RS-232 2165746

$C.$ 1

8232-27/065746

00000001 -

Exploratory Battery Technology Development and Testing Report for 1985

Nicholas J. Magnani, Robert P. Clark, Jeffrey W. Braithwaite,
Donald M. Bush, Paul C. Butler, James M. Freese,
Kenneth R. Grothaus, Kevin D. Murphy, Paul E. Shoemaker

1076279

Exploratory Battery Technology Development and Testing Report for 1985

Nicholas J. Magnani
Power Sources Department
Robert P. Clark, Jeffrey W. Braithwaite, Donald M. Bush,
Paul C. Butler, James M. Freese, Kenneth R. Grothaus,
Kevin D. Murphy, and Paul E. Shoemaker
Storage Batteries Division

Sandia National Laboratories
Albuquerque, NM 87185

Abstract

Sandia National Laboratories, Albuquerque, has been designated as Lead Center
for the Exploratory Battery Technology Development and Testing Project, which
is sponsored by the U.S. Department of Energy's Office of Energy Storage and
Distribution. In this capacity, Sandia is responsible for the engineering develop-
ment of advanced rechargeable batteries for both mobile and stationary energy
storage applications. This report details the technical achievements realized in
pursuit of the Lead Center's goals during calendar year 1985.

Contents

Figures

Figures (continued)

Figures (continued)

Tables

Acronyms and Abbreviations

ANL	Argonne National Laboratory
BCT	Battery Components Technology (a section of NBTL)
BEST	Battery Energy Storage Test Facility
BET	Brunauer, Emmett, Teller method for determining particle surface area
CAPM	Capital Asset Pricing Model
CI	constant current
COMSAT	Communications Satellite Corporation
CRT	cathode ray tube
CSOM	customer side of the meter
CSPL	Chloride Silent Power, Ltd.
CV	constant voltage
CY	calendar year
DOD	depth of discharge
DOE	Department of Energy
EDA	Energy Development Associates
EDS	energy-dispersive spectroscopy
EDX	energy-dispersive x ray
EECI	Electrochemical Engineering Consultants, Inc.
EHP	Electric and Hybrid Propulsion (a division of DOE)
EPD	electrophoretic deposition
EPI	Eagle-Picher Industries
EPRI	Electric Power Research Institute
ERC	Energy Research Corporation
ETD	Exploratory Battery Technology Development
ETX	electric transaxle experimental test vehicle and testing project
EV	electric vehicle
EVEM	Electric Vehicle Engineering Model
FACC	Ford Aerospace and Communications Corporation
FUDS	Federal Urban Driving Schedule
IGCB	improved gell-cell, lead-acid battery
IR	internal resistance; infrared analysis
ISOA	improved state of the art
JCI	Johnson Controls, Inc.
LL	load leveling
LMSC	Lockheed Missiles and Space Company
NBNM	Natural Bridges National Monument
NBTL	National Battery Test Laboratory
NMR	nuclear magnetic resonance
NPV	net present value
OCAC	open circuit after charge
OCV	open-circuit voltage
ORNL	Oak Ridge National Laboratory
PASTF	Photovoltaic Advanced Systems Test Facility
PHS	Public Health Service
PS	polysulfone
PV	photovoltaic
PVC	polyvinylchloride
Redox	reduction oxidation
RF	recharge factor
S^3D	slurry solution, spray-dried

Acronyms and Abbreviations (continued)

S⁴D	seeded slurry solution, spray-dried
SCR	silicone-controlled rectifier
S.E.A	Studiengesellschaft für Energiespeicher und Antriebssysteme
SEM	scanning electron microscopy
SERI	Solar Energy Research Institute
SES	stationary energy storage
SNL	Sandia National Laboratories
SOC	state of charge
SWRES	Southwest Residence Photovoltaic Evaluation Facility
TBR	Technology Base Research Project
TD	Technology Demonstration
TEP	triethylphosphate
WACC	weighted average cost of capital
WTG	wind turbine generator

Exploratory Battery Technology Development and Testing Report for 1985

Chapter 1. Aqueous Battery Development

Introduction

During 1985, several aqueous electrolyte advanced secondary battery systems were developed. These included zinc/bromine (Exxon Research and Engineering Company and Energy Research Corporation), zinc/ferricyanide (Lockheed Missiles and Space Company), and hydrogen/nickel oxide (COMSAT Laboratories). The contractors receiving support in 1985 also dedicated their own funds to these efforts.

Exxon phased out its zinc/bromine program in 1985. The firm successfully established technology licensing agreements with several international companies, including Johnson Controls, Inc. (JCI) in the United States. Activities supported by the Exploratory Battery Technology Development (ETD) program were limited to delivery of units for evaluation and drafting of the final contract report. In June, an Exxon battery (Z30-A), based on technology developed under previous ETD programs and fabricated under a DOE/EHP-sponsored program, successfully powered an experimental test vehicle at Ford Motor Company.

In September, Sandia National Laboratories (SNL) contracted the Energy Research Corporation (ERC) to continue the development of zinc/bromine core technology and to address the engineering issues associated with zinc/bromine stationary systems. This three-year, $5.1M program was the result of a lengthy competitive procurement process. The Electric Power Research Institute (EPRI) also contracted ERC to design, qualify, and deliver a 500-kWh zinc/bromine battery to be evaluated at the BEST facility in 1989. The EPRI battery will be based on the technology developed under the ETD-funded Sandia contract.

Since 1981, Lockheed (under contract with SNL) has performed engineering development studies on the zinc/ferricyanide battery. The second contract phase was completed in December 1984, with two basic technical issues still not completely resolved:

(1) identification of a suitable low-cost membrane, and (2) the development of a low-cost electrode that is amenable to a bipolar design. A new, 18-month contract was placed with Lockheed in October 1985 to address these issues. In the period between contracts, Lockheed used internal funding to perform marketing and economic studies directed at future commercialization of this battery system.

Six hydrogen/nickel oxide cells and one battery were built and evaluated in 1985 by Communications Satellite Corporation (COMSAT). JCI was a major subcontractor in this effort. One of the most encouraging developments was improvement of the system's performance by the use of thicker positive electrodes; cell capacity was increased 40%, with fewer parts and no volume increase. A cost study was completed that indicated that a hydrogen/nickel oxide battery could be made cost-competitive with lead-acid on a life-cycle cost basis.

The aqueous battery systems under development continued to show promising results. A major shift in zinc/bromine developers resulted in a pause in the rate of development, but it continued to be the most extensive program in this ETD element. Significant progress in the hydrogen/nickel oxide system warrants further support for this system, particularly as applied to stand-alone solar applications.

Zinc/Bromine Battery—Exxon

The zinc/bromine battery is a flowing electrolyte battery that uses a combination of recent developments: soluble, reversible, bromine complexing agents; the control of shunt current effects; and a conductive carbon-plastic electrode technology. Previous attempts to develop a zinc/bromine battery were unsuccessful because of problems related to self-discharge caused by bromine diffusion between the

electrodes, irregular and dendritic zinc growth during recharging, and corrosion problems caused by the high reactivity of bromine. In the present approach, self-discharge is controlled by the use of a bromine complexing agent to store bromine outside the cell. Electrolyte circulation helps provide uniform zinc deposition. The electrolyte circulation process provides common electrolyte pathways for shunt current. Electrical shunt current protection methods have been developed in which current is passed through the common electrolyte, which effectively eliminates the shunt current effects. Electrode corrosion is avoided by the use of conductive carbon-plastic and other plastic components that are bromine-resistant. The extensive use of plastic components in the battery system provides a low-cost, easily producible battery module.

Using its extensive background in fuel cells and a previously developed carbon-plastic electrode, Ex-xon's formal involvement in the zinc/bromine battery began in 1975. Sandia entered into a cost-shared, three-phase contract with Exxon in 1980 to develop an evaluation battery suitable for solar applications. A follow-on program to adapt the technology to electric vehicle (EV) applications began in 1983. Both programs continued through 1985.

The objective of the last phase of the development program was core technology, that is, the development of both an electrolyte technology and a versatile electrode structure that would be adaptable to various battery applications. The most significant 1985 achievement was the delivery of a 20-kWh stationary battery for testing at SNL (Figure 1-1). The EV battery development program focused on the evaluation of higher-voltage, high-capacity designs in support of the DOE/Ford Motor Company ETX program.
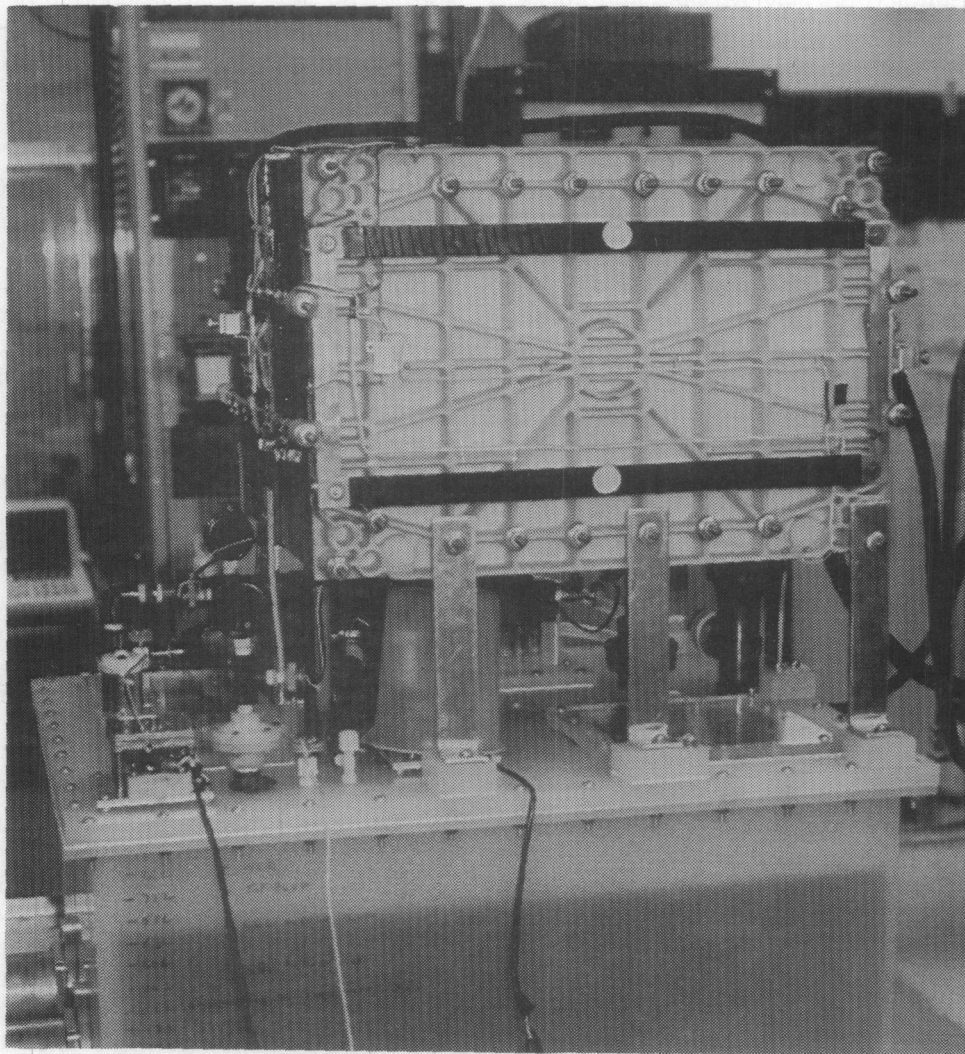
Figure 1-1. 20-kWh, 120-V Zinc/Bromine Battery (Z-20)

In 1981 Exxon developed an attractive, low-cost battery stack structure based on coextruded electrodes and molded integral separator/flow frames. The conductive electrode material is extruded with two nonconductive borders. The electrode material is cut to size and holes are punched to produce the manifold tunnel and bolt holes. The microporous separator material in the flow frame is also extruded. A section of the separator is cut to size, and a plastic flow frame is injection-molded around the edges of the separator material. The flow frame has electrolyte channels and flow distributors and collectors, and holes for manifolds are molded into the nonconductive upper and lower borders. The active electrode of this low-cost electrode structure was scaled up to 1200 cm^2 during 1982. The 1200-cm^2 components are shown in the foreground of Figure 1-2. Rolls of extruded electrode and separator materials demonstrating the productivity of the extrusion technique are shown in the background of this figure.
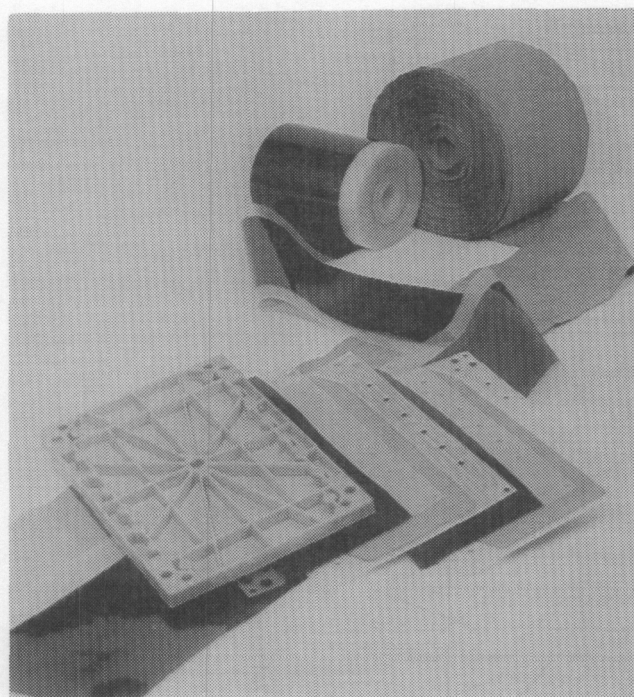
Figure 1-2. 1200-cm^2 Zinc/Bromine Battery Components

Before the fabrication of a multikilowatt-hour battery design, a single-stack 10-kWh battery (120 V) was built and cycled to 50 cycles to qualify this design point. Performance over the 50 cycles was stable, and no further modifications in the design were required.

State of Development

During 1984-85, system scale-up of the 1200-cm^2 components was accomplished with nominal 20-kWh batteries. Three 20-kWh batteries (120 V) were built and cycled over 25 times. One of these, shown in Figure 1-1, was selected for delivery to and evaluation at SNL. Specific energy density for this design, including all auxiliaries except the controller, is ~55 Wh/kg. The 20-kWh battery exceeded the nominal design capacity in tests at SNL.

These 20-kWh, 120-V batteries use two stacks of 78 bipolar cells (1200-cm^2 area). Internal stack configurations are shown in Figure 1-3. The two stacks are connected in parallel to produce the rated current and power. Voltage tabs are placed at intervals in the cell stacks. Voltage monitoring of these banks of cells has shown closely matched average cell voltages throughout charge and discharge. The two-stack design also demonstrated close matching of current use and delivery throughout the charge and discharge. Typical cell bank voltage, stack and battery system voltage, and current during a charge and discharge are shown in Figure 1-4.

The performance matching of the cells, stacks, and components is encouraging and promotes consideration of systems with higher voltage, power, and capacity. The largest resistive component in the battery stack is the gap between the electrodes that is filled with electrolyte; this gap resides mainly in the electrolyte-filled separator. This arrangement contributes to internal performance damping and provides uniform stack performance. Uniform mixing and the supply of electrolytes to the electrodes by circulating the electrolyte help to match the stack performance. Circulating the electrolytes also provides good heat exchange and uniform temperatures within the stacks.
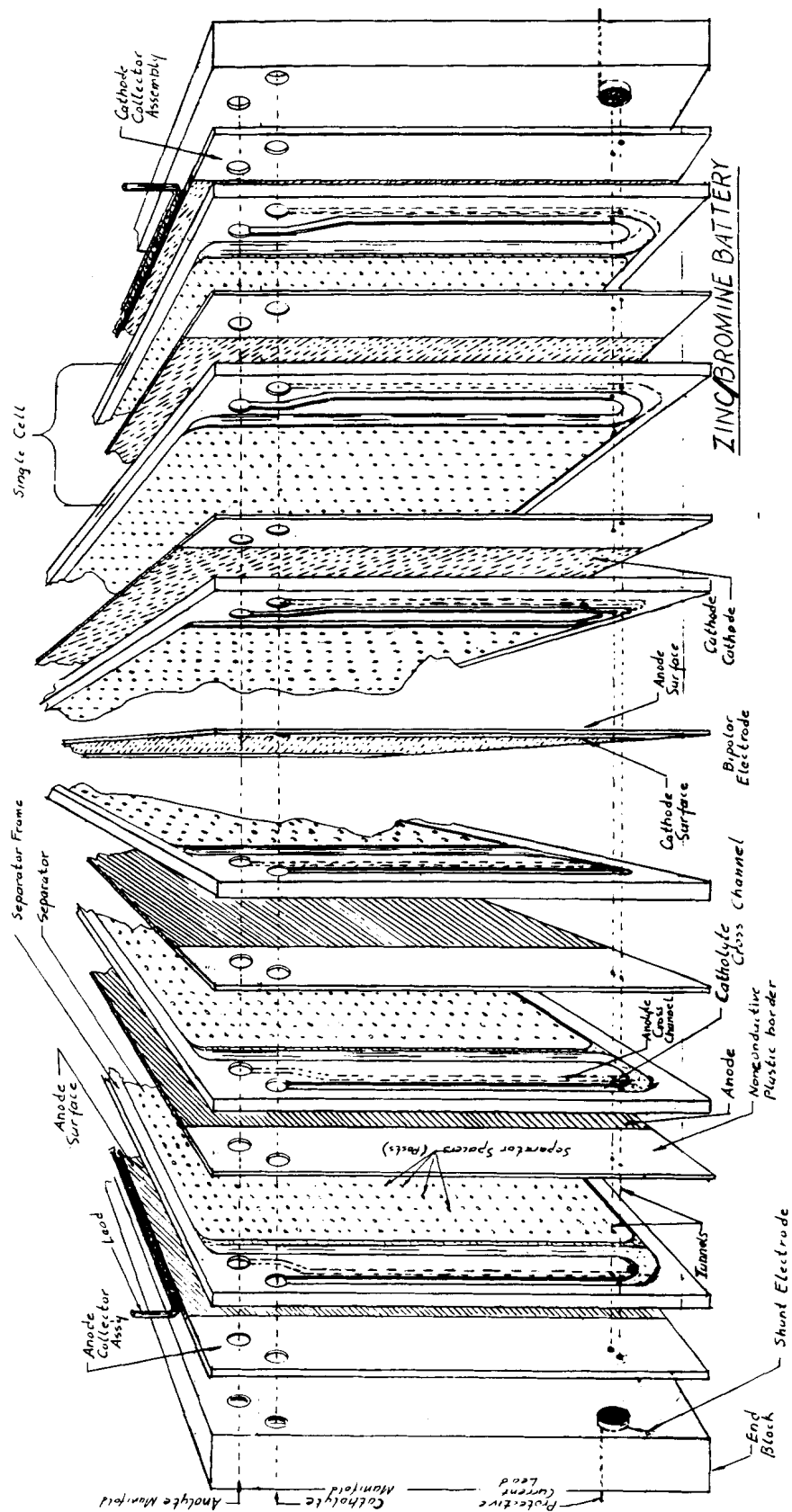
Figure 1-3. Exploded View of Z-Design Battery Stack

14
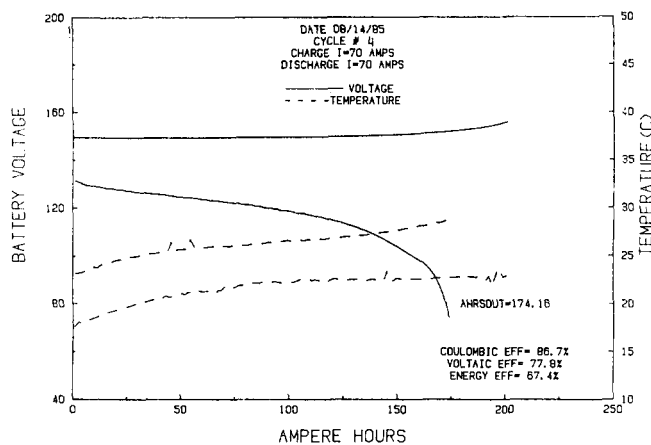
(a) Cell Bank Voltage Behavior
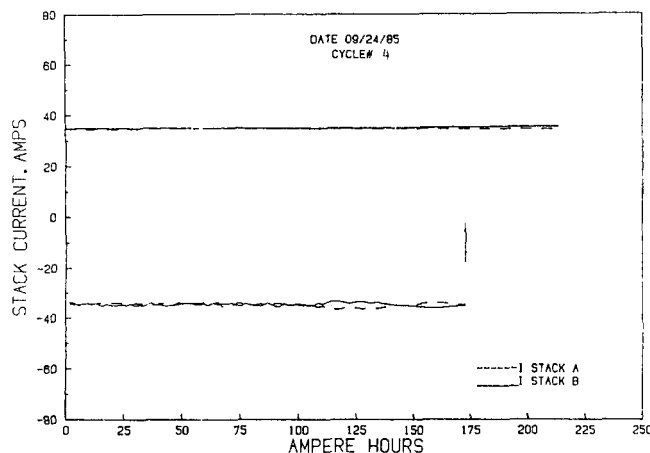
(b) Charge/Discharge Stack Current Behavior
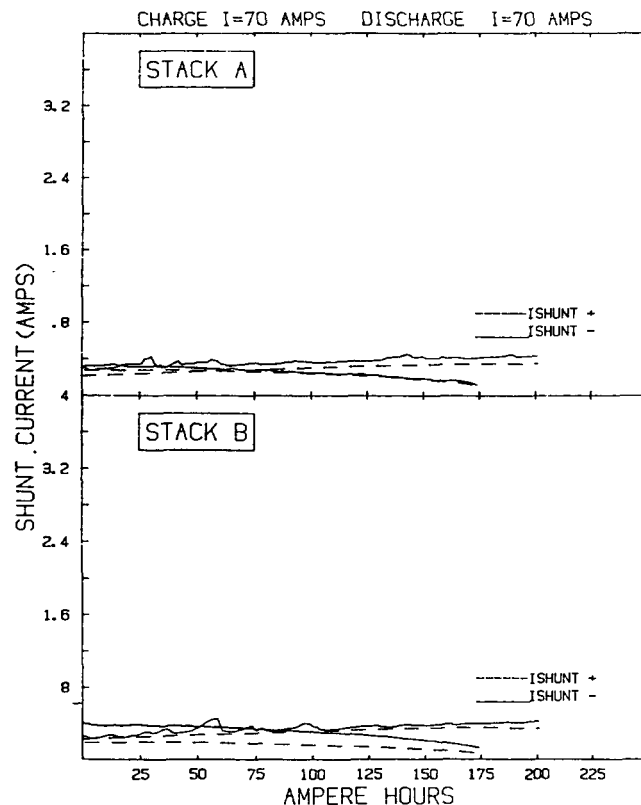
(c) Charge/Discharge Shunt Current Behavior

Figure 1-4. PV-20 Zinc/Bromine Battery Performance Characteristics

The "tunnel" shunt current protection system was applied to the 78-cell bipolar stacks. The power and energy, which would be shunted in unprotected systems, were slightly augmented and passed through the commonly shared electrolyte manifold channels and tunnels connecting the channels. The tunnels are located between the electrolyte channels close to the point at which the channels enter or leave the cells. The effects of shunt currents through the common electrolyte include reduction of capacity, maldistribution of capacity through the stack, zinc metal growth into the channels, and corrosion of electrodes. Because none of these effects is desirable, shunt current protection is an important feature of the system's design. The 20-kWh batteries were self-protected with the protective tunnel electrodes directly hard-wired to the system's terminal electrodes.

Heat is produced in the battery during operation through internal-resistance heating, self-discharge, and auxiliary equipment. Heat exchanger/radiators are required for thermal management. Coolant coils of polyolefin plastic tubing are provided in the anolyte reservoir. To remove the heat, water is circulated through these coils and to the external radiator. The 20-kWh batteries are also provided with temperature-sensor probes in the anolyte reservoir and in the coolant loop.

The 20-kWh battery delivered to SNL was equipped with in-line flowmeters to monitor the anolyte and catholyte flow. Pressure gauges and sensors also monitor the circulating electrolyte. Electrolyte liquid-level sensors are incorporated into the anolyte and catholyte reservoirs. Data loggers gather battery information for display on an HP/87 computer CRT

15

and in periodic printouts. Also displayed are voltages and currents of the electrolyte pump motors, total ampere-hours and kilowatt-hours into and out of the battery, and the currents internally supplied within the battery to the system, which protects the electrodes from the effects of shunt current.

Reservoirs, support structures, and auxiliaries were heavily overdesigned in this battery. This overdesign can easily be engineered out and in future batteries specific energy and power densities are projected to exceed 60 Wh/kg and 100 W/kg in stationary applications. As noted below, separators from recent shipments performed poorly. By incorporating separators that perform better and auxiliaries that weigh less, specific energy densities >70 Wh/kg can be projected.

Various auxiliaries required to demonstrate full-scale battery operation underwent steady development in 1984-85. An improved controller/controller interface for the battery was constructed and qualified with the Z-20 unit. The controller for the battery system is an HP/87 personal computer. Future designs for mobile and stationary use will probably be based on a single-board microprocessor. The functional specification and programming for the single-board microprocessor will be similar to the present HP/87 program. Efforts continued in 1984-85 to develop air-cooled radiators and to match various ac and dc motors coupled to the magnetically driven centrifugal pump heads for various designs.

Many variables and constraints must be considered in the design of any new battery system. Designs vary significantly over the range of possible uses of the zinc/bromine battery. These applications include load leveling, electric vehicles, photovoltaic energy storage, and standby/emergency power. The complexity of interactions between design variables, constraints, and performance criteria is so great that the only practical means to evaluate design options and trade-offs is through use of a computerized model of zinc/bromine battery interactions.

A simple model of a zinc/bromine battery was developed during the second phase of this development effort. The major electrochemical cell effects incorporated into the model were internal resistance and bromine diffusion across the separator. This model considered the number of cells in a stack and the system voltage, geometrical factors of the manifolds/channels and cells, stack component dimensions, separator thickness, tortuosity and porosity, electrolyte flow rates, density, conductivity, aqueous bromine concentration, self-discharge, shunt current protection, and pumping power. These relationships, together with charge/discharge currents and time of charge, allow computation of capacities and efficiencies.

During the third development phase, the model was expanded to include ranges of electrolyte composition and use, and system component dimensions and densities (to compute volume and weights) for multiple stacks. The effects of parameter changes on peak power and volumetric and gravimetric energy and power densities, for example, can be computed and graphically displayed with this expanded model.

During 1984-85, parametric testing concentrated on extending life and controlling various potential failure mechanisms. An extended electrolyte test continued through 1400 cycles (including use in five separate parametric stacks) and showed no decline in electrolyte performance. This particular electrolyte has been in active use for 30 months. Periodic analysis of this electrolyte showed no change in the nuclear magnetic resonance (NMR) spectra, indicating stability of the quaternary ammonium complexing agents. Elemental analysis of the electrolyte showed a slight increase (at the ppm level) in aluminum and silica, probably due to discharging from the filler in the separators. Stack life for the 1200-cm^2 components was demonstrated in a 1-kWh stack for over 500 cycles at the full- (90-mAh/cm^2) design zinc loading. Final failure of this stack was associated with electrode warpage. The use of thicker electrodes (50 vs 30 mils) reduced the rate and intensity of warpage, although the longest life with these electrodes has been 325 cycles. Earlier work with 100-mil electrodes showed no sign of warpage after 640 cycles. The longest-life zinc/bromine battery completed over 1500 cycles by the end of 1985, with stable performance. This battery was sent to SNL after 20 qualification cycles at Exxon and has now been on test since 1982. This stack has eight cells made from 600-cm^2 electrodes with a 500-Wh capacity.

Progress was made on controlling a number of failure mechanisms. Limiting the maximum charge voltage to 2 V/cell avoids voltage excursions at the end of charge, which can cause rapid pH increases. These excursions are related to a depletion of zinc in the anolyte in heavily supported electrolytes. Experience continues to show that electrode warpage can be controlled either by using thicker electrodes or by using electrodes made with mixtures of carbon-plastic that show less expansion in the presence of bomine. Finally, safety cutoffs were installed in all parametric stations to shut down the battery cyclers in the event of a burnout of a pump motor brush.

Experimental studies aimed at improving battery operating efficiency have indicated that coulombic losses are due to the mass transport of elemental bromine across the separator into the anolyte where the bromine reacts indirectly with the zinc deposit in the anode. In particular, we found that the microporous separator used in our battery is wetted preferentially by the polybromide complex rather than by the aqueous phase. This characteristic facilitated bromine transport and was a major cause of a significant portion of the observed coulombic loss. In an attempt to gain a better understanding for this behavior, we found an additive that changes the wetting characteristics of the separator in an aqueous phase-polybromide complex mixture, producing significant improvement in coulombic efficiency. This additive is introduced into the electrolyte in very small amounts and is inexpensive. An eight-cell parametric battery has yielded 90% coulombic efficiency at full loading (90 mAh/cm^2) and deep cycling.

Various studies were initiated to aid in solving basic problems with the zinc/bromine battery system. Laser Raman spectroscopy was used to quantitatively identify liquid ionic complexes between zinc and halide ions, as well as complexes formed with complexing agents and/or supporting cations. The addition of supporting electrolytes will shift the zinc halide ion equilibria toward higher ionic forms. It appears that the complexing agents stabilize the mono-negatively-charged zinc halide species by forming ion pairs (charged or neutral). The Raman spectra of the complexing agents exhibit differences and can serve as a method of quaternary ion analysis. Laser Raman spectra are, therefore, a good tool for the scientific analysis of electrolytes. The ionic complexes mentioned above adversely influence battery performance. The use of laser Raman spectra provides much-needed quantitative data on these complexes, the absence of which has hindered the understanding of various mass transfer effects in the battery. Other spectra studies have investigated the interaction between carbon and bromine, interaction that can be interpreted as a significant increase in the interlamilar spacing of carbon crystallites in the presence of bromine. Further studies are needed.

The most significant new component demonstrated was a separator that exhibited an increase in coulombic efficiency of ~10% over the best recent Daramic® separator material, with no loss of voltaic efficiency. We recently noticed a gradual decline in coulombic efficiency in successive batches of Daramic. In particular, a typical coulombic efficiency dropped 8–10% from the 1982 performance level. Studies to understand the differences between the new separator and Daramic reveal some differences that affect coulombic efficiency. These observations led to the identification of a class of electrolyte additives that improve the efficiency of Daramic to comparable levels noted earlier.

Other improved components were tested, including solid bromine complexing agents that could reduce the escape of bromine in the event of reservoir ruptures. A resilient polymer was incorporated in flow frames in recent experiments. This resilient polymer reduced the need for internal battery adhesives to prevent leakage because the material acted as its own gasket. Carbon-plastic coextrusion, first demonstrated in 1982, was improved, finally showing precise control of the bond between conductive and nonconductive plastic as well as uniform part tolerances.

A 20-kWh battery (PV-20) has been installed and is operating at SNL. Performance curves are shown in Figure 1-5. The performance meets specifications. In the latter part of 1985, the plastic coils of heat exchangers in this battery were replaced with titanium tubes for greater reliability. The PV-20 will be connected to a photovoltaic array in 1986.

EFFICIENCIES & ENERGY OUTPUT VS CYCLE NO.
EXXON'S PV20 BATTERY

COULOMBIC EFFICIENCY	VOLTAIC EFFICIENCY	ENERGY EFFICIENCY	DISCHARGE (kWh)
—+—	—+— —	— — —▲— — —	· · · · ·□· · · · ·

EFFICIENCY (%) OR ENERGY (kWh)
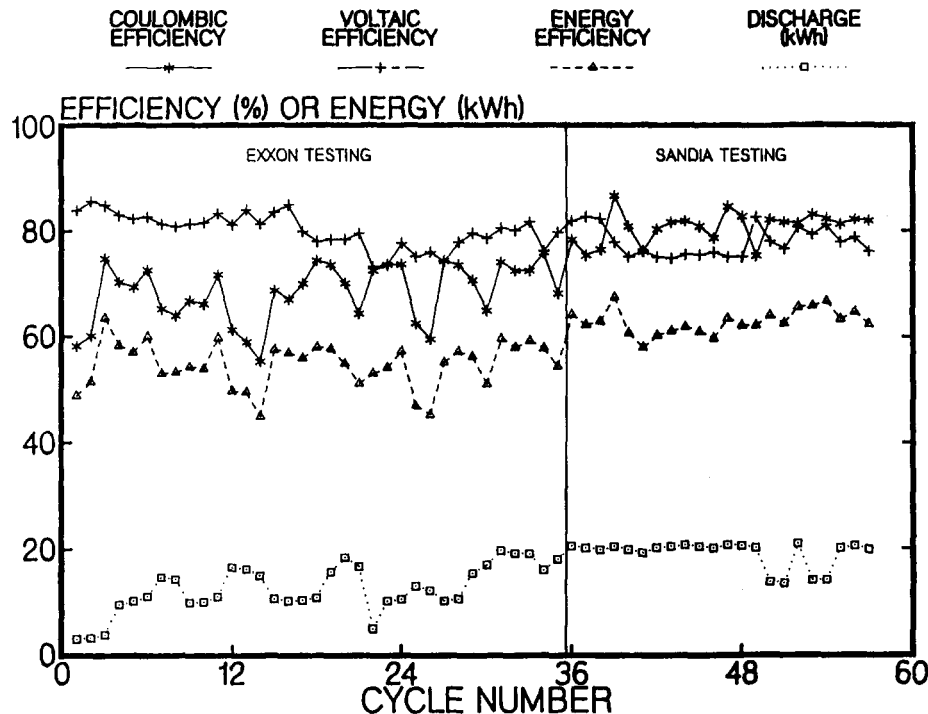
Figure 1-5. PV-20 Performance Data

Zinc/bromine battery technology was also advanced in other related programs, which drew heavily upon the technology developed in the Phase III Core Technology program.

In the EV battery development program, the use of zinc/bromine technology for electric vehicles was initially demonstrated in a 200-V, 124-cell battery module (Z-15). To meet EV power performance requirements, the stack was tested with supported electrolytes. The cell components were the same as those in the 78-cell stacks. Z-15 demonstrated 15-kWh capacity with power exceeding 40 kW over most of the discharge. Sustained power of 25 kW was demonstrated, and the performance was stable over 50 cycles. However, the electrolyte flow rates were less than optimal, and the efficiency was also less because of additional shunt losses related to more conductive electrolytes. Various constraints did not permit a redesign of the cell components. Z-15 was a success, and the performance encouraged building a 30-kWh, two-module system with specifications and design suitable for the Ford ETX vehicle.

Z-30A was built and tested for more than 50 cycles at Exxon. It was the first advanced secondary battery to successfully power the state-of-the-art, full-sized, 200-V ac drive ETX vehicle at Ford Motor Company in Dearborn, Michigan. The Federal Urban Driving Schedule (FUDS) testing was successful. The battery had the appropriate range capacity but its power was limited at later states of discharge.

A second battery (Z-30B) was delivered to Argonne National Laboratory (ANL) in the second half of 1985. Subsequent characterization tests and vehicle simulation runs were successful and continued into 1986.

Technical Challenges Remaining

Testing of large batteries is particularly important to the future development of the zinc/bromine batteries. Large-scale battery tests will be needed to demonstrate the capabilities of the zinc/bromine system to various potential consumers of advanced batteries, such as electric utilities, manufacturers of

photovoltaic energy storage systems, and manufacturers of electric vehicles.

Stack sealing continues to be a major problem in building these large batteries. Sealing now involves the use of a solvent-based adhesive applied to the mating surface of the electrodes and separators. These adhesive application techniques have virtually eliminated external leaks, although occasional small seepage and some internal cross-flow are still problems. Additional efforts should be devoted to improving the thermal bonding techniques, which could prove more reliable than adhesive sealants.

Battery coulombic losses during prolonged shutdown require further study. This capacity loss is related to complexed bromine trapped in the separators and the cathode activation layer. Reducing the quantities of bromine in the separator and in the cathode activation layer should limit the losses.

Exxon now holds 30 U.S. patents on various aspects of the zinc/bromine battery design, fabrication, and application. Long-range plans for the overall zinc/bromine battery program at Exxon now call for worldwide development efforts by licensees of this technology. Johnson Controls, Inc., a leading manufacturer of lead-acid batteries, is the United States codeveloper; S.E.A., a division of OIAG in Austria, is the European codeveloper; Sherwood Engineering is carrying out codevelopment in Australia; and the codeveloper in the Far East is a major Japanese auto manufacturer. Work at JCI and with other codevelopers will adapt the technology to several applications (electric vehicles and large- and small-scale bulk-energy storage). It is anticipated that these adaptations will be based on principles of electrolyte formulations and electrode technology developed under the Sandia contract. These worldwide efforts will continue to augment the zinc/bromine battery technology.

Zinc/Bromine Battery—ERC

A zinc/bromine battery development program has been underway at ERC since late September 1985 under Sandia's sponsorship. Previous work at ERC on the zinc/bromine battery had been conducted since 1983 under a program supported by EPRI.

Several characteristics of the zinc/bromine system make it a promising candidate for utility energy storage as well as for other applications (electric vehicle, photovoltaic, etc.). The reactants (zinc and bromine) are abundant, low-cost materials. The electrodes used

in the battery are low-cost molded carbon-plastic composite materials. These electrodes serve as substrates on which battery reactions occur. Unlike other commonly used battery systems, the electrodes themselves do not change chemically during the operation of the cell. This unique characteristic means that under ideal conditions a cycled battery, when fully discharged, would be physically identical to a new battery. The zinc/bromine battery, therefore, has the potential to exhibit unprecedented useful life.

To realize this potential, the wide-scope development program presently underway at ERC ranges from studies of the fundamental electrochemistry of the zinc/bromine couple to engineering studies on full-size utility battery design concepts. Two separate but closely coordinated projects are presently underway: one supported by DOE/Sandia, the other by EPRI. Both programs are cost-shared by ERC.

The three-year Sandia-supported program involves core technology studies to develop and optimize the battery design. This includes basic research on the battery electrochemistry and supporting research and development activities to optimize the cell and component designs. Development studies on the battery system will include hardware design and battery scale-up. After two years of development, a design will be chosen and two 50-kWh prototypes will be built and tested in the third year of the program. Successful operation of the 50-kWh prototypes will qualify the design and initiate the fabrication of a 500-kWh demonstration battery (in the companion EPRI-supported program). During the third year of the Sandia program, while the 50-kWh prototypes are built and tested, the R&D activities will focus on design issues involved in other battery applications, primarily for EV energy storage.

The zinc/bromine battery is a flowing electrolyte system in which an electrochemical stack is fed with electrolyte from two (anolyte and catholyte) recirculation loops. The electolyte is an aqueous solution of zinc bromide, with supporting salts and additives used to increase conductivity and improve zinc electrode performance. On charge, the zinc bromide salt is electrolyzed to form metallic zinc and molecular bromine. Bromine is formed as a liquid dissolved in the catholyte. Zinc is plated out as a sheet of metal on the surface of carbon bipolar electrodes. The cell and stack configurations are shown in Figures 1-6 and 1-7, respectively.
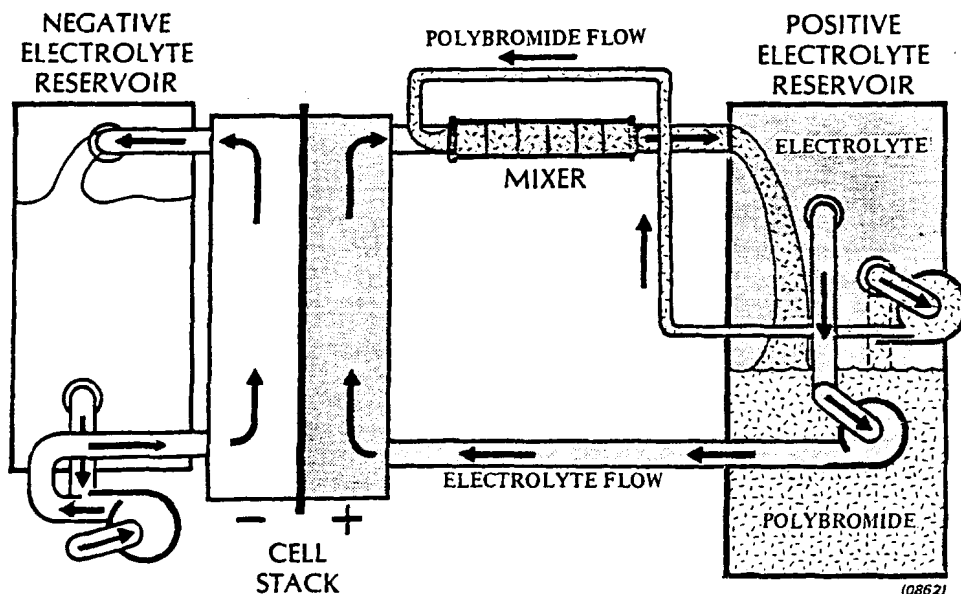
Figure 1-6. Schematic of Simplified Battery Flow System
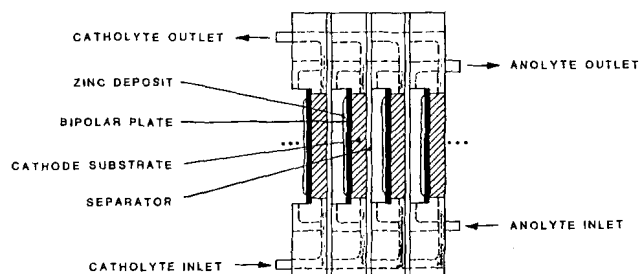
Figure 1-7. Cell Stack Design Concept

To prevent self-discharge of the system (from nonfaradaic reaction of zinc and bromine), a porous membrane is used to separate the anolyte and catholyte fluids, limiting the rate of bromine diffused into the anolyte fluid. To further limit the rate of bromine diffusion, bromine levels in the catholyte are kept low by extracting evolved bromine with an organic complexing agent. Because of the resulting low levels of bromine in the catholyte, a high-surface-area carbon felt flowthrough electrode is used to improve bromine electrode performance on discharge.

The overall objective of the Sandia-supported program is to advance the battery technology to the point at which the system is demonstrated to be a reliable, low-life-cycle-cost candidate in its targeted applications. The program is organized into two major tasks. Task 1, Core Technology Research and Development, involves development activities to optimize

the component and system design. Task 2, Battery Engineering and Testing, occurs in the third year of the program and involves the fabrication and testing of 50-kWh prototypes incorporating the optimized battery design.

The Core Technology Research and Development task of the program is broken down into five subtasks, described below:

- **Basic Research and Development** consists of studies on the fundamental electrochemistry of the battery system and components. The subtask includes investigations on bromine electrode kinetics, bromine storage techniques, zinc electrode kinetics, electrolyte properties, separator properties, bipolar electrode development, electrolyte pH maintenance, and computer modeling studies.

- **Supporting Research and Development** involves component and system design activities using the results of the Basic R&D subtask activities. For each area of study listed for the Basic R&D subtask, a corresponding design activity occurs in the Supporting R&D subtask, in which the actual component designs are developed.

- **Hardware Design** consists of optimizing the stack hardware configuration. In the present stack design, the bipolar stack is held together with compression applied by tie bolts and endplate assemblies. The Hardware Design subtask

includes development work to optimize the stack clamping assembly. The feasibility of heat-sealing the stack components together is also being investigated. Studies on scaling up the electrode's active area (from the 872 cm² presently used) are also included.

- **Hardware Testing** involves the fabrication and testing of full-scale multicell stacks incorporating the optimized cell, hardware, and system designs.

- **Material Qualification** consists of chemical and electrochemical stability studies on battery components and materials of construction.

Figure 1-8 shows the overall program schedule and the plan for the companion EPRI-supported program. The Sandia-supported program began in late September 1985, so CY85 activity included slightly more than three months of work. As shown in the program plan, many of the activities described above had not yet begun. A discussion of the activities conducted over this period is presented below.

State of Development

Bromine Electrode Development

This activity of the program involved investigating the kinetic performance of novel (other than carbon felt) bromine electrode designs. Work conducted included the completion of bromine electrode catalyst stability tests and polarization testing of porous flow-by and ribbed electrode structures.

Bromine electrode catalysts are being investigated as a means of improving cell performance by reducing activation polarization of the bromine electrode. A number of catalysts were studied including ruthenium oxide, cobalt spinels, perovskite, and gold-palladium alloy catalysts. The ruthenium oxide material was found to be the only stable catalyst. This is unfortunate since it is one of the more expensive catalyst materials.

The flow-by and ribbed electrodes are being studied as a means to circumvent the limitations of the carbon felt electrode. One of these limitations is that the felt entraps some of the bromine complex formed

YEARS INTO PROGRAM:		1	2	3	4
	'85	1986	1987	1988	1989
SANDIA PROGRAM					
BASIC ELECTROCHEMICAL RESEARCH					
SUPPORTING R&D–UTILITY LOAD LEVELING					
SUPPORTING R&D–EV APPLICATION					
50-kWh PROTOTYPE FABRICATION & TESTING					
EPRI PROGRAM					
UTILITY APPLICATIONS STUDIES					
PRELIMINARY BEST BATTERY DESIGN					
FINAL BEST BATTERY DESIGN					
50-kWh PROTOTYPE FABRICATION & TESTING					
500-kWh BEST BATTERY FABRICATION ACCEPTANCE PRETEST					

Figure 1-8. Four-Year Program Plan for Zinc/Bromine Battery Development at ERC

in the cell channel that is meant to be expelled from the stack to limit self-discharge. Another is that the felt is not produced or engineered for electrochemical applications; therefore, material quality and uniformity has been a problem.

Ribbed electrode structures perform comparably to carbon felt, but require much higher electrolyte flow rates. Porous flow-by electrodes also require high catholyte flow rates to achieve acceptable polarization characteristics, but do not perform as well as the ribbed electrodes. The incorporation of a ruthenium oxide catalyst on ribbed electrodes reduced electrode discharge polarization by $\sim$100 mV at 30 mA/cm^2.

Bromine Storage Development

In this activity of the program, the chemistry of alternate methods of storing evolved bromine was examined. The materials investigated included solid storage media (carbon, solid quaternary ammonium materials) and organic solvents. The feasibility of removing bromine as a vapor for external storage (as elemental bromine or bromine hydrate) will also be studied.

Work in the first three months of the program included setting up flow systems for the investigation of bromine storage in packed beds of carbon or solid complexing agents. Also, equipment was ordered to study the vapor-liquid equilibrium of bromine over the electrolyte used in the battery.

As a first step in the study of bromine storage in packed fluidized beds, a number of candidate powder materials were analyzed for density (bulk and absolute) and specific surface area. The specific surface area of the materials ranges from 1400 m^2/g for black pearl carbon black to 40 cm^2/g for solid quaternary ammonium compounds.

Zinc Deposition Studies

The electrochemistry of zinc deposition was investigated. Analytical equipment was set up and electrolyte solutions were made. The first tests examined zinc deposition kinetics from electrolyte solutions with various zinc bromide and supporting salt concentrations.

The electrolyte currently used in cell and battery tests at ERC is designated MOD-1. It consists of an aqueous solution of 0.5 mol zinc bromide, 3.0 mol potassium chloride, 1.5 mol zinc/chloride, and 2.0 mol potassium bromide. An inorganic zinc plating additive is also used.

Tafel plots were made for the MOD-1 electrolyte (with additives) and for unsupported 3 mol of zinc bromide electrolyte. The exchange current density for plating zinc on glassy carbon from the MOD-1 electrolyte was $\sim$130 μA/cm^2. The exchange current density for the unsupported 3-mol zinc bromide solution was about the same. The exchange current densities for plating zinc on zinc were about ten times higher, $\sim$1 mA/cm^2. The Tafel slope for the unsupported electrolyte solution was lower than that observed for the MOD-1 electrolyte.

Potential step measurements were also made on the two electrolyte solutions to observe the onset of zinc nucleation and deposition. At an overpotential of 20 mV, no deposition occurred at the MOD-1 electrolyte until $\sim$10 s into the test. When the unsupported 3-mol zinc bromide solution was used, a 20-mV potential step induced a current of 30 mA/cm^2 within 5 s. This illustrates the significant effect that supporting salts and additives have in slowing down the kinetics of the zinc deposition process. It is a beneficial effect since it tends to shift the deposition process from diffusion control (which promotes dendritic deposits) to activation or kinetic control. In other words, the deposition process is limited by the reactivity of zinc ions at the electrode surface, as opposed to being limited by the rate of diffusion of zinc ions from the bulk solution to the electrode. This is preferred for the deposition of a uniform, dense zinc layer on the electrode surface.

Separator Development

This activity of the subtask was limited by the availability of sample separators. Evaluation of extruded polyethylene materials in the previous EPRI program had shown that the use of thicker films (above the 25-mil thickness presently used) would increase battery efficiency. The increased voltage loss in thicker films is more than offset by the decrease in bromine permeability.

Attempts were made to get samples of extruded polyethylene films (Daramic® from W. R. Grace Company and Submicro® from Evanite Corporation) 30 mils thick or greater; however, these materials were not available. Samples of a 30-mil-thick extruded PVC material, Amer-Sil® (Amerace Corporation), were obtained late in 1985 and testing will begin in early 1986.

Bromine Electrode Design

This activity of the program involves the design and optimization of the bromine electrode. Initially, the work centered on optimizing the carbon felt electrode currently used in the system. Later in the program, the focus will shift to scale-up and engineering of promising alternate electrode concepts arising from the Basic Research and Development subtask work.

One of the problem areas associated with the carbon felt electrode has been the difficulty in obtaining uniform material within a given thickness and density specification. The problem stems from the fact that suppliers who produce the material for other applications have not had the incentive to optimize process techniques or specifications for application of the material to batteries.

As a result of earlier work done on the development of fuel cell materials, ERC has accumulated a substantial amount of carbonization equipment and expertise. Carbon felt samples were prepared by heat-treating rayon felt material. Cell tests were made on samples produced with various heat-treatment temperatures and cycles. Samples tested at 1200°C performed similarly to felt used in the program to that point.

A large quantity of the felt precursor was obtained and 50 pieces were carbonized. The pieces were cut into 20×20-in. squares, which shrink to about 13×13 in. when carbonized. The pieces were trimmed and then used to build single cells having an active area of 872 cm^2. A poor end electrode contact limited the performance of the first cell tested, which exhibited a dc-to-dc energy efficiency of 64% to 70% on cycle test. A second cell was fabricated after correcting the end plate problem. This cell exhibited up to 76% energy efficiency on cycle test, and was continuing at the end of 1985.

Scale-Up Studies

In this activity, the issues involved in electrode size scale-up were investigated. Cost studies conducted at ERC identified significant cost reductions that could be realized by increasing the electrode size above the 872-cm^2 level currently used.

A preliminary design was generated for a flow frame using a 3000-cm^2 electrode. Discussions with vendors were initiated to determine the feasibility of injection-molding the large flow frame in PVC.

Stack Compression Assembly Optimization

In this activity, the technique used to assemble compressed stacks was examined in an effort to optimize the design and to identify the cost/performance limits. The major drawback of the compressed stock design is the high cost of the end plate "strongback" assemblies. This high cost arises from the large quantities of materials (polypropylene and coated steel) needed to provide uniform stack compression.

Work began with a comprehensive review of the hardware currently used. Changes were made to correct minor problems in the hardware, and new drawings were issued.

A second-generation compression assembly was then designed in which structural rib members were used to provide rigidity in the strongback assembly. The additional rigidity allows the use of a thinner plastic end plate and eliminates the need for heavy leaf-spring assemblies to distribute compressive force over the stack area. Belleville washer spring discs were employed to ensure proper tie bolt tension. Fabrication of the first prototypes of the new strongback assemblies began in December 1985.

End Electrode Design

The end electrode—a 1/4-in.-thick titanium plate—is used to distribute current evenly over the active cell area from a central terminal. This design was originally used in stacks where the end plates were exposed to the electolyte. In this stack configuration, the end electrodes are normally dry but they can be exposed to electrolyte in the event of a leak in the cell hardware or end plate gaskets.

The objective of this activity is to develop a low-cost alternate to the titanium end electrode. Two approaches are being investigated: coating a copper current collector by molding carbon-plastic material around the copper insert, and using thick graphite end electrodes.

Samples of carbon-plastic electrodes with copper inserts were prepared by compression-molding the carbon-plastic material around the copper insert. A solvent-based primer was developed to improve adhesion between the Kynar®/graphite material and the copper insert.

Technical Challenges Remaining

Because of the timing of the start of the program, this report covers only the first three months of a three-year project, but the work done in this period establishes a firm foundation for the continued success of the program. Improvements in stack hardware and in the development of in-house carbon felt production techniques have resulted in single-cell energy efficiency of over 75%. If this level of performance is demonstrated in multicell stacks on extended cycle tests, it could lead to a revision in one of the program's goals, which called for 74% dc-to-dc efficiency (65% efficiency was typically observed at the time the program plan was established). The Basic Research and Development studies are expanding our understanding of the principles involved in such critical areas as zinc deposition at high loading levels, and alternate bromine electrode and bromine storage approaches.

Work planned for 1986 includes continued development of electrode scale-up, hardware design, and stack construction techniques. The electrode size and

the stack construction approach will be chosen late in 1986, and procurement of tooling will begin. Other work planned for the year includes the design and development of a hydrogen/bromine recombiner that would automatically maintain electrolyte pH at the proper level. Battery testing will include testing 240-W (5-cell) stacks and 3-kW stacks at ERC and at SNL.

Hydrogen/Nickel Oxide Battery—COMSAT/JCI/SNL

Work continued at COMSAT/JCI during 1985 to develop a sealed, 100-Ah hydrogen/nickel oxide battery for deep-discharge, terrestrial applications. The main thrust of the cost-sharing contract was to reduce the cost of the aerospace design without unduly compromising the desirable features of the system, such as long cycle life and zero maintenance. The goal was to be cost-competitive with lead-acid batteries in a system designed for a 20-yr life.

A completely new hydrogen/nickel oxide battery design has evolved, cell and battery performance has been very good, and significant progress has been made in reducing the cost. The COMSAT baseline cell design consists of a multiplate rectangular configuration similar to a conventional lead-acid cell, with a number of cells in a common pressure vessel. In the assembly of the cells and batteries, JCI was able to use existing production equipment as well as commercially available plastic cell cases. A six-cell battery in a reuseable pressure vessel is shown schematically in Figure 1-9.

Specific tasks under the present contract (51-5767) follow.

- **Cost Study.** Refine the cost study conducted on the previous contract and identify areas where cost reduction would have the greatest impact.

- **Modeling.** Continue the battery modeling study, with particular emphasis on thermal management.
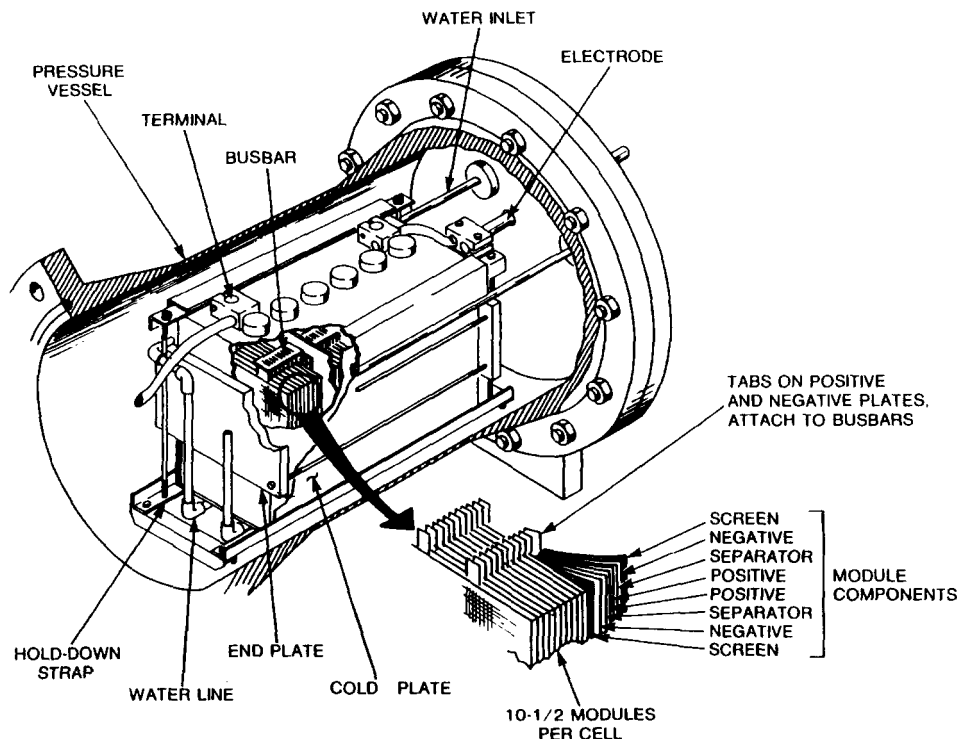
Figure 1-9. Six-Cell Battery

- **Module Design.** Prepare detailed design drawings for 4-kWh (28-V, 150-Ah) and 15-kWh (98-V, 150-Ah) modules incorporating the results from the cost and modeling studies above. One key element is the pressure vessel, with an option for the remote storage of hydrogen.

- **Cells and Batteries.** Fabricate and test single cells and six-cell batteries to evaluate new design concepts that would reduce component cost.

- **Deliverables.** Deliver six cells and one six-cell battery to Sandia during the 12-mo period following placement of the contract.

State of Development

A detailed study was performed to determine the cost of manufacturing a 15-kWh hydrogen/nickel oxide battery system at a JCI pilot line facility using the 100-Ah, six-cell battery as the building block. The objectives of this cost study were as follows:

- Provide a preliminary, well-thought-out benchmark against which later cost estimates could be measured.

- Identify areas that, because of their cost implications, warrant futher development in this or future programs.

- Determine whether the ambitious cost goal (6¢/kWh/cycle based on 6000 life cycles) for a battery designed for an autonomous photovoltaic system can be achieved.

Details of the study are presented in SAND85-7219. The pilot plant production level turned out to be 72 units per year. Costs are compared with other production levels in Figure 1-10. Also included is the cost of the aerospace design. Even at the low production rate characteristic of a pilot plant, the first cost-per-kilowatt-hour is more than an order of magnitude less than for the aerospace design. In a number of areas identified by the cost study, further development would lead to additional cost reductions, even at the pilot lot production rate. At a higher but reasonable production rate, the goal of 6¢/kWh/cycle is achievable.
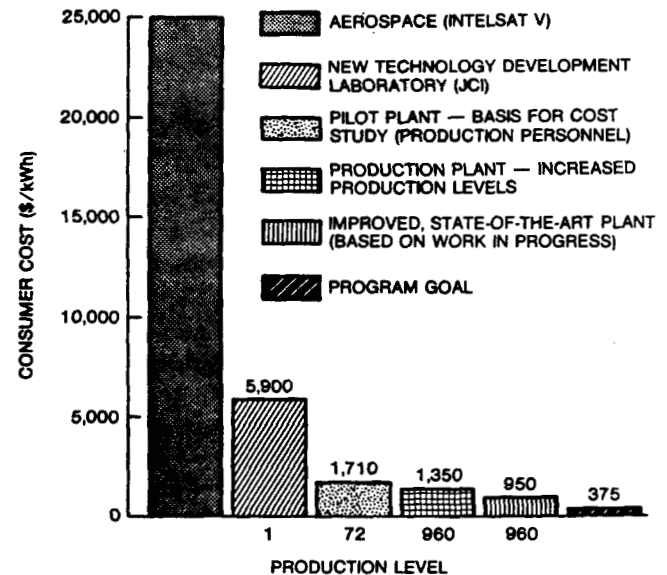
Figure 1-10. Summary of Cost Study Results

A transient heat transfer program was developed to model the thermal performance of the hydrogen/nickel oxide battery under various boundary conditions. The program can be used in either a two- or three-dimensional mode, and accepts input on cycle time, charge and discharge currents, and voltage profiles to determine heat generation rates. The pressure profile is also input since the rate of convective heat transfer is a function of the density of the hydrogen gas. Good correlation between experimental results and model predictions have been obtained. The thermal model is proving very useful in the design of the multikilowatt-hour battery.

One design for a 4-kWh battery system is shown in Figure 1-11. It incorporates a prototype pressure vessel and an active cooling system. The individual batteries are mounted directly onto a cold plate, and heat is conducted from the battery case to the cold plate through a thin copper sheet clamped by straps around the two long sides and the bottom of the case. This design allows the batteries to be assembled and instrumented outside the vessel. The assembly can then easily be inserted and removed from the vessel by sliding the plate along rails that join the cross-beams. This pressure vessel is 16-in. in diameter and made of stainless steel; it is designed for operation in either a vertical or a horizonal orientation.

PRESSURE VESSEL

VESSEL HANDLE

COLD PLATE

END SUPPORT PLATES

BATTERY
HOLD DOWN
STRAPS

COOLANT
INLET

BOLT COLDPLATE
TO VESSEL

37"

TWO ORIENTATIONS
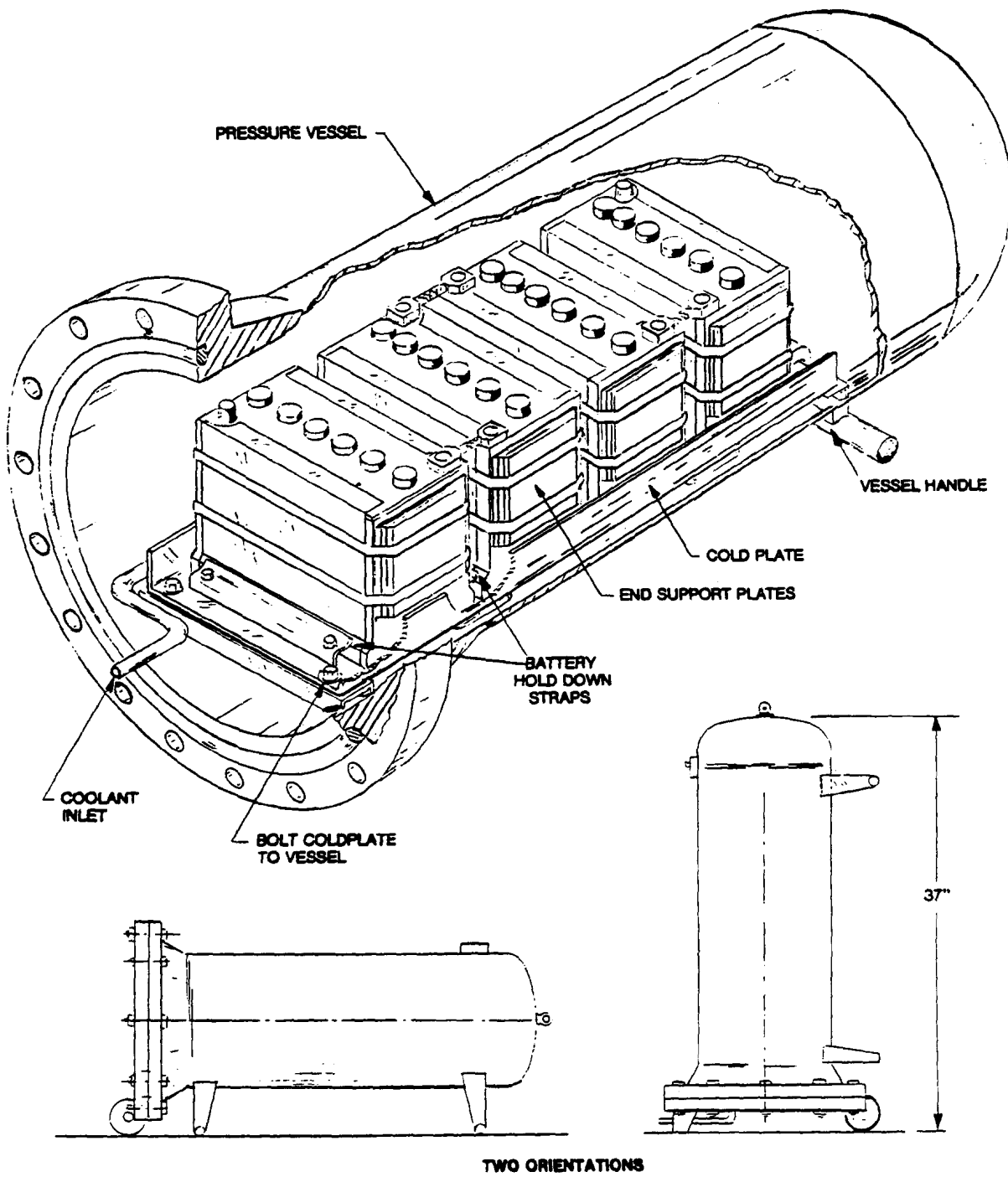
Figure 1-11. 48-V 150-Ah Battery System

Six cells and one 6-cell battery were fabricated and assembled during 1985. The design variations, summarized in Table 1-1, are discussed below.

Cells 15, 16, and 17, and Battery 03 all had the standard 32-mil-thick positive electrode, asbestos separator, and reservoir cell design. The negative electrodes had a rolled nickel screen rather than the standard nickel expanded metal in an effort to reduce cost. Cell 17 differed from the others in that it did not have the Gortex® backing on the negative electrode; this was the result of another attempt to reduce cost.

Cells 18, 19, and 20 had the thicker 68-mil positive electrode, asbestos separator, and peripheral seal design. Instead of the rolled nickel screen in the negative electrode, these cells had an electroformed nickel screen, also as a cost-effective measure.

The three cells differed in that Cells 18 and 20 had a lithium additive in the electrolyte and Cell 20 did not have the Gortex backing on the negative. Obtaining a thicker positive was an important achievement in 1985. It resulted from a program at JCI to improve the impregnation process of the thicker nickel plaques, which increased the capacity ~40% in the same volume, and resulted in significantly fewer cell parts. Actual test results are presented below.

Evaluation of the hydrogen/nickel oxide cells and batteries was conducted at SNL. The cells and batteries were received as contract deliverables from COMSAT Laboratories after having completed acceptance testing. Four cells and one 6-cell battery were on test at the beginning of 1985, six additional cells and one battery were put on test during the year, and four cells were removed from test. Thus, at year's end six cells and two batteries were on test.

Both cycling and characterization tests were conducted. The cycling regime consisted of a set of 50 cycles to 80% DOD and, later in the year, to 1 V/cell (100% DOD). Charging was terminated when the pressure-time slope dropped to 50% of the linear value. This was followed by two capacity tests to 1 V/cell with the charge to 25% of the linear slope.

Characterization tests included continued development of a method to terminate charging when the pressure-time slope reached a preselected fraction of the linear slope, investigating methods of charging to maximize coulombic efficiency, studying the effects of precharge pressure and coolant temperature on performance, and determining stand-loss characteristics.

Cell 12 and Battery 02 represent the baseline design at the beginning of 1985. Variations from this design are noted briefly in Table 1-2, and in greater detail in Table 1-1 for the cells and batteries fabricated during 1985. Also in Table 1-2 are the total cycles accumulated at the end of the year and the latest capacity, using the coolant temperature indicated. As noted, four cells were removed from test during the year. Capacity of Cell 03 declined after ~1000 cycles, and it was noted upon removal from the pressure vessel that the unrestrained cell case had bulged considerably; later cells were restrained with plastic or metal plates.

Table 1-1. Design Variations

| S/N | Positive Electrode | | Negative Electrode | | Cell Type |
	Thickness (mils)	Lithium Additive	Nickel Screen	Gortex	
Cell 15	32	No	Rolled	Yes	Reservoir
Cell 16	32	No	Rolled	Yes	Reservoir
Cell 17	32	No	Rolled	No	Reservoir
Battery 03	32	No	Rolled	Yes	Reservoir
Cell 18	68	Yes	Electroformed	Yes	Peripheral seal
Cell 19	68	No	Electroformed	Yes	Peripheral seal
Cell 20	68	Yes	Electroformed	No	Peripheral seal

Table 1-2. COMSAT Nickel/Hydrogen Test Summary, 1985

S/N	Variations	Rating (V)	Rating (Ah)	Coolant (°C)	Cycles	Capacity (Ah)
Batteries						
02		7.50	100	10	743	91.5
03	Screen substrate in negative	7.50	100	20	345	87.0
Cells						
03		1.25	90	RT	1106	69.6*
09		1.25	90	RT	754	75.1
10	Thick positive	1.25	120	10	352	113.2
12		1.25	90	20	666	102.6
15	Screen substrate in negative	1.25	90	RT	263	59.1*
16	Screen substrate in negative	1.25	90	RT	142	69.3*
17	Screen substrate in negative†	1.25	90	RT	180	66.3*
18	Thick positive with lithium additive	1.25	125	10	98	137.1
19	Thick positive	1.25	125	10	27	125.8
20	Thick positive with lithium additive†	1.25	125	10	27	133.8

*Removed from test.
†No Gortex backing on negative.

Cells 15, 16, and 17 all exhibited capacity decline early in life. As noted above, these cells had the pressed nickel screen in the negative. During posttest analysis, it was found that a number of nickel tabs were broken from the screen. This collector has been replaced with the electroformed screen. Also, these cells had negatives containing what was suspected to be a bad lot of catalyst; this has also been corrected.

Concerning the units still on test, the capacity of Battery 03 has declined, but not as rapidly as Cells 15, 16, and 17, which were of similar construction. Cell 12 and Battery 02 are doing very well after ~700 deep cycles, as indicated in Table 1-2.

The performance of the latest cells using the thicker positives is particularly encouraging. Capacities range from 125 to 137 Ah in the same size cell that previously yielded a nominal 100 Ah. The lithium additive to the electrolyte appears to be beneficial, with Cells 18 and 20 outperforming Cell 19. Cell 18 with the Gortex backing on the negative is doing slightly better than Cell 20, but additional testing will be required to determine the trade-offs between performance and cost with the elimination of the Gortex backing. In the meantime, Cell 18 is the new baseline design.

Technical Challenges Remaining

Technical challenges remaining include finalizing the design, and building and evaluating a 24-V, 7-kWh battery suitable for solar applications. Evaluations are currently underway at SNL on lead-acid and nickel/cadmium batteries of this size using an existing photovoltaic array, and the larger hydrogen/nickel oxide battery could be included in the study. A string of 20 cells will be required to obtain 24 V, and two strings will be necessary to obtain the desired capacity. The ramifications of this series/parrallel configuration need to be evaluated. To date, cells and batteries have all been assembled in boiler-plate, reusable pressure vessels. A study is required to develop a low-cost pressure vessel for the 7-kWh battery that is suitable for commercial applications. Thermal management of the larger battery is a consideration and will need to be addressed with the aid of the thermal model.

At the cell level, research and development efforts must continue in order to optimize the performance and economics of the system. Areas to be investigated are those seen in prior cost studies and cell and battery testing to have significant impact on life-cycle cost. They include the type and quantity of catalyst in the negative electrode, the need for the Gortex backing,

and the development of a lower-cost substrate for the positive electrode and its optimum thickness. Other areas that could profit from more study include development of a synthetic separator, enhanced electrolyte management, and improved thermal management within the cell.

Zinc/Ferricyanide Battery— Lockheed

Development of the zinc/ferricyanide battery was initiated in 1978 by scientists at Lockheed Missiles and Space Company (LMSC). The battery's technology is based upon solid storage of both charged and discharged active materials. On charge, zinc is electrodeposited on the negative electrode; on discharge, it is stored as zinc oxide. The active positive electrode materials (sodium/ferro- and ferricyanide) are stored as precipitates. This solid storage results in a more compact but obviously more complex process. The battery, having 1.74-V OCV and 1.59-V discharge at 35 mA/cm^2, is intended for bulk electrical energy storage applications. Its advantages include high cyclic efficiency, high cell voltage, near-ambient temperature operation, low toxicity with biodegradable reactants, potentially long cycle life, and low projected costs.

As stated in the introduction, a gap in the ETD-sponsored development of the zinc/ferricyanide technology existed between December 1984 and November 1985. During this period, LMSC sponsored an evaluation of the technology that included marketing and techno-economic studies aimed at commercializing a zinc/ferricyanide battery. The initial results of this LMSC-sponsored activity are presented in this section. The limited results available from the new ETD contract will be discussed in the 1986 Annual Report.

State of Development

The technical and economic feasibility of the zinc/ferricyanide system in a variety of possible stationary applications has been a concern of the DOE-funded programs at Lockheed for some time. Interim results from these early programs were published in the report, *Zinc/Ferricyanide Battery Development: Phase IV* (SAND85-7195, May 1985). Early in 1985, LMSC began funding its own analyses of preliminary engineering and commercial feasibility of the zinc/ferricyanide system. The preliminary engineering analyses are being performed by Lockheed personnel in collaboration with Electrochemical Engineering Consultants, Inc., (EECI) under contract to LMSC.

The LMSC/EECI techno-economic studies of the zinc/ferricyanide battery were divided into three phases, the first two of which were performed during 1985. In the first phase, cost projections were made of a preliminary zinc/ferricyanide battery design to be used in residential solar and customer-side-of-the-meter (CSOM) applications. Of the many possible stationary applications that could have been considered, the solar and CSOM applications were chosen for analysis because it was felt that these might provide the earliest opportunities to commercialize the zinc/ferricyanide system, and because they would permit sensitivity analyses to be performed to delineate the economic feasibility of the system for a variety of applications. In the second phase of the study, detailed designs of batteries for these two applications were developed, and preliminary (outline) designs for load-leveling and village solar applications were made. In the third phase of the study, the residential solar and CSOM designs will be analyzed. Modifications will be made to the designs to maximize performance and reliability and to minimize initial costs. More detailed cost projections of batteries for these two applications will be prepared, and technical and cost analyses on the outline designs for the load-leveling and village solar applications will be performed. During the upcoming third phase of the preliminary engineering work, the design for a prototype zinc/ferricyanide battery will be detailed. It is anticipated that the prototype will help determine the feasibility of using a zinc/ferricyanide battery in a number of potential applications.

At the outset of the first phase of the work, the requirements for, and the arrangement of, the various components and subsystems of a zinc/ferricyanide battery were critically examined to effect simplification and to reduce anticipated costs relative to earlier designs. The outline designs for residential solar and CSOM batteries, and hence the first-cut projected costs, were based on the first iteration of a simplified design. The flow schematic was re-examined as part of the detailed design work performed during the second phase, and further simplification steps were identified. The flow schematic ultimately used as the basis for the detailed design work is shown in Figure 1-12. We anticipate that large zinc/ferricyanide batteries (e.g., those intended for the CSOM applications) will be built-in modules capable of independent operation. The modules will be interconnected only electrically, with no chemical flows (except for the infrequent "watering" required) between the modules. Each module will consist of one (residential solar) to four (CSOM) or more cell stacks connected hydraulically and electrically in parallel; pumps and pump motors, heat exchangers, storage chambers, and other battery components and subsystems will be custom-built for each size module.
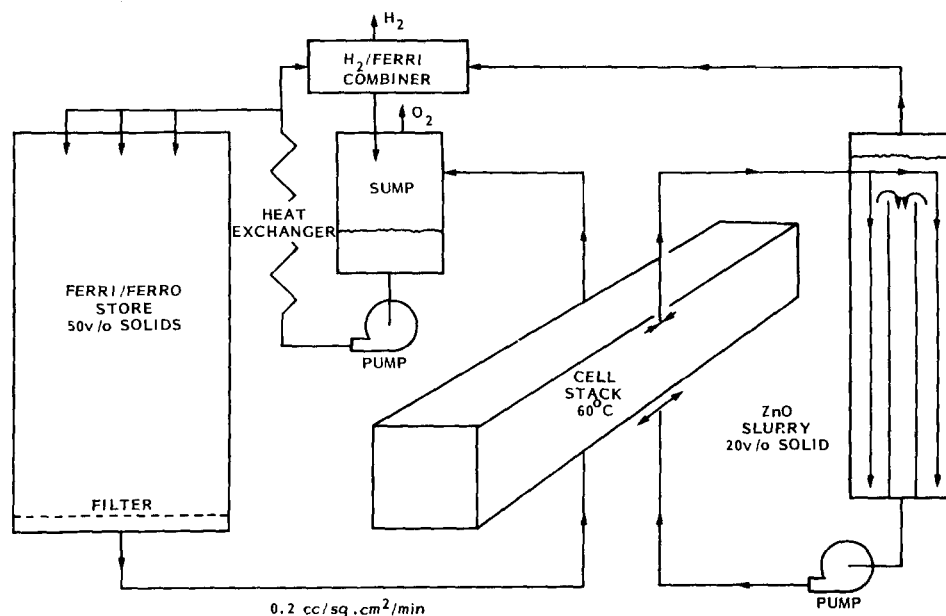
Figure 1-12. Flow Schematic of Zinc/Ferricyanide Battery

We expect that a bipolar design will be used for the cell stacks, the bipolar partitions consisting of plastic/graphite composite sheets coated with nickel on the positive side and with cadmium on the negative side. Zinc will be electrodeposited on the negative side during charge from a flowing sodium zincate solution (generated in the negalyte store from solid zinc oxide produced during the preceding discharge) to form the negative electrodes. We also anticipate the positive electrode substrate to consist of electroless nickel-plated graphite felt through which the redox solution (a mixture of sodium ferro- and ferricyanides) is flowed. The concentrations of the ferro- and ferricyanides flowing to the cells will be maintained constant (at constant temperature) because both sodium ferro- and ferricyanide (in their respective hydrated forms) will be contained as crystalline solids in the redox store. Ion exchange membranes will be used to separate the posilyte and negalyte compartments of zinc/ferricyanide cells.

In normal operations (including periods of stand that do not exceed design limits), we plan to operate a zinc/ferricyanide battery of the type shown in Figure 1-12 at constant temperature. Two pumps will be required in each zinc/ferricyanide battery module, one for the posilyte (redox) flow and the other for the negalyte (sodium zincate) flow. We anticipate that the same flow rates will be used for the posilyte and negalyte, and that the flow rates and directions will be the same in charge and discharge. We plan to use one pump motor to drive both pumps of each module. The

requirements for effective and straightforward filtration in the redox store, and those for a well-managed flow, lead us to believe that a sump (Figure 1-12) will be needed for the posilyte flow. The flow schematic shows one heat exchanger (in the posilyte flow loop) to remove heat resulting from coulombic and voltaic inefficiencies in the battery cells. A subsystem to combine hydrogen (generated in a side reaction between zinc and the caustic soda electrolyte on the negative side) with ferricyanide is included as an integral part of the flow scheme to ensure that the half-cell capacities remain in balance during extended cycling. Figure 1-12 clarifies the arrangement of the various components and subsystems, and of the various material flows required.

During the first phase of the LMSC-funded preliminary engineering study, a somewhat more complicated version of the flow schematic was used as a basis for making "first-cut" designs for a number of residential solar and CSOM batteries. For these first-cut designs, generalized concepts for cell stacks and other battery components were used so that a preliminary evaluation of the projected capital cost could be made. A number of outline designs were generated for the two applications, with battery capacity, discharge rate, zinc electrode capacity, electrode dimensions, and module size as the primary variables. Cost projections were made using the latest version of the EPRI Utility Battery Costing Guidelines, combined with our best estimates for the acquisition cost for purchased components. Wherever possible, the published

cost and design analyses performed on other flow batteries were used to provide input data for our cost projections.

The cost projections made for zinc/ferricyanide residential solar batteries are shown in Figure 1-13 along with those made for lead-acid batteries designed for the same service. We can see that these first-cut projected capital costs could be competitive in residential solar applications if the battery capacity required by the customer were greater than ~50 kWh. The economic advantage that might be offered by zinc/ferricyanide batteries in this application would be greater if the zinc electrode capacity could be increased from the currently attainable 240 mAh/cm^2 to a value closer to 500 mAh/cm^2. We should bear in mind, however, that a special "chopper-charger" may be needed to effect smooth zinc plating, even to the currently attainable zinc capacity densities, given the economically imposed power limitations of solar photovoltaic arrays. It appears unlikely that relatively small zinc/ferricyanide batteries of 40-kWh discharge capacity and less (as well as other flow battery technologies) will be economically competitive in the residential solar or similar applications.
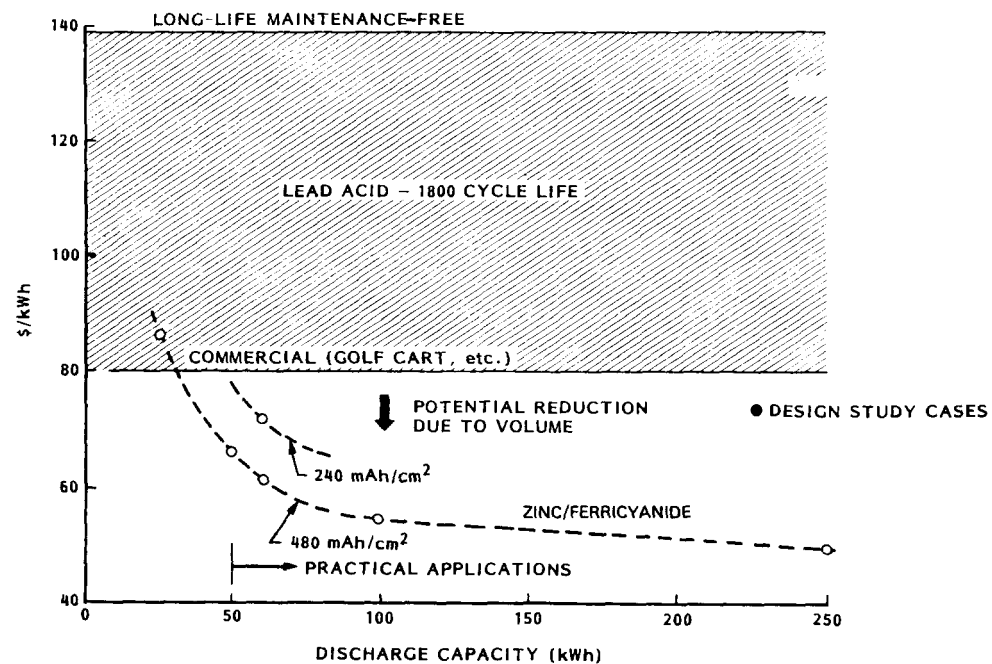
Figure 1-13. Battery Cost Comparison: Remote Power

Figure 1-14 shows the results of the first-cut capital cost projections made for CSOM zinc/ferricyanide batteries plotted against discharge duration, together with comparable costs for lead-acid batteries. The three points shown refer to batteries with capacities of ~1 MWh (1-h discharge duration at 1-MW power), 2 MWh (2 h, 1 MW), and 2.25 MWh (3 h, 750 kW), but all three batteries would use the same number and size of cell stacks. It appears that zinc/ferricyanide batteries may offer considerable economic advantages over lead-acid batteries in this CSOM application; this is particularly true for the shorter discharge duration. The outline designs prepared to make these first-cut cost projections indicated that the physical size of zinc/ferricyanide CSOM batteries would be comparable to the lead-acid batteries.
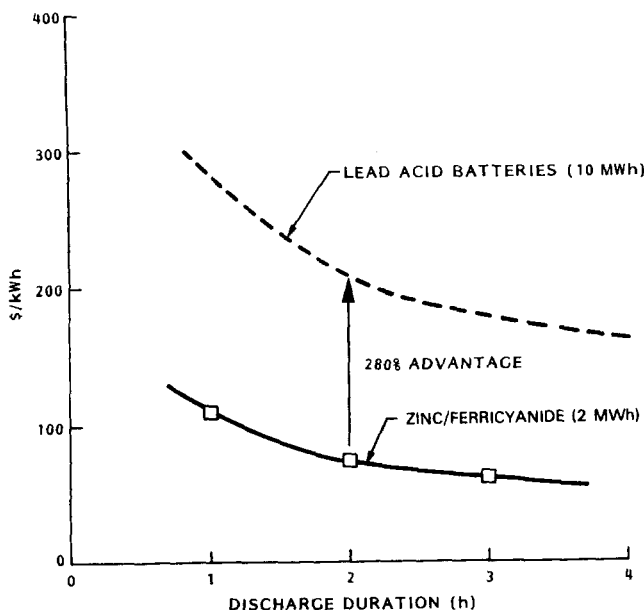
Figure 1-14. Battery Cost Comparison: CSOM

The parts and components we believe to be the most important from a capital cost standpoint, together with the figures used to compute the projected battery costs, include the following:

- Ion exchange membranes ($2/ft^2)
- Nickelized graphite felt for positives ($1.10/ft^2)
- Metal-coated bipolar partitions ($0.70/ft^2)
- Ferro/ferricyanide storage (cost depends on battery capacity)
- Hydrated sodium ferrocyanide ($0.20/lb)
- Pumps, motors, and controls (cost depends on battery capacity)

Even if pessimistic values are used for these critical components (e.g., $5/ft^2 for ion exchange membranes), the total projected capital costs will probably not be more than 25% greater than those cited above. We believe that the costs we have projected for labor and factory equipment in the battery assembly facility are reasonable, compared with those derived by other advanced battery developers. It should be noted, however, that an analytical simulation of the assembly process has not yet been undertaken.

In the second phase of the LMSC/EECI preliminary engineering study completed at the end of 1985, a microcomputer design-aid program was developed to facilitate the analyses. This program was used to prepare outline designs for batteries used in load-leveling, CSOM, village solar, and residential solar applications. These outline designs were made in such a way that the same electrode dimensions (~2 ft^2 active area), and thus the same basic cell-stack design, could be used in the batteries for all four applications.

Detailed drawings were prepared for the cell stack and its components, and for complete residential solar and CSOM batteries. Apart from the number of cell stacks and modules required, the main difference between the cell stacks for the two applications lies in the number of cells in series in the stacks: 64 cells for residential solar and 80 for CSOM. The 50-kWh residential solar battery, with a one-cell stack, is projected to be 4 ft long × 3 ft wide × 5 ft high. The 2-MWh (1-MW) CSOM battery with 16 modules (including four redundant spares), each with four cell stacks, is contemplated to be 32 ft long × 20 ft wide × 10 ft high. Both batteries were designed in a way that allows for ease of maintenance, and with high reliability in mind.

The residential solar and CSOM battery designs include details of the plumbing that interconnects the stacks, stores, pumps, etc. This plumbing is sized on the basis of material flow and balance calculations included in the design-aid program. The program also allows calculations/estimations of the shunt current and pumping power losses that will be experienced because of the electrolyte flows in the cell stacks. The sum of these two losses in a charge/discharge cycle is projected to result in a requirement for an increase of ~7% (residential solar) or 2% (CSOM) in the charging energy, these values being somewhat lower round-trip losses than have been estimated for other flow batteries.

The detailed design analyses performed during the second phase of the preliminary engineering study revealed nothing to indicate that the cost projections made in the first phase were markedly in error. In

addition, the emphasis on the residential solar and CSOM applications appears to remain well-justified. As indicated above, the batteries designed for these two applications will be analyzed in greater detail in the third phase of the preliminary engineering study, to be completed in 1986. A detailed design for a prototype zinc/ferricyanide battery will also be prepared in this third phase. Preliminary engineering studies performed to date revealed that some redirection of the experimental effort at LMSC was desirable, and these changes were made. More attention is now being directed to the zinc electrode, particularly with regard to decreasing hydrogen evolution and to increasing the charge capacity density. As indicated above, the latter could be particularly advantageous for residential solar batteries. Experiments to verify that zinc/ferricyanide cells can be discharged at the high rates necessary for the CSOM application, and evaluations of materials for the bipolar partition have been initiated. Alternative positive electrode materials, which might be less expensive than the nickel-graphite felt presently used, are being considered. The technology of solids management in zinc/ferricyanide batteries will be investigated later in 1986.

In parallel with these LMSC-funded efforts, an ETD-funded program at LMSC on ion-exchange membranes for zinc/ferricyanide batteries was reinitiated late in 1985, and continues with further tailoring of low-cost sulfonated polystyrene membranes (provided by RAI Research Corporation) and sulfonated polysulfone membranes (provided by C. Arnold of SNLA). Cyclic data obtained during a previous contract indicated that a problem had developed with the cadmium-plated substrate used for the zinc electrode: the coulombic efficiency was reduced from $\sim$95% to $\sim$85%. A study of cadmium-plated substrates is now underway. An approximate 97% level of coulombic efficiency on the zinc electrode is the goal. A 60-cm^2 cell currently under test with a Nafion N-117 membrane (Figure 1-15) exhibits a mean energy efficiency of 76.7% $\pm$ 4.9%, but is currently operating at a steady 85% energy efficiency. The cell was initially operating out-of-balance for the first 130 cycles with the zinc half-cell operating at $\sim$85% and the redox half-cell at $\sim$97%. The cell was then brought into balance using hydrogen reduction of ferricyanide on a platinum-catalyzed surface. After that, both half-cells operated at $\sim$95%. The hydrogen reduction of ferricyanide is envisioned as a practical means of maintaining cell balance in large zinc/ferricyanide batteries, since hydrogen is produced by both zinc half-cell parasitic reactions, namely, self-corrosion and sluff-off of nonadherent zinc. During previous studies, the best results had been $\sim$75% energy efficiency for the same cell configuration.
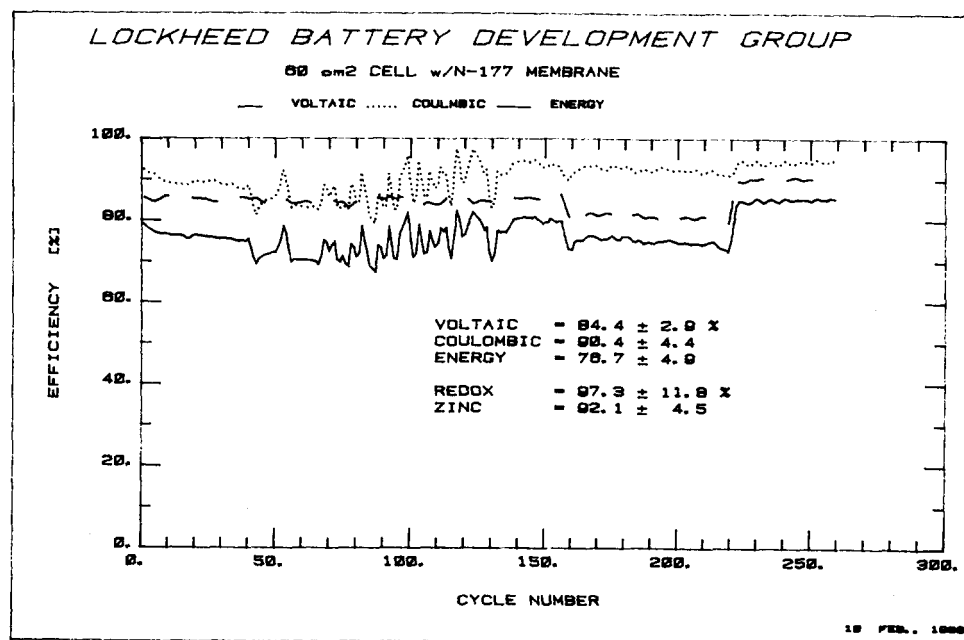
Figure 1-15. A 60-cm^2 Cell With Nafion Membrane

Chapter 2. Nonaqueous Battery Development

Introduction

The objective of this ETD activity is to support the development of nonaqueous secondary battery technologies that have the potential to satisfy the requirements of mobile and stationary energy storage applications. In 1985 this effort focused exclusively on the sodium/sulfur system. Programs were supported through development contracts with industrial participants and other national laboratories. In most cases these contracts were cost-shared by the industrial participants.

The following programs were supported in 1985: Sodium/Sulfur Battery Development at Chloride Silent Power, Ltd. (CSPL); Sodium/Sulfur Cell and Module Evaluation at Ford Aerospace and Communications Corporation (FACC); Cell Posttest Analysis at Argonne National Laboratory (ANL); and Beta″-Alumina Electrolyte Improvements at Ceramatec, Inc.

The placement of the Sodium/Sulfur Battery Development contract with CSPL met an ETD Director-Controlled Milestone. This three-year, $8.5M program was initiated in September. CSPL's cost-share was approximately 35%. Sodium/sulfur core technology development and stationary battery engineering are the contract's major tasks. The objective of the second task is the development of a 50-kWh module that would be representative of a basic building block for a 500-kWh utility battery. This battery will be designed and qualified by EPRI under a coordinated program.

The Sodium/Sulfur Cell and Module Evaluation program with FACC was a continuation of the testing activities initiated under the tripartite contract between the Department of Energy, FACC, and Ford Motor Company. The technical effort on this contract concluded early in 1985. A significant accomplishment in this program was the successful completion of over 1000 C/3 cycles on 19 prototype EV cells.

ANL conducted a posttest analysis on six FACC sodium/sulfur cells. These included EV cells, stationary energy storage cells, and one modified EV cell tested for satellite baseload applications at Wright Aeronautical Laboratories. The ANL analysis focused on polysulfide phase identification, electrode morphology, and cell case and seal stability.

Programs were initiated in 1985 with Ceramatec to improve the properties and processing of beta″-alumina electrolytes. The incorporation of yttria-stabilized zirconia into the beta″-alumina structure was an important part of this effort. This was done to improve the fracture toughness of the electrolyte, and represented a transfer of technology from a TBR-sponsored research project (with Rockwell International) to an ETD development program. Optimization of the seeded slurry solution spray-drying process and development of the semiautomated proof-testing apparatus were also included in this effort.

Calendar year 1985 was a transition year for the ETD-sponsored sodium/sulfur battery development programs. Major activities began at CSPL and Ceramatec as the FACC effort came to a close. Promising results from these programs, along with the encouraging progress of other worldwide developers, continue to make sodium/sulfur battery technology a leading candidate for meeting advanced energy storage needs.

Sodium/Sulfur Battery Development—CSPL

The Department of Energy and the Electric Power Research Institute sponsored joint programs to continue advances in sodium/sulfur battery technology and to study, design, build, and test a 500-kWh battery for the BEST facility. Chloride Silent Power, Ltd., of Runcorn, England, started the DOE-funded core technology and battery engineering section of the joint program in September 1985.

The objective of the core technology program is to advance the state-of-the-art of existing sodium/sulfur component, cell, and battery technologies. The program is divided into two distinct tasks:

- Task 1—Core Technology Research and Development

- Task 2—Battery Engineering and Testing.

Task 1 is devoted to research and development in areas that are generic to both stationary and EV applications of sodium/sulfur batteries. Performance, reliability, safety, and cost are emphasized. The following subtasks are included:

- Subtask 1.1—Electrolyte Research and Development
- Subtask 1.2—Materials Development and Qualification
- Subtask 1.3—Cell Development
- Subtask 1.4—Cell Testing and Posttest Analysis
- Subtask 1.5—Module Development and Testing.

Task 2 is directed toward stationary applications. The program is structured to support the companion EPRI 500-kWh battery program and will culminate in the design, manufacture, and test of a segment of the proposed 500-kWh battery incorporating the cells and modules developed in Subtasks 1.3 and 1.5.

CSPL's established sodium/sulfur cell designs were central sulfur cells, that is, cells with the sulfur electrode contained within the beta-alumina electrolyte. The most mature cell of the program was known as the NaS7 cell (150 Ah), which included an electrolyte tube 580 mm long × 30 mm ID. A 30-Ah Technology Demonstration (TD) cell—a smaller version of the NaS7 cell included an electrolyte that is 120 mm long × 30 mm ID—was used to investigate new developments in cell technology and to determine the interactions of cell size with performance and reliability.

The invention of small electrode seals, particularly appropriate to cells of the central sodium configuration, led CSPL to incorporate a small central sodium cell into its EV cell and battery development program. These small electrode seals used the sealing technology developed for the NaS7 cell. The seals were produced within the diameter of the cell electrolyte and occupied a small volume. This major reduction in seal volume offered an opportunity to design small cells that satisfied energy density and power density targets for sodium/sulfur batteries. The simple cell design encompassing the new seal concept is illustrated in Figure 2-1. The 20-Wh cell, code-named the PB cell, included an electrolyte 30 mm long × 30 mm ID. With respect to earlier cell designs, the PB cell offered the following potential benefits at the cell level:

- Simplified cell design
- Lower-cost cell manufacture
- Higher energy and power densities
- Higher reliability (smaller electrolytes include fewer defects and are less subject to critical stresses during manufacture and use).
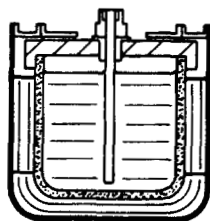
EV APPLICATIONS

PB CELL 20Wh
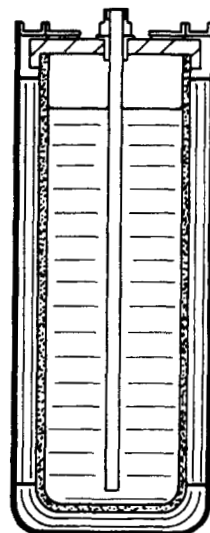
UTILITY APPLICATIONS

EXTENDED PB CELL 55Wh

Figure 2-1. PB and Extended PB Cell Designs

During the PB cell development program, it was realized that the new cell design could provide the basis for a family of cells, individually tailored to each advanced battery application. An analysis specifically considering stationary (load-leveling) applications indicated that the optimum cell for this application would include an electrolyte 100 mm long × 30 mm ID. This cell, known as the Extended PB cell, is also illustrated in Figure 2-1.

State of Development

As noted above, the current, DOE-funded contract is split into several tasks. Progress in each of these is described below.

The objective of Task 1 was to carry out the basic research, cell development, cell testing, materials studies, quality control, and computer modeling required to support a battery engineering program directed to fabricating and testing a subscale version of a battery designed for stationary applications. The issues of performance, reliability, safety, and cost were specifically addressed.

The objective of Subtask 1.1 was to provide the necessary research and development to ensure that the properties and processing of the beta-alumina electrolyte were acceptable for eventual cost-effective

commercialization. Before beginning the DOE-funded work, CSPL's electrolyte development program included two significant phases:

- Electrolyte research/development and process development based upon isostatic pressing

- Electrolyte research/development and process development based upon electrophoretic deposition (EPD).

The transfer from the isostatic approach (which is still available at CSPL, although inactive) to the EPD approach was based upon a thorough investigation of the potential of each for the cost-effective manufacture of high-quality electrolyte. The EPD approach coincidentally provided the flexibility to successfully manufacture small electrolyte tubes of uniform wall thickness that were vital to the realization of the small-cell concept. First-generation EPD electrolyte possessed excellent physical and electrical properties:

- Low resistivity: 3.3 ± 0.3 Ω-cm at 350°C

- High sintered density with a volume porosity of 1% or less

- Uniform, fine porosity with a pore size of 2 to 3 μm

- Uniform, fine-grained microstructure with matrix grain size of 2 to 3 μm and restricted secondary-grain growth

- Phase content of 93% beta''-alumina, uniform throughout the electrolyte.

Low-cost starting materials, coupled with proprietary methods of suppressing impurity-induced resistance rise, resulted in resistance rises of <0.0004 mΩ/cycle (2 × 10^{-4} Ω-cm^2/cycle) in NaS7 cells tested for over 3000 cycles. Mean-times-to-failure of 3000+ cycles was observed in cells including EPD electrolyte, and early failures were almost eliminated in the mature cell designs.

The fundamental electrolyte research and development program focused on toughening the electrolyte by incorporating zirconia in the composition. The EPD process was ideal for the zirconia addition, and 60% to 80% tetragonal retention, improved densification, and reduced grain growth were obtained. Optimum additions of zirconia increased electrolyte strength by up to 80% (to 260–320 MPa) and fracture toughness by 50%. Eight TD cells (with electrolytes that contained zirconia) completed 500 cycles without any failures, exhibiting stable resistance (equivalent to 0.96 Ω-cm^2).

A preferred zirconia-toughened composition was identified and, as illustrated in Figure 2-2, excellent grain size control was observed. High concentrations of zirconia improved the electrolyte properties but also increased sensitivity to moisture.

Process improvement and quality control development were important features of the electrolyte development program. Before the DOE-funded work began, drying procedures for green shapes had already been improved, and surface porosity had been eliminated. Also, degassing the EPD suspension had reduced the incidence of blow holes and increased green shape density. Alcohol reclaimed from EPD suspensions was demonstrated to be technically suitable for reuse.

CSPL's electrolyte quality plan was based upon extensive analysis of incoming materials and 100% inspection at each process stage, followed by a final quality audit on electrolyte tubes before issue. Quality standards for electrolyte tubes included dimensions, density, strength, and incidence of surface defects (as observed by a fluorescent dye test). Grading of tubes was introduced at each stage so that the quality standards necessary for full-scale production of electrolyte tubes could be reviewed, based upon the results of cell-testing and posttest analysis programs. Yield of the highest standard electrolyte tubes, from green shape manufacture to cell build, was typically 45%.

A number of significant improvements have been realized during the DOE-funded program. A four-chamber EPD rig was designed, fabricated, and commissioned; this was an important step toward manufacturing scale-up. A new particle-size analyzer for improved on-line process control was obtained. The first production run with the optimum addition of zirconia to the electrolyte yielded 30 electrolyte tubes (65%), suggesting that yield improvements may be associated with the new compositions. A second source of low-cost alumina appropriate to EPD was identified. This was an important commercial objective. Manufacturing trials with this alumina produced fine-grained electrolyte of improved strength (240 N/mm^2 for standard material, 340 N/mm^2 for zirconia-toughened material). The eight TD cells with zirconia-toughened electrolyte completed 800 cycles with no failures.

Major electrolyte research and development objectives for 1986 are

- Continued assessment of new sources of alpha-alumina

- Improved understanding of the role of zirconia in electrolyte compositions and of the sensitivity of the compositions to moisture

- Introduction of zirconia-toughened material as the standard for cell manufacture

- Increased yield

- Redefinition of electrolyte quality control techniques and quality standards

- Support of the manufacturing engineering program to increase electrolyte output.

Materials development and qualification activities in 1985 were intended to qualify candidate materials for cell and system design, demonstrating that the materials would fulfill the performance and durability targets set for the sodium/sulfur battery. Emphasis was placed on accelerated life tests to increase the understanding of degradation mechanisms and to enable predictions to be made about the real durability of materials used. Posttest analysis of cells contributed significantly to this program. Processing procedures and quality controls for materials, components, and subassemblies were addressed, as were material costs.
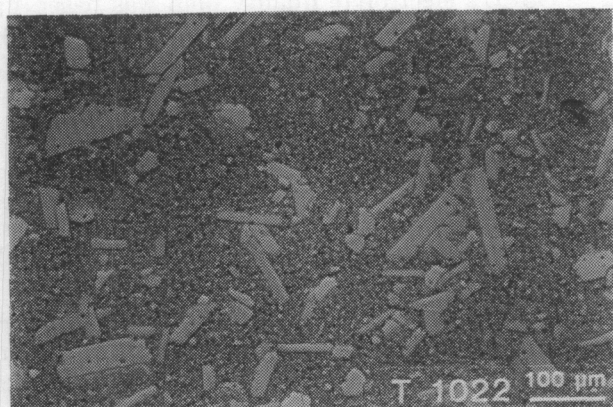
(a) Microstructure Without Zirconia
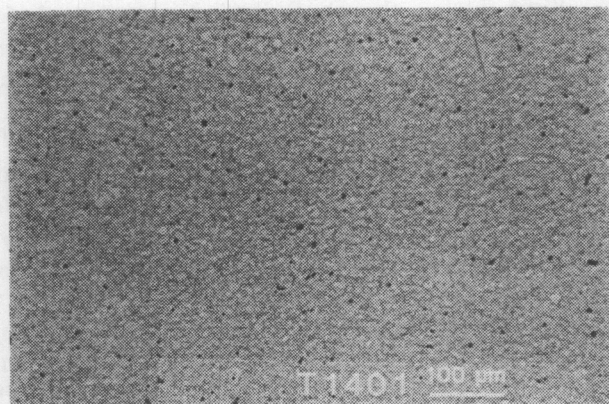
(b) Microstructure With Zirconia
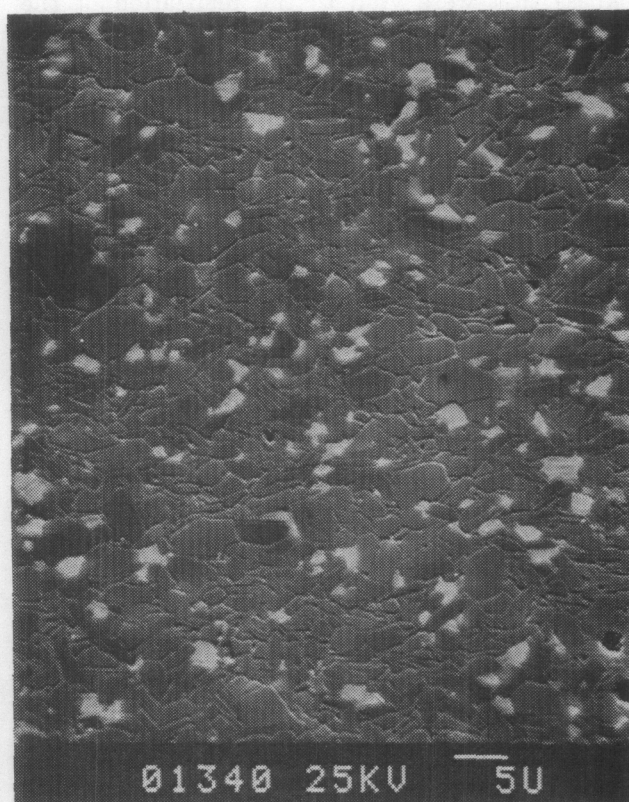
(c) Scanning Electron Micrograph of Zirconia Beta″-Alumina

Figure 2-2. Microsections of Beta″-Alumina

CSPL had built up a significant database on its own on cell materials through long-term cell testing of mature cell designs. Continued testing and posttest analysis of such cells within DOE- and EPRI-funded programs expanded that database. Table 2-1 shows the progress of the materials qualification program (using PB cell materials) at the time the DOE-funded program began.

Table 2-1. Qualification of PB Cell Materials in Mature Cell Designs

| | Experience | |
Item	Cycles	Hours
Electrolyte composition	2561	21,048
Glass composition	2561	21,048
Thermocompression seals	3236	26,688
Sodium electrode	2561	21,048
Sulfur electrode	2945	24,360
Containment	—	24,500

The state of development of CSPL's beta″-alumina/glass/alpha-alumina seals at the beginning of the DOE-funded work is characterized below:

- Sodium resistance of preferred glass composition is predicted to be adequate for a 5-yr life cell.

- Established procedures are available for manufacturing and processing the glass composition into the form required for seal manufacture.

- Proprietary approaches are available for manufacturing alpha-alumina/beta″-alumina seals of increased strength and improved thermal stability.

During the DOE-funded program, a glass composition was manufactured that melted at a lower temperature than the standard glass. A lower melting point was desired to permit more flexibility in manufacturing the cell. High-temperature sodium exposure testing and photoelastic stress measurements on seals began.

The state of development of CSPL's metal/alpha-alumina seals at the beginning of the DOE-funded work is summarized below:

- Materials technology and thermocompression bonding procedures were validated by long-term testing of mature cell designs (3236 cycles in 26,688 h).

- Cells with PB electrode seals containing an aluminium interlayer between a weldable metal and alpha-alumina completed 652 cycles of test (5200 h).

- Cells with proprietary PB electrode seals completed 500 cycles (4000 h).

- A prototype production machine was designed, manufactured, and commissioned. The machine, illustrated in Figure 2-3, manufactured batches of consistently high-quality seals.

- PB electrode seals were found to be unaffected by rapid thermal cycling.

Late in 1985, electrode seals with a deformable aluminium interlayer were developed further. Existing laboratory equipment to manufacture the seals was recommissioned, and thermocompression bonds to chromise mild steel were manufactured. One of the subassemblies originally manufactured as a preliminary to thermocompression bonding (an aluminium ring friction-welded to a metal cap) was eliminated from the manufacturing sequence. The effect of cell reliability on electrode-sealing procedures was investigated.
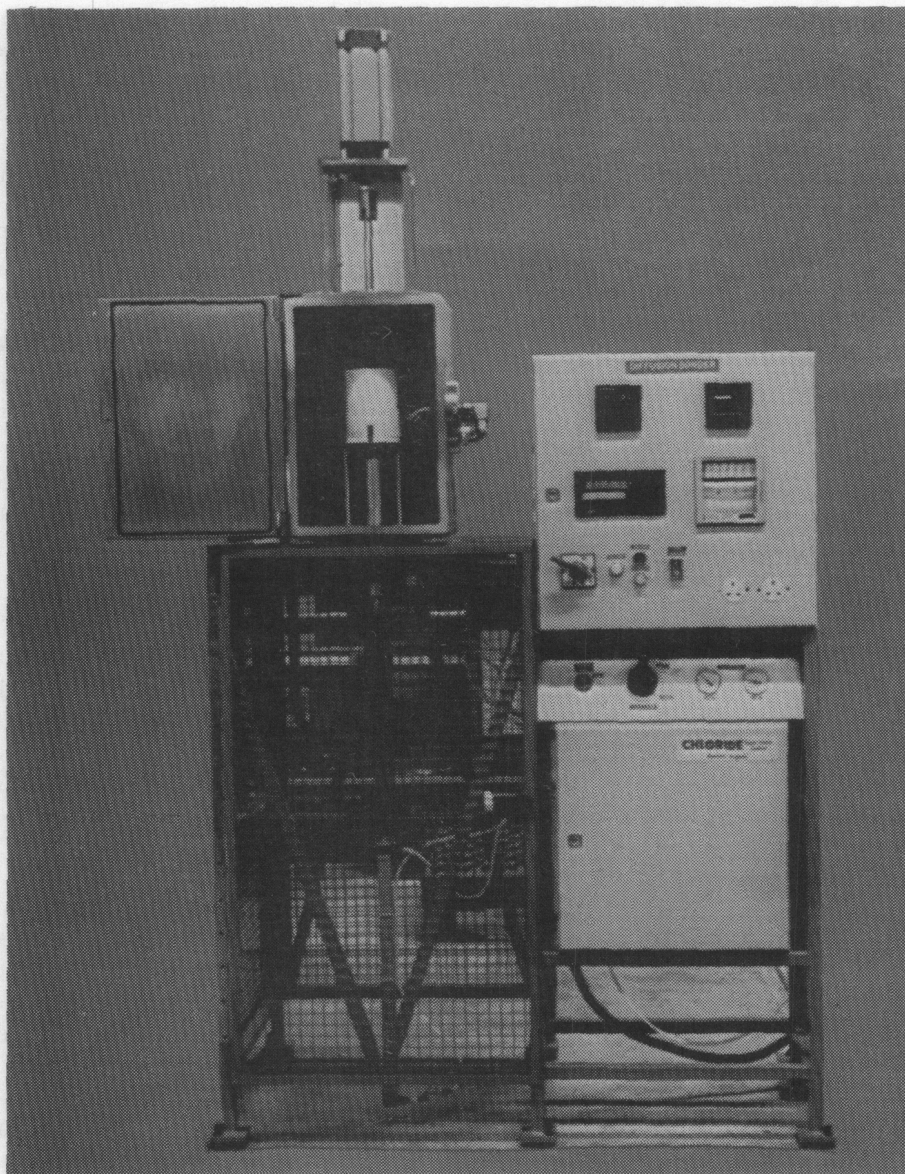
Figure 2-3. Prototype Production Machine for Ceramic-to-Metal Sealing

CSPL's sodium electrode had been developed to the following level when work began on the DOE-funded program.

- Processing equipment was available to reduce the impurities in commercial sodium to levels acceptable for cell manufacture.

- Sodium electrode infill materials were available that gettered electrode impurities and promoted resistance stability.

- Electrolyte surface treatment was available that avoided impurity-associated resistance rise at the sodium/electrolyte interface.

- Proprietary sodium wicks were available that ensured that the electrolyte in PB cells and Extended PB cells remained covered with sodium at all times during operation (even when discharged at 250 mA-cm^{-2}).

Sodium electrode wicks, while not an essential feature for PB cells, were required for the longer Extended PB cell, and under the DOE-funded program the wick designs for Extended PB cells developed further. The wicks, contained within an annulus between a metal shim and the electrolyte, were investigated by sodium-sodium cell testing. As illustrated in Figure 2-4, the Extended PB cell wick was effective

when discharged in a sodium-sodium cell at 85 mA-cm^{-2} although it was slow to wet with sodium in the initial stages of cycling.

Surface treatments of electrolyte to reduce the sodium wetting temperature and the time to achieve good wetting were investigated. Although treatments with a number of metals with low melting points were investigated, the lowest wetting temperature was achieved with lead-coated electrolyte, which was shown to promote a significant decrease in the start-up resistance of PB cells.

CSPL's sulfur electrode technology was well-advanced when the DOE-funded program began.

- Low-resistivity electrode structures were developed (0.27 Ω-cm).

- Uniform electrode operation was achieved by incorporating alumina into the carbon fiber matrix. Alumina was preferentially wetted by sodium polysulfide with respect to sulfur.

- Good rechargeability was demonstrated (85% theoretical capacity was obtained at 1000 cycles, 75% at 3000 cycles).

- No evidence of materials degradation was found in cells tested >24,360 h.

Since September 1985, sulfur electrode development included an initial examination of alternative methods of dispersing alumina in the electrode structure.

CSPL's containment development program was also well-advanced when the DOE-funded program began.

- Extensive test experience (up to 24,790 h) was available on inexpensive mild steel containment with a chromised surface.

- Static corrosion tests in Na_2S_3 at elevated temperature projected a life of at least 5 yr for the preferred containment.

- A second source of chromised material was identified, providing higher quality coatings at reduced cost.

- A proprietary variant of chromising was tested in small cells for 334 cycles (2700 h).

Under the DOE-funded program, the cell testing program on containment continued and selected cells were removed from test to be subjected to posttest analysis. New materials, which could provide the resistance to polysulfide corrosion required from metallic components in contact with the cell environment, were also introduced into sulfur electrodes for subsequent test and posttest analysis.
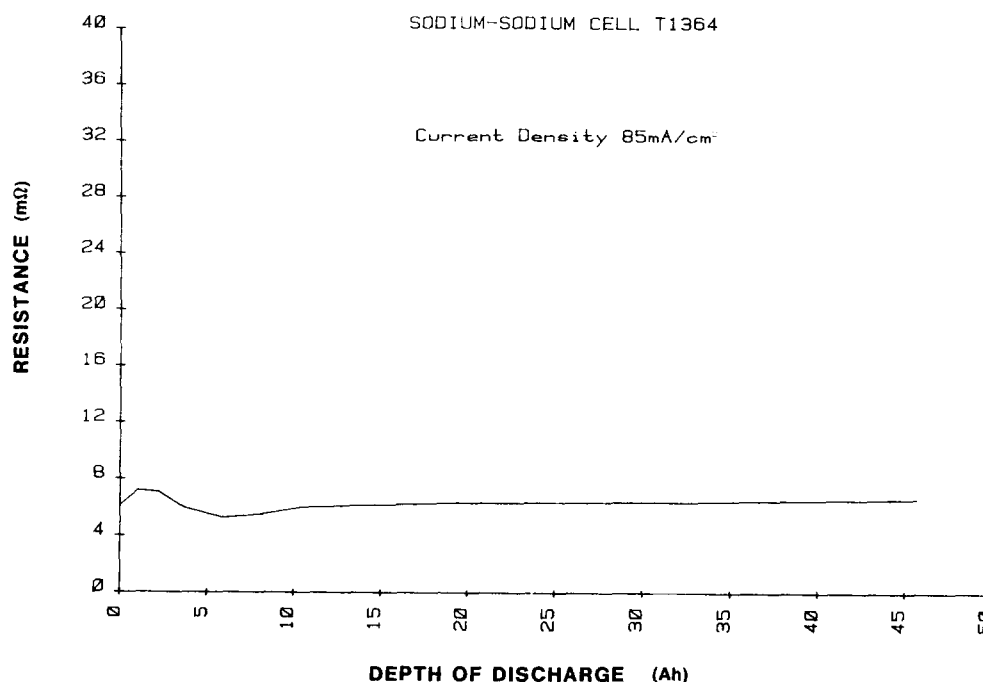
Figure 2-4. Sodium-Sodium Testing of Extended PB Wick Resistance vs Depth of Discharge

In the coming year, containment activities will include

- Improvement in the stability of the electrode seals
- Commencement of accelerated life tests on established materials and alternative materials offering the prospects of increased durability or reduced cost
- Redefinition of materials requirements based upon feedback from cell, module, and battery manufacture
- Further development of the materials quality plan.

The objective of CSPL's cell development work in 1985 was to design and develop cells for the EV application and for stationary applications (specifically for the BEST module). The materials technology and component designs developed by CSPL were to be used to create cells satisfying the important issues related to battery development and testing (e.g., energy density, power density, reliability, safety, cost, freeze-thaw survivability, infant mortality, fabrication, failure-resistance consistency). Another important objective was the development of a computer program to simulate the electrical and thermal characteristics of cells. Following the manufacture of prototype cells meeting performance requirements, the processing technology was to be transferred to the manufacturing engineering team (Figure 2-5).

Before the DOE-funded program the status of CSPL's cell development was as follows:

- Numerous cells of the mature designs had completed more than 2000 cycles.
- A controlled experiment using the mature cell designs (NaS7 and TD cells) showed that cell reliability was a function of electrolyte length.
- The Weibull characteristic life of hybrid PB cells (PB cells with the mature seal design) was 2237 cycles, as measured at 750 cycles.
- The Weibull characteristic life of true PB cells was ~500 cycles, indicating a need for further seal development.
- Initial scoping trials on hybrid versions of the extended PB cell had begun.
- PB cells had successfully survived 14 thermal cycles in the fully charged state.
- The safety of PB cells was demonstrated to be affected by the pressure inside the sodium compartment.
- Controlled resistance behavior was not observed in PB cells that failed.

In 1985 the controlled experiment to investigate the effects of electrolyte length on cell reliability was continued in a parallel EPRI-funded program. The 15-cell population of TD cells completed 2544 cycles (22,632 h) and the 15-cell population of NaS7 cells completed 1846 cycles (15,624 h). Table 2-2 shows the results of Weibull analyses on the cycle life data for the two groups.
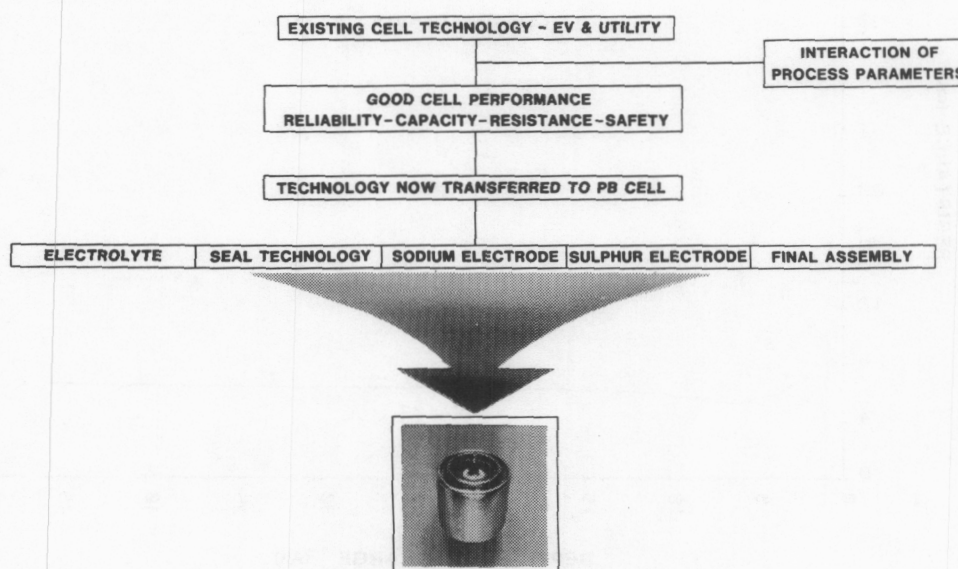
Figure 2-5. Transfer of Existing Technology Into PB Cells

The subscripts and superscripts on the predicted values of Weibull characteristic life and shape parameters in Table 2-2 indicate 95% upper and lower confidence limits, respectively.

Life test data on hybrid PB cells (electrolyte length: 30 mm) further illustrated the sensitivity of reliability to electrolyte length, thus supporting the small cell strategy. The Weibull characteristic life of a 12-cell group of hybrid PB cells was 3464 cycles when predicted after 1100 cycles of test.

The status of PB cell performance at the end of CY85 is summarized in Table 2-3, which also includes the performance targets set for the PB cell. These performance targets were substantially met, but cell reliability was constrained by the effectiveness of the seals.

Table 2-2. Data From Size vs Reliability Experiment*

Cell Capacity (Ah)	Electrolyte Length (mm)	No. of Cells	Cycles Completed	Weibull Analysis	
				Characteristic Life (cycles)	Shape Parameter
30	120	15	2544	$_{1385}3072^{6818}$	$_{0.51}0.94^{1.73}$
150	580	15	1846	$_{630}1165^{2154}$	$_{0.59}0.96^{1.58}$

*December 1985

Table 2-3. Performance Goals of Electric Vehicle Cell

Parameters	Target 1985	Target 1986	Status December 1985
Equivalent characteristic life	1800 1100 or	2200	435* 3464[†]
Shape parameter	1.5 2.0	2.0	3.00* 1.36[†]
Design cycles, 95% confidence	250	500	165
Resistance (Ω-cm^2)	1.0	1.0	$\left(\begin{array}{l}1.12^* \text{ norm}\\0.98 \text{ BEST}\end{array}\right)$
Resistance rise (mΩ/cycle)	0.006	0.003	$\left(\begin{array}{l}\leq 0.006^†\\0.012^*\end{array}\right)$
Capacity (% theoretical)	85% at 250 cycles	85% at 500 cycles	Achieved*
Energy density (Wh/kg)	200	240	200
Energy density (Wh/L)	380	440	350
Freeze-thaw (cycles)	10	25	3×10 1×14
Safety	No breach/ distortion, $\Delta T \leq 200°C$	Safe under abuse conditions	224°C (worst case)

*PB cells, proprietary seal
†Hybrid PB cells including PB electrolyte and electrode features

43

The Scoping Trials on the hybrid versions of the Extended PB cell were continued, although one cell failed after 244 cycles. The remaining cells—one with a sodium wick and one with no wick—continued on test until 268 standard cycles had been completed. Their discharge limit was then adjusted from 1.90 V open circuit to 1.76 V open circuit so as to discharge the cells more deeply and determine the effectiveness of the sodium wick. The resistance of the cell without the wick increased by 25% at the end of discharge. The resistance of the cell with the wick remained stable.

An automatic freeze-thaw cycling facility was designed and the feasibility of using nondestructive testing techniques to examine the sulphur electrode during freeze-thaw cycling was explored. The safety testing facility was upgraded to accommodate the cell safety and module safety test programs.

In 1986, cell development will focus on the following:

- Further development of the PB cell and Extended PB cell designs

- Repeatability Trials on PB cells and Extended PB cells to illustrate that reliable, repeatable, and predictable cell behavior can be obtained.

In 1985, the Cell Testing section sought to establish that reliability and performance targets for EV applications and stationary applications were met by the cell designs developed in other parts of the program. In addition to repetitive charge/discharge cycles using test regimes appropriate to the different applications, the test program included tests to determine the limits of cell operation (e.g., the effect of high recharge overvoltages on cell reliability, the effect of high rate charge and discharge rates on cell reliability, and the effect of operating temperature on cell life).

Before the DOE-funded work, CSPL's cell performance testing program had generated the following results:

- Low cell resistance (<1 Ω-cm^2)

- Stable cell resistance (resistance rises <0.0004 mΩ/cycle achieved in NaS7 cells tested to 3000 cycles)

- Excellent rechargeability (75% of theoretical capacity obtained at 3000 cycles)

- Predictable and repeatable performance

- High efficiency ($>85\%$)

- Excellent resistance to high recharge overvoltage (cells held permanently at 8 V survived over 10,000 h).

Testing of hybrid PB cells (cells with the electrolyte and electrode features of the PB cell but with the mature thermocompression-bonded seal used in TD cells) indicated that the technology transfer from the central sulfur cell design to the central sodium cell design had been accomplished. A test schedule equivalent to that of the mature cell designs was used: discharge at the 3-h rate using an adjustable load resistor. However, unlike cells of earlier designs, which were discharged to a limit of 1.76 V open circuit, discharge was terminated at 1.9 V open circuit. Recharge was carried out at constant voltage (2.8 V) for 5 h with a maximum current density limit. A limited number of true PB cells exceeded 500 cycles of test. The ability of the small-cell design to discharge at high current density was illustrated when a hybrid cell that had completed 500 discharge/charge cycles was discharged at increasing current density. The current density was increased from 100 mA-cm^{-2} in 100 mA-cm^{-2} increments over 10 cycles and finally the cell was effectively short-circuited. The cell survived short-circuiting and continued to operate normally. Another was operated for 240 cycles at a discharge rate of 200 mA-cm^{-2}, after completing 360 cycles at 100 mA-cm^{-2}.

In 1985, the database of PB cells was extended to 224 cells. Hybrid PB cells continued to cycle and 12 cells exceeded 1000 cycles. Figure 2-6 shows the behavior of a hybrid PB cell tested for 1100 cycles and that of the true PB cell tested for 650 cycles. As expected, the resistance and capacity behavior of the two cells was similar, with good capacity retention, $\sim80\%$ theoretical capacity, and stable resistance. The initial testing of the Extended PB cell concept proposed for stationary applications was carried out using a hybrid version of the cell. The resistance and capacity behavior of the cells, shown in Figure 2-7, indicated that no major performance problems were encountered with the larger cell design.
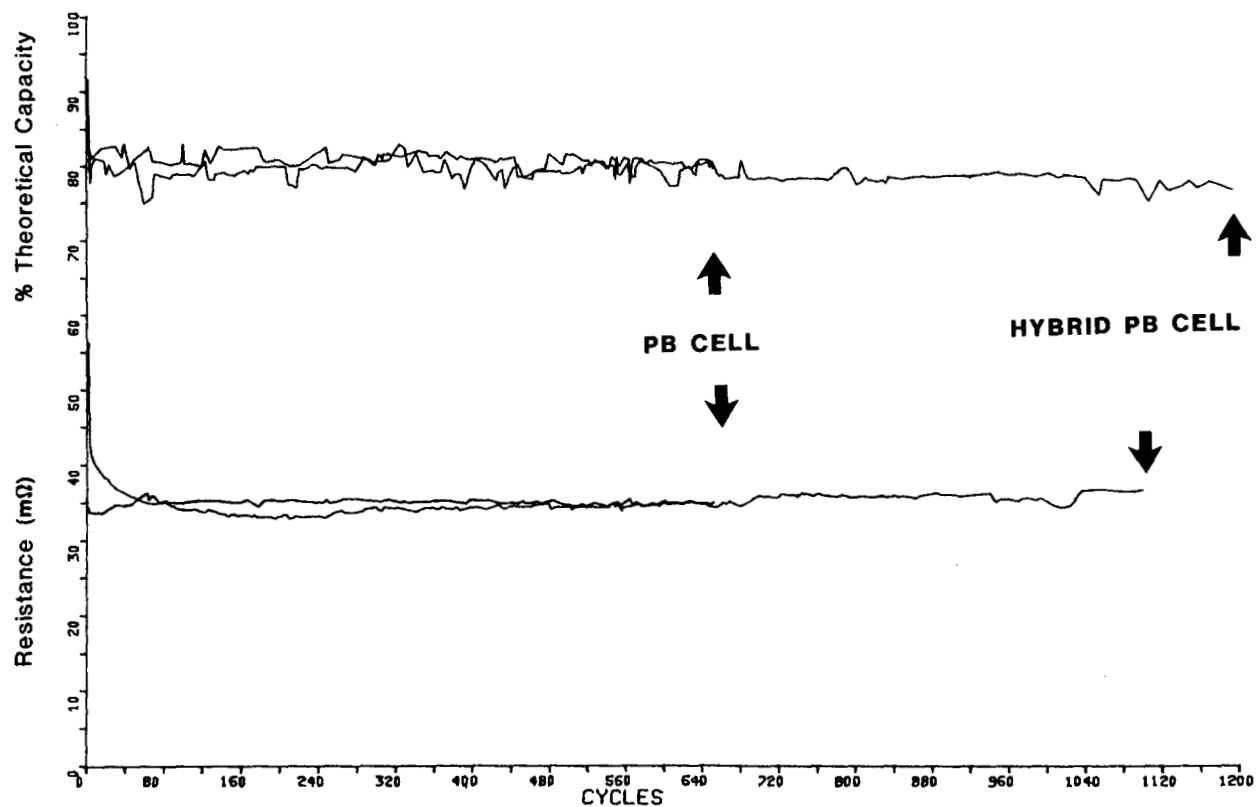
Figure 2-6. Comparison of Capacity Retention and Resistance Stability for Hybrid PB and PB Cells
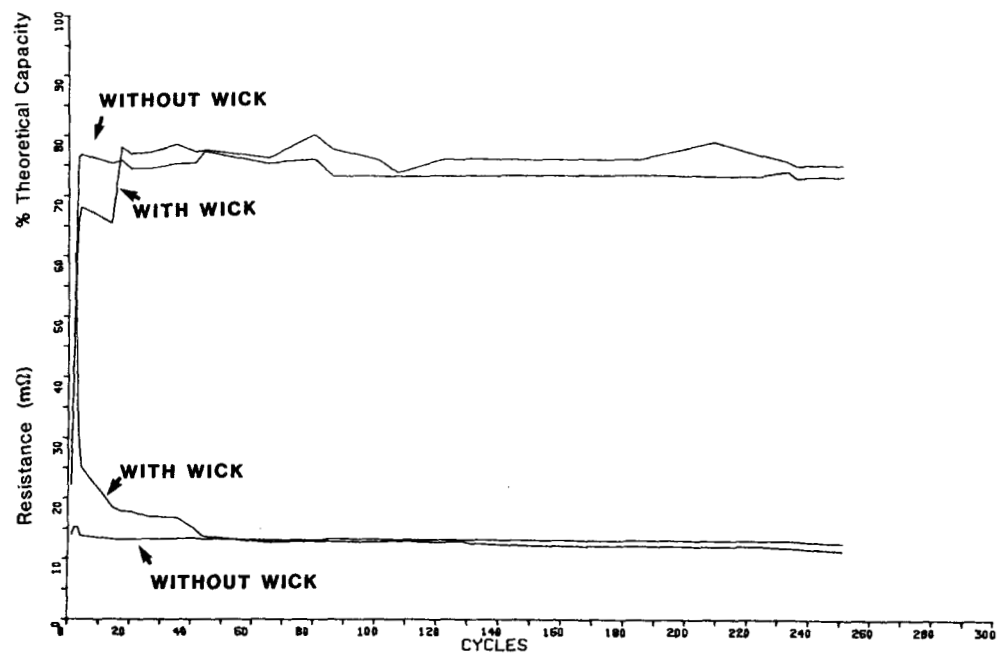
Figure 2-7. Performance of Hybrid Extended PB Cells With and Without Wicks

In 1985, test data were collated to support the computer simulation of cell bahavior. These data were required for electrical and thermal modeling for CSPL's battery simulation activity.

CSPL's cell testing activities also included posttest analysis of cells. The posttest analysis facilities at CSPL were upgraded and expanded to meet the needs of the DOE-funded program. Cells were selectively removed from test for subsequent posttest analysis to identify the following:

- Sites of cell failure, where appropriate
- Sites of incipient cell failure
- Component design concerns
- Materials degradation mechanisms and corrosion rates
- Relationships between cell fabrication steps and observed cell behavior.

Posttest analysis was used to build up the database on materials and component performance. Samples of materials and components were archived to provide the basis of investigations into the rates and mechanisms of degradation. Information generated from posttest analysis in 1985 included the behavior of the proprietary container coating up to 800 cycles of test (6963 h). As indicated in Figure 2-8, no significant deterioration in the coating was observed, suggesting that the new and potentially lower cost coating could prove acceptable for future cell development.

Major testing objectives for CY86 include

- Continued cell testing in support of the cell development programs
- Testing of cells in Repeatability Trials to measure cell performance against targets
- Posttest analysis of cells in support of the development programs.
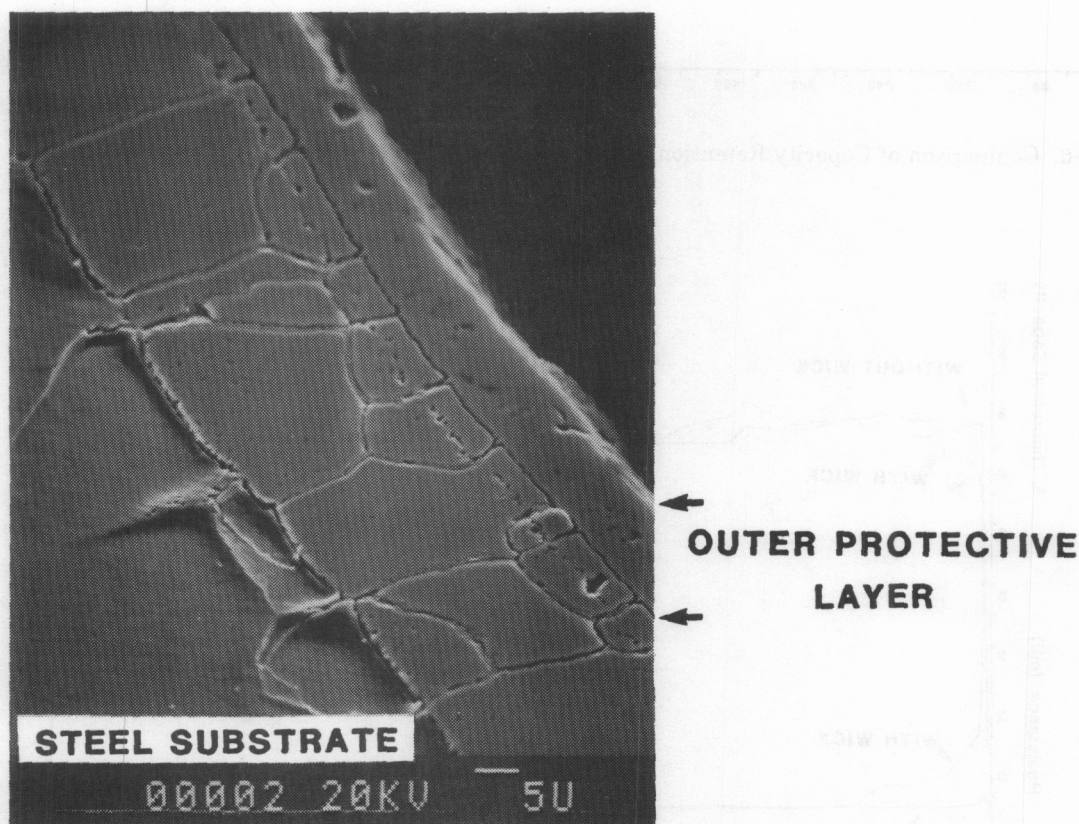
Figure 2-8. Photomicrograph of Proprietary Container Coating After 800 Cycles on Test

The electrical and thermal behavior of small groups of interconnected cells was also addressed in 1985. Activities included designing and testing modules and networks appropriate to the EV applications (PB cells) and stationary applications (Extended PB cells). The battery computer model developed earlier was to be used to predict the electrical and thermal characteristics of the modules.

Before September 1985, CSPL tested networks of NaS7 and TD cells. The status of CSPL's network tests follows:

- Stable performance was obtained from four-cell strings and networks of four-cell strings.

- No degradation of cell performance or reliability was observed in four-cell strings and networks of four-cell strings.

- Electrical consequences of cell failure was accommodated in networks of four-cell strings.

Two approaches can be used for the electrical networking of sodium/sulfur batteries: parallel connection of individual cells and series connection of individual cells. The approach selected for battery development is dependent on the behavior of cells on failure (open-circuit or short-circuit) or on the ability to provide a device external to each cell, activated upon cell failure, that effectively simulates the open-circuit or short-circuit failure mode. The variable failure characteristics of cells and the absence of reliable failure control devices compelled CSPL to use a four-cell string as the basic building block of electrical networks. A short string avoided the occurrence of unacceptably high overvoltage on the cell in the string that reached top of charge first. Further, the consequences of short-circuit failure were limited to the string in which the failure occurred, since the cells connected in series to a failed cell were charged by adjacent strings until their high resistance at the top of charge prevented further current flow. Nevertheless, the availability of a reliable device external to each cell that effectively reproduces open-circuit or short-circuit failure conditions was sought to eliminate some constraints on battery design.

A consequence of using the four-cell string approach in battery design, particularly for EV batteries, was that the use of a large-capacity cell limited the number of parallel paths in the battery, making the battery design vulnerable to early failures. A battery designed with small cells included a multitude of parallel paths, and the accommodation of cell failure was much improved. Statistical analysis showed that the ability to provide more parallel paths had a strong influence on maintenance strategy. The analysis indicated that battery maintenance frequency could be

reduced from a 3-mo period with large cells to over 5 yr (i.e., maintenance-free) for small cells having identical reliability.

A four-cell string approach to battery networking was tested before starting the DOE program. A 16-cell network (four parallel strings, each including four cells) behaved as predicted when tested for over 400 cycles with a failed cell in one string.

The first testing of four-cell strings in the DOE-funded program was of four PB cells connected in series. A string that included high-resistance interconnections operated at predicted resistance ($\sim$200 mΩ), providing 78% of theoretical capacity until a cell failed after 87 cycles.

The results achieved in CSPL's battery/module design efforts before the start of the DOE-funded program were as follows:

- Close packing of cells was achieved.

- Local heat generated by heaters or failing cells was dissipated by the thermal design.

- Effectiveness of vacuum enclosures was demonstrated.

- Cell and battery insulation methods and materials were proved.

Before the start of the DOE-funded program, CSPL addressed the issues of module and battery design in the design, fabrication, and testing of a 120-cell (16-V, 330-Ah) battery of TD cells (2 series banks, 15 parallel strings per bank, 4 series-connected cells per string). The battery consisted of a close-packed array of cells in a vacuum-insulated enclosure. The thermal management approach was developed by modeling the proposed battery design and the thermal characteristics of cells on failure and during normal operation. The target was to limit the temperature variability within the battery to $\pm$10°C during normal operation and to limit the temperature excursion in cells adjacent to a worst-case failure to 20–30°C. The method of thermal management was validated by safety-testing a small module of cells. Close correlation was observed between predicted behavior and actual behavior. On testing the battery, the variability in cell temperature was $\pm$4°C. The battery was tested for 9 mo, and the vacuum insulation remained effective throughout this period. Subsequent posttest analysis of the battery indicated that none of the battery components was subject to deterioration. Busbars, instrumentation leads, heaters, and framework and electrical insulation were all in excellent condition.

Late in 1985, the first module of PB cells, illustrated in Figure 2-9, was designed and assembled for initial studies of thermal and electrical behavior. It

consisted of five strings of four cells surrounded by sixteen dummy cells. The thermal management and electrical insulation methods used on the TD-cell battery were used. The ends of each cell were separated from their neighbors above and below by simple press-molded insulative components. Low-resistance intercell connections developed from computer-modeling various terminal-weld configurations were used. As shown in Figure 2-9, the strings were located by a metal plate at each end, to which they were attached by low-energy welding. The plate provided the parallel interconnection distributing the current between the strings. Mathematical modeling was used to study the voltage drop across one of the plates to determine if the location of a four-cell string, including a failed cell, could be detected. A significant movement in voltage contours resulted from a cell failure, suggesting that a technique based on this approach could be used to detect cell failure in batteries requiring maintenance.
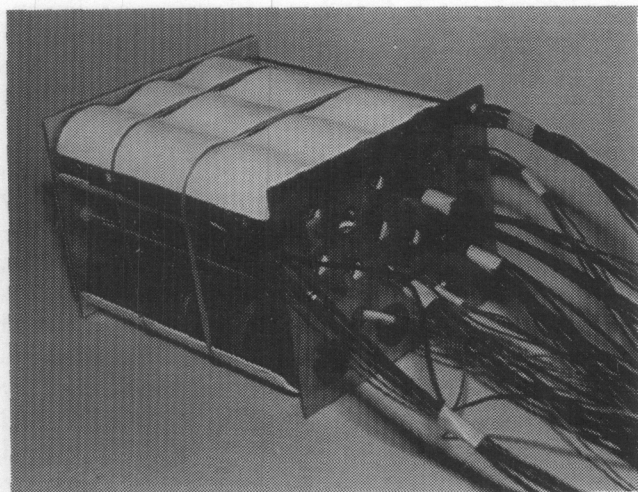
Figure 2-9. Photograph of 36-Cell PB Module

In 1986, CSPL's module development and testing activities will include

- Further development of battery components
  - low-resistance interconnections
  - failure control devices (open circuit/short circuit)
- Design, fabrication, and qualification of PB cell modules
- Design, fabrication, and qualification of Extended PB cell modules
- Calibration of mathematical models against module behavior.

The major objectives for CSPL's battery engineering and testing work are to design, fabricate, and test a subsize version of the BEST battery from suitable cells and modules and to develop a computer model simulating battery operation. Successful completion of these objectives is to be validated by the results obtained from testing two subsize batteries, one at CSPL and another at a site in the U.S. The battery would be expected to achieve projected performance, demonstrating effective electrical and thermal management, system control, and auxilliary systems.

The status of module and battery engineering at CSPL is described above. As noted, CSPL's approach to module design incorporates many small cells. The small-cell approach offered the following advantages in battery design.

- The prospect of maintenance-free batteries. The multiplicity of parallel paths allowed an occasional cell failure to be tolerated without a large loss in capacity.
- High power and energy densities
- Improved battery safety as a result of the extensive multipartitioning of the reactive materials
- Flexible battery design to fit a wide range of applications
- Improved tolerance to thermal and mechanical perturbations.

Within the DOE-funded program, a model was developed to predict the effects of cell variables (size, reliability, temperature, failure mode) and battery variables (interconnection strategy, control strategy, maintenance strategy) on the characteristics of a battery system (thermal behavior, electrical behavior, reliability, and cost). The model was to be used to optimize stationary battery system designs, and was to be calibrated initially against the observed characteristics of modules consisting of five strings of four cells connected in parallel. The battery computer model adopted is illustrated in Figure 2-10.

Analyses of cell/battery reliability and cell/battery systems were started. In the systems analyses, the value of different battery approaches was assessed as a function of cell cost. It was assumed that structural costs, interconnection costs, and thermal management costs were a fixed fraction of cell cost, regardless of size. The principle adopted can be illustrated using the value of a short-circuit failure device to the four-cell string. When an open-circuit cell failure occurred, three live cells would be essentially lost, but if a short-circuit device was provided for each cell only the failed cell would be lost. The value of the short-circuit device would, therefore, be three-fourths of one

cell: the number of cells effectively saved divided by the number of devices needed to save them.

In 1986, CSPL's battery engineering work will focus on

- Design of the subsize version of the BEST battery
- Development and calibration of the battery computer modeling program.

Development of Beta″-Alumina Ceramic Electrolyte—Ceramatec

Sodium beta″-alumina, prepared in the form of closed one-end tubing, is the apparent preferred choice as a separator/electrolyte in many moderate-temperature electrochemical devices including the sodium/sulfur battery. The sodium/sulfur battery has been under extensive development for over 15 years for such diverse applications as electric vehicles, load leveling, and space power. In recent years, significant improvements in cell lifetime and performance have been demonstrated. One of the major obstacles remaining in commercializing this battery system is the demonstration of reliability. The reliability of the sodium/sulfur battery depends on a number of factors including the cell interconnect configuration, electrode deterioration, container corrosion, and electrolyte failure. In turn, the reliability of the electrolyte itself is a function of several properties, including its strength variability and fracture toughness. Beta″-alumina tubes, being brittle components, are prone to failure under various conditions. The failure may be electrolytic in origin or may result from mechanical stress. In either instance, failure generally initiates at flaws such as cracks, voids, large grains, and inclusions, which are typical defects introduced during processing.

Preparation of beta″-alumina powders has been performed by a number of different techniques. Predominant among these methods have been the zeta process and the slurry solution spray-drying process. The zeta process is a dry powder process that involves mixing and calcining alkali salts with alpha-alumina and subsequently milling the resultant powder product. Although this process produces electrolytes of high mass density, possessing a fine-grained microstructure and high intrinsic conductivity, it has distinct disadvantages: the process is both equipment- and labor-intensive, requires multiple operations, and produces a nonflowable powder. Scaling of this process to a mass-production level is, therefore, considered difficult and costly.
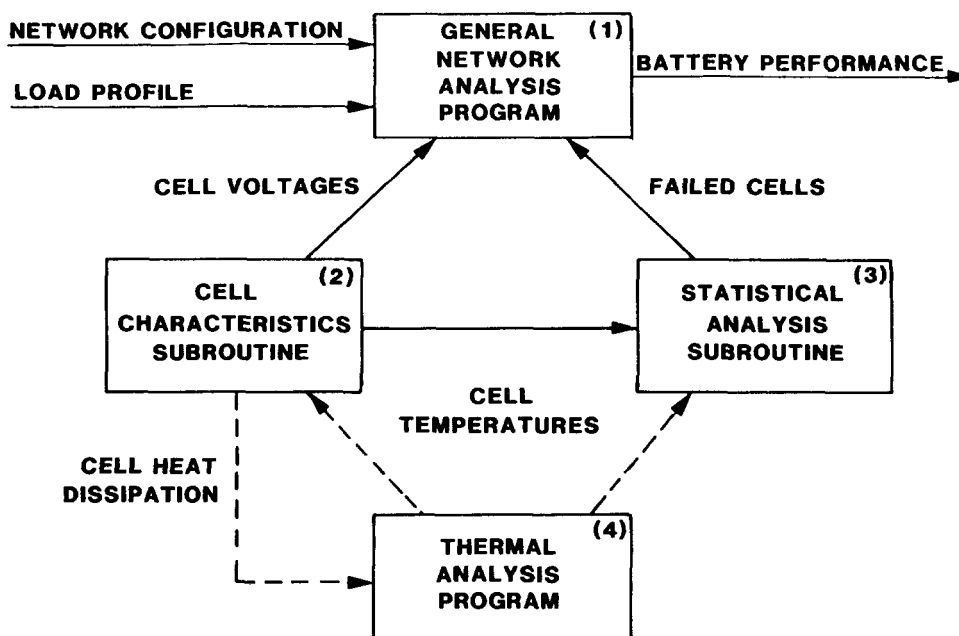
THE DIAGRAM ABOVE SHOWS THE FLOW OF INFORMATION BETWEEN THE COMPUTER PROGRAMS AND SUBROUTINES THAT WILL BE USED IN THE BATTERY SIMULATION EFFORT.

Figure 2-10. Schematic of Battery Computer Modeling

As an alternative, the spray-drying process was developed as a single-step manufacturing route to the powder preparation. In slurry solution spray-drying, various alkali salts are dissolved in water and subsequently slurried with alpha-alumina and beta″-alumina seeds. After mixing, the slurry solution is evaporatively dried in a conventional spray dryer. Flowable powders, which are suitable for automatic isostatic pressing, have been prepared using this process and inexpensive sources of alpha-alumina. The technique of seeding has been incorporated into the spray-drying process to (1) catalyze conversion to the beta″-alumina phase during sintering, and (2) produce electrolytes of controlled grain size yielding excellent electrical and mechanical properties. Slurry solution spray-drying is attractive because the expensive operations of calcination and ball-milling are eliminated from processing. This process is also easily scaled to mass-production levels.

Since small-size defects are always present in ceramics, toughening of the beta″-alumina ceramic has been pursued in an effort to improve its average mechanical properties. This toughening has been accomplished by several techniques, but the method of interest in this program has been transformation toughening. In this process, fine particles of zirconium oxide (unstabilized or partially stabilized with yttrium oxide) are incorporated into the beta″-alumina ceramic. Work performed simultaneously at the University of Utah and at Rockwell International has demonstrated that both the fracture strength and fracture toughness can be substantially increased by the incorporation of zirconia. However, high toughness values are critically dependent upon the amount of metastable transformable tetragonal phase within the sintered body. In turn, the amount of transformable tetragonal phase is a function of the zirconia particle size and stabilizer content. For an unstabilized zirconia, only particles within a certain size range will transform in the presence of a propagating crack. For partially stabilized zirconia, slightly coarser zirconia particles are permissible because the yttrium oxide tends to reduce the driving force for transformation. Thus, in this system both composition and particle size are important parameters controlling transformation of the zirconia. However, work done previously in the partially stabilized system was conducted only at 3-mol% yttrium oxide. Under the current program, an investigation was made of yttria contents ranging from 0 to 3 mol% at a zirconia content of 15 wt%.

Burst-testing was an integral part of the process development efforts outlined above. In this method, electrolyte tubes were subjected to a uniformly increasing internal pressure until failure. The flaw patterns developed on the fractured electrolytes permitted identification of fracture origins. Evaluating the fracture origins provided information on processing defects. As a feedback loop for processing, burst-test data were compiled on various process modifications to determine the effects of composition variables or other process parameters on fracture strength.

State of Development

The specific objectives of work done in 1985 for DOE included (1) development of an automated proof-tester to perform routine nondestructive testing of EV-size electrolytes (25 mm OD × ~250 mm length × 1.4 mm wall thickness); (2) optimization of the seeded slurry solution spray-drying process; (3) investigation of yttria-doped zirconia/beta″-alumina composites and processing procedures to determine fracture toughness and strength at various yttria contents; and (4) characterization of these process or compositional modifications by burst-testing.

The proof-test/burst-test apparatus (developed under an earlier program) was redesigned to allow it to be operated in a semiautomatic mode. As designed, this unit used hydraulic fluid to expand an internal elastomer bag against the electrolyte tube, generating a uniform hoop stress to the electrolyte and allowing components to be either pressurized to failure (burst-tested) or pressurized to a preset level (proof-tested). Originally, application of the pressure was performed using a manually operated hand-pump. Consequently, parameters such as the pressure application rate and overshoot were difficult to control. Under the newly designed apparatus, the system is constructed with high-pressure pumps and a pressure-transducer sensing system integrated with a micrprocessor controller. In this design, the rate of pressure application can be controlled, and pressure overshoot is eliminated. This test equipment was upgraded as part of Ceramatec's cost-sharing portion of the DOE-funded program.

Initial burst-test results are summarized graphically in Figure 2-11 for entire tubes of several beta″-alumina process modifications including (1) conventionally sintered zeta-process electrolytes; (2) hot isostatically pressed zeta-process electrolytes; (3) seeded slurry solution spray-dried electrolytes; and (4) zirconia-toughened electrolytes. To amplify on these statistics, additional data were generated by sectioning individual tubes into rings ~2 cm long for burst-testing. By cutting the electrolytes into rings, determination of strength, flaw size, and flaw size population could be documented more readily without the need to prepare significant quantities of electrolyte tubes. The results of these ring tests are given throughout the remainder of this report.
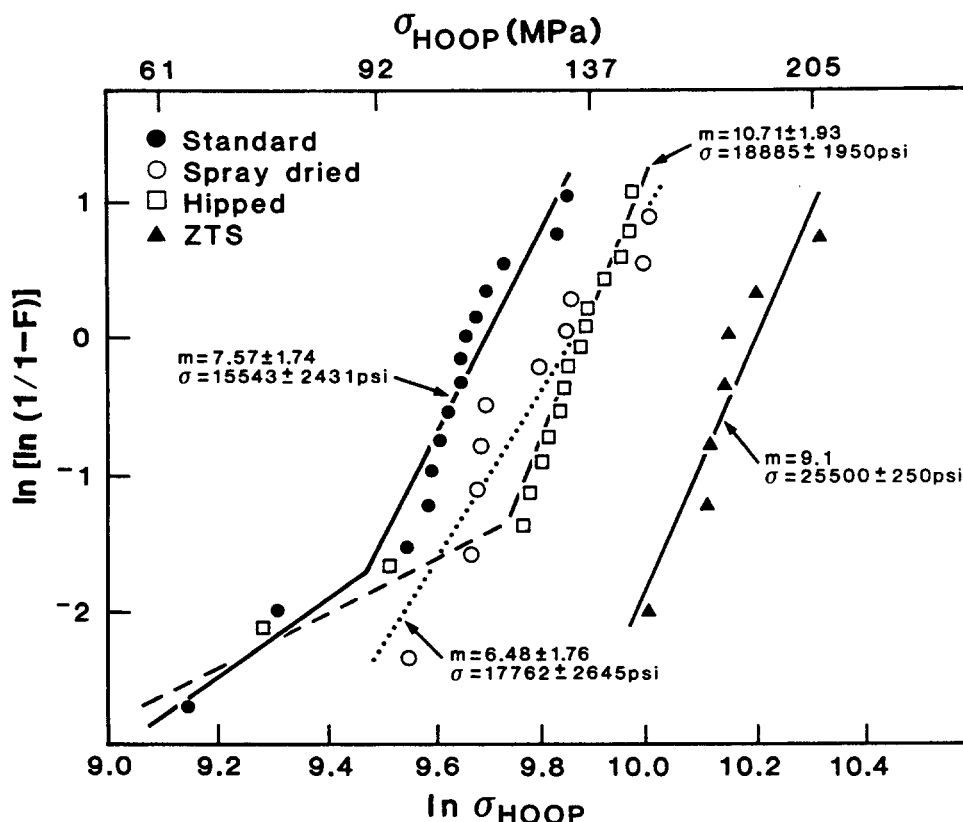
Figure 2-11. Burst-Test Characteristics of Beta″-Alumina Electrolytes

Work on the seeded slurry solution spray-drying technique focused on (1) investigating various methods of seed preparation; (2) optimizing the solids content of the spray-drying process; (3) examining various alkali raw material sources and organic additives for their compacting and sintering characteristics; and (4) characterizing these variables by burst-testing.

Various methods of preparing seeds were examined, including techniques for milling and classifying the seed material. Several comminution methods were investigated including (1) dry-ball milling, (2) jet-milling, and (3) vibratory grinding. The particle size distribution and impurity contamination were examined for each method. Of these milling techniques, vibratory grinding gave the narrowest particle-size distribution and lowest level of contamination. Following these experiments, vendor tests of air classifiers were conducted to determine the best equipment for classifying seeds into the required size range. An appropriate model and manufacturer of this equipment were located, and a unit was procured as part of Ceramatec's cost-sharing portion of the DOE-funded program.

The solids content of the slurry is deemed an important parameter for efficient spray-drying. To minimize energy consumption, solids contents in the range of 40% to 60% are essential. However, because of the high pH of the slurry solution (~13), low-viscosity slurries are difficult to achieve without excessive water. Most conventional dispersing agents are ineffective at these high pH ranges. Therefore, as part of the program, preparation of high-solids slurries using nonconventional agents was investigated. It was found that certain surfactants (generally nonionic types) are able to provide reasonable dispersion of solids as high as 60%.

Experimental powder batches were prepared at the three solids-content levels shown in Table 2-4. Theoretical densities >98.5% were routinely achieved at all solids contents. The resistivity values of these electrolytes are among the best reported values for any beta″-alumina. The burst-strength data indicated that the higher solids contents gave higher average strengths with smaller standard deviations. With the exception of the 40% solids material, the remaining batches gave high Weibull moduli (>10). The lower Weibull modulus of the 40% solids material was determined to result from poor sample preparation.

51

Table 2-4. Physical Properties of Seeded Slurry Solution Spray-Dried Electrolytes—Solids Content Study

	Solids Content		
	40%	50%	60%
Mass density (g/cm)	3.23 ± 0.00	3.24 ± 0.01	3.22 ± 0.01
Resistivity (Ω-cm, 300°C)	4.1	4.2 ± 0.0	4.6 ± 0.6
% Linear shrinkage	9.8 ± 0.0	10.6 ± 0.0	—
Bisqued weight loss	12.6 ± 0.1	12.6 ± 0.1	12.8 ± 0.1
Burst-Test strength (MPa)	113 ± 23	130 ± 11	148 ± 14
Weibull modulus	4.8 ± 0.5	12.1 ± 2.0	11.4 ± 1.7

Sintering conditions: 1580°C for 12 min; 1475°C for 1 h.
Burst Test and Weibull data were compiled from approximately 25 ring sections for each condition. All other data represent 1 to 6 samples of each condition.

In addition to the data presented above, two alkali sources (hydroxides and carbonates) were investigated, along with alternative organic additives, to determine their combined effects on ceramic properties. To evaluate the effects of these various additives, the compaction characteristics and densification behavior of these materials were compiled. Of the alkali sources, the use of hydroxides was preferred. Hydroxide-based powders consistently gave the best compaction behavior and sintered properties. The carbonate-based system gave lower overall pressed and sintered densities at all conditions investigated. Some of the organic additives included lubricants, humectants, and anticaking compounds. The data indicated that the addition of these agents improved the compaction and densification characteristics of the spray-dried powder.

To demonstrate the beneficial effects of these additives, Figure 2-12 shows the comparative Weibull characteristics of beta″-alumina ring sections prepared from a zeta process and two spray-drying modifications. A comparison of this data with those in Figure 2-11 demonstrates that significant improvements have been achieved. The overall strength increase in these samples results partly from the testing of smaller volume elements. However, note that the Weibull modulus for the zeta-process material is essentially equivalent to values determined previously, whereas a significant improvement was obtained in the moduli for spray-dried process modifications (from ~6.5 to between 10.4 and 13.2). This represented an increase of more than 38%.

Using scanning electron microscopy (SEM), the flaws in a number of these electrolytes were characterized. Shown in Figure 2-13 (a) and (b) are representative failure origins for zeta-process and spray-dried electrolytes, respectively. In all instances, electrolyte failure was characterized by the presence of a void.

In zeta-process electrolytes, these voids were generally associated with large grains. Energy-dispersive x-ray (EDX) analyses of these defects indicated the presence of iron as an impurity. It is believed that the iron was present as an inclusion at the void site. During sintering, the iron presumably diffused into the surrounding matrix, leaving the void and promoting exaggerated grain growth.

In the spray-dried electrolytes, no large grains were observed adjacent to the voids. Except for isolated instances, no impurities were present at the void sites either. A slight sodium oxide compositional gradient was observed near some of the voids, leading to the speculation that voids resulted from local high concentrations of sodium that diffused into the surrounding bulk during densification.
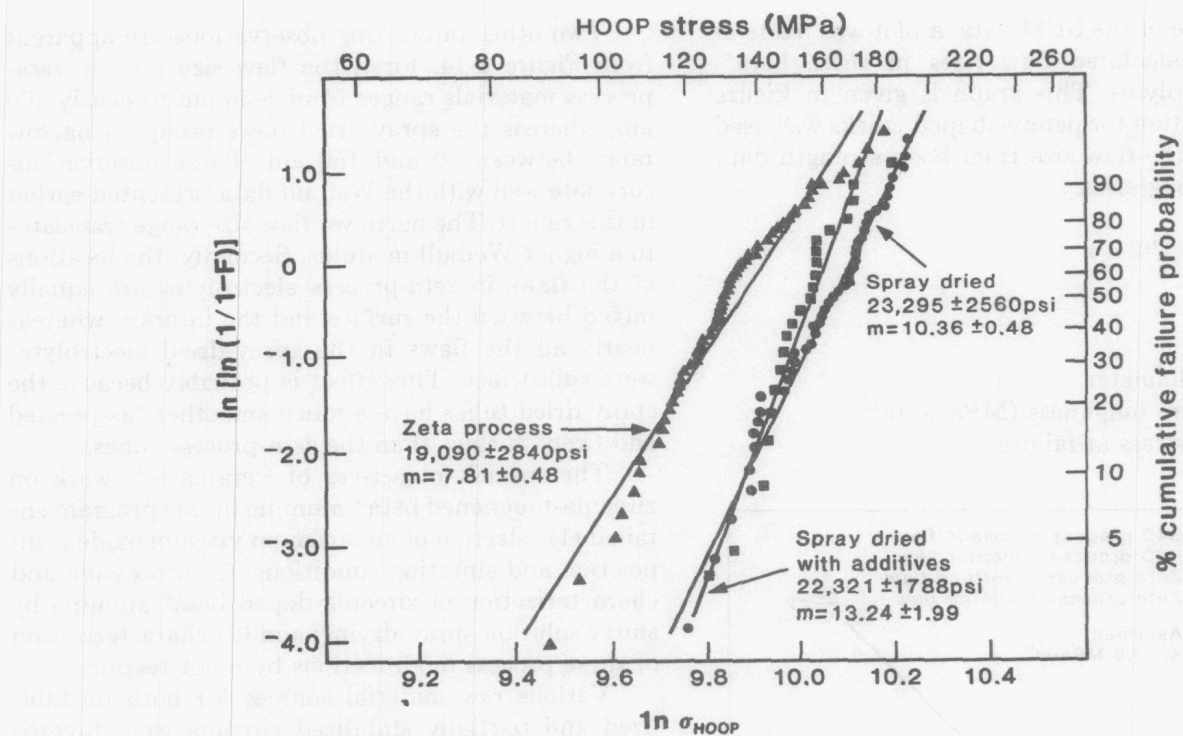
Figure 2-12. Weibull Characteristics of Beta″-Alumina Ring Sections Prepared From Zeta Process and Two Spray-Drying Modifications
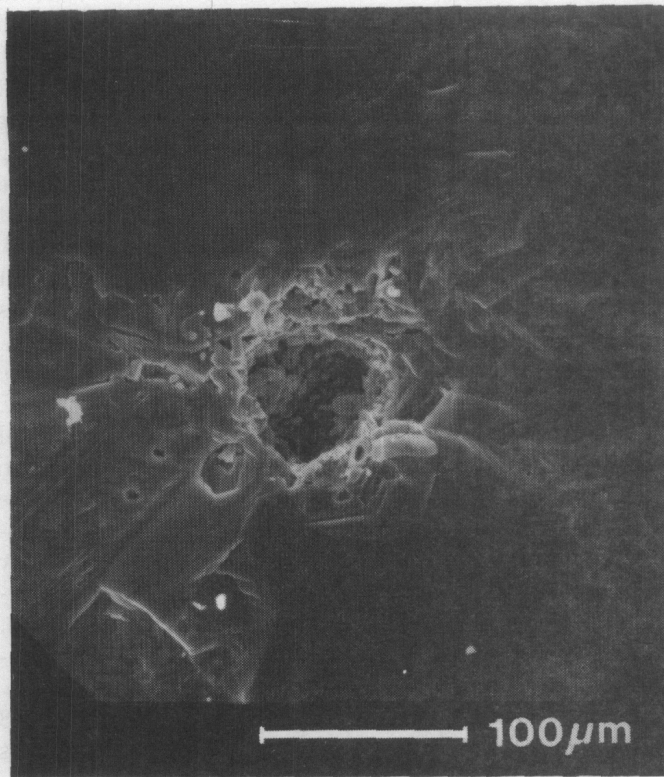
(a) Zeta Process
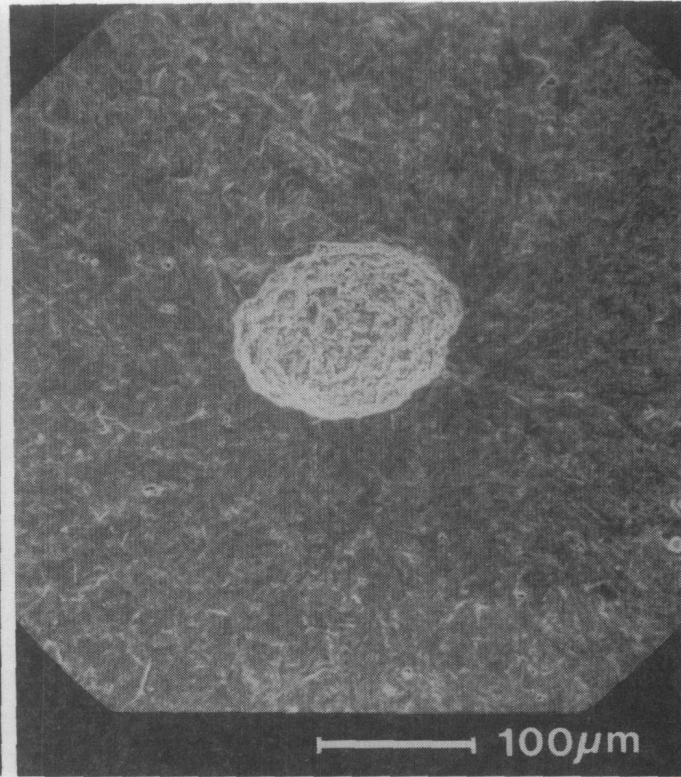
(b) Seeded Spray-Dried Process

Figure 2-13. Typical Failure Origins of Burst-Tested Beta″-Alumina Electrolytes

Using some of the SEM data, a plot was made of observed vs calculated flaw sizes in these beta″-alumina electrolytes. This graph is given in Figure 2-14. The equation for penny-shaped cracks was used in calculating the flaw size from hoop strength data and fracture toughness:

$$2C = (K_{IC}^2 \times \pi)/(2\,\sigma^2)$$

where

$2C$ = flaw diameter
K_{IC} = fracture toughness (MPa $\times$ m$^{1/2}$)
σ = hoop stress at failure.
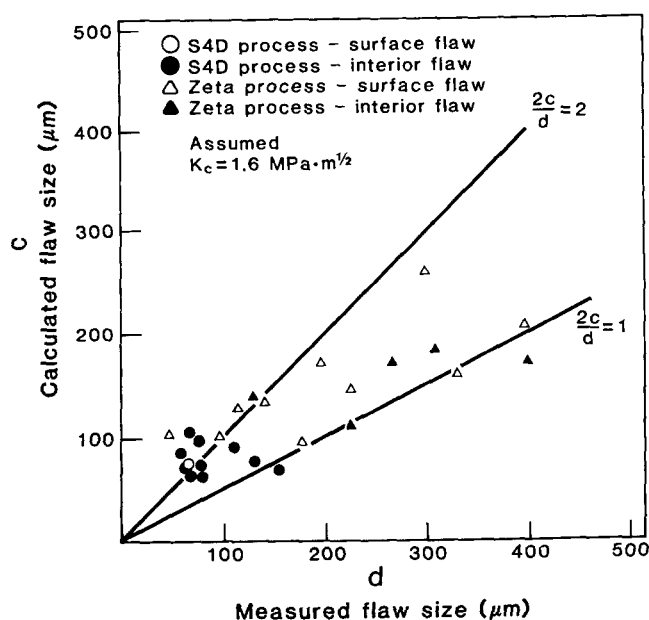
Figure 2-14. Comparison of Observed vs Calculated Flaw Sizes for Beta″-Alumina Ceramics

Initially, when calculating these flaw sizes from fracture data, a stress intensity factor of 2.1 MPa/m² was used. (This average value was obtained using double-cantilever beam tests.) In correlating the observed vs calculated data, however, the observed flaws were between two and four times the calculated values. This suggests that the actual fracture toughness of the material in regions near these flaws must be lower. Using a K_{IC} value of 1.6 MPa/m², all the observed flaws lie approximately one to two times within those of the calculated values. (This is the lowest average fracture toughness value obtained using an indentation method.) This result suggests that the fracture toughness near defects is lower than the measured bulk toughness.

Two other interesting observations are apparent from Figure 2-14. First, the flaw size for the zeta-process materials ranges from ~50 μm to nearly 400 μm, whereas the spray-dried flaws occupy a narrow range between 50 and 150 μm. These observations correlate well with the Weibull data presented earlier in this report. The narrower flaw size range translates to a higher Weibull modulus. Secondly, the locations of the flaws in zeta-process electrolytes are equally mixed between the surface and the interior, whereas nearly all the flaws in the spray-dried electrolytes were subsurface. This effect is probably because the spray-dried tubes have a much smoother "as-pressed and fired" surface than the zeta-process tubes.

The specific objectives of Ceramatec's work on zirconia-toughened beta″-alumina in this program entailed (1) selection of an optimum yttrium oxide composition and sintering conditions; (2) processing and characterization of zirconia-doped beta″-alumina by slurry solution spray-drying; and (3) characterization of these process modifications by burst-testing.

Various raw material sources for both unstabilized and partially stabilized zirconia were investigated at compositions ranging from 0 to 3 mol% yttrium oxide. The zeta process was initially used as the base powder for incorporation of the zirconia. Powder compositions at 0, 1, 2, and 3 mol% yttrium oxide were studied. These compositions were sintered over a range of temperatures from 1575°C to 1600°C. Qualitatively, it was found that the tetragonal content of these powders generally increased with increasing yttrium oxide content, or decreased at higher sintering temperatures or times. The 3-mol% yttrium oxide composition showed no detectable monoclinic content regardless of sintering conditions. On the other hand, unstabilized materials varied in tetragonal content from 50% to 70% depending on firing conditions. As expected, the tetragonal contents for 1% and 2% yttrium oxide were intermediate between the two other experimental end-members. Density, resistivity, strength, fracture toughness, and microstructural features were obtained for these materials. When compared with nontoughened beta″-alumina, the zirconia-toughened material showed equivalent porosity levels (>97% of theoretical density), slightly higher resistivities at 300°C (4 to 6 Ω-cm for toughened material vs 3 to 5 Ω-cm for standard material), fracture strengths ~20% higher than standard material, and fracture toughness values averaging 50% above nontoughened material (2.8 MPa/m² vs 1.8 MPa/m²). The highest values for fracture toughness occurred at the 1-mol% yttrium oxide level.

Using techniques that were developed for slurry solution spray-drying (described above), zirconia-

toughened beta″-alumina electrolytes were prepared by this process as well. Compositions ranging from 0 to 3 mol% were also investigated for the spray-drying process.

In general, values equivalent to toughened zeta-process materials were achieved. Ring sections from these electrolytes were burst-tested. The average hoop stresses at failure were calculated for a number of electrolyte modifications and ranged between 152 and 180 MPa, which are lower than the whole tube data presented earlier but generally higher than nontoughened zeta or spray-dried materials. (It is speculated that the zirconia-toughened materials may be more susceptible to machining damage when cut into ring sections. This may explain the low values obtained in some of the rings.) Overall, these data demonstrate that zirconia-toughening substantially improves average mechanical properties without seriously compromising the ionic conductivity of the material.

Technical Challenges Remaining

In summary, Table 2-5 presents comparative data on electrolytes prepared from zeta, seeded slurry solution spray-dried, and zirconia-toughened processes. This information demonstrates that significant improvements in beta″-alumina electrolytes have been achieved by using the spray-drying and zirconia-toughening processes for electrolyte fabrication. Of these processes, the spray-drying process is clearly the preferred choice from standpoints of cost, processing simplicity, and physical properties. Adding zirconia to this process is easily accomplished and results in additional physical property improvements. Both processes are now at a point where scale-up from their current pilot plant level to a full-scale manufacturing facility is appropriate, pending increases in electrolyte demand.

Table 2-5. Properties of Beta″-Alumina Electrolytes Fabricated From Several Powder Processes

Properties	Zeta	Seeded Spray-Dried	Zirconia-Toughened
Mass Density			
(g/cm)	3.25 ± 0.01	3.24 ± 0.01	3.48 ± 0.01
(% of theoretical)	99.4 ± 0.3	99.1 ± 0.3	99.5 ± 0.3
Ionic Resistivity			
(Ω-cm @ 300°C)	4.4 ± 0.3	4.3 ± 0.3	5.9 ± 0.6
Fracture Strength			
(4-point bend, MPa)	194 ± 25	242 ± 1	300
(Diametral, MPa)	321 ± 41	—	380
Hoop Strength (Burst Test)			
(EV tubes, MPa)	108 ± 17	123 ± 18	176 ± 2
(2-cm rings, MPa)	132 ± 20	161 ± 17	182 ± 21
Weibull Modulus			
(EV tubes)	7.57	6.48	9.10
(2-cm rings)	7.81 ± 0.48	10.36 ± 0.48	7.94 ± 1.20
Fracture Toughness			
(DCB technique, MPa/m²)	1.93 ± 0.12	2.04 ± 0.09	2.56 – 3.98
Microstructure			
(Average grain size, μm)	3	15	1-2
(Morphology)	Duplex	Uniform	Uniform
Cell Test Life			
(Na/Na cells, Ah/cm²)	>2400	>2500	>2400
(Na/S cells, cycles)	>5000	>1800	—
Critical Current Density			
(A/cm² @ 300°C)	8	—	28

EV Tubes: 25 mm OD, 230 mm length, 1.4 mm wall.

Posttest Examinations of FACC Sodium/Sulfur Cells—ANL

Selected sodium/sulfur cells fabricated and tested by FACC underwent posttest examinations at Argonne National Laboratory. These examinations were directed toward increased understanding of the morphology of the sulfur electrode, the materials behavior of cell hardware, and the underlying causes of cell failure. The findings were reported to FACC in support of its efforts to achieve improved cell performance, cycle life, and reliability. During the past year, examinations were completed for three load-leveling cells and two EV cells. In addition, one cell was examined that had been operated at Wright Aeronautical Laboratories for satellite baseload energy applications. Descriptions of these cells and the posttest findings are summarized in Table 2-6. The following sections offer a more descriptive discussion of polysulfide phase analysis, electrode morphology, and cell hardware performance.

State of Development

One cumulative finding in the sulfur electrode examinations has been that the compositional gradients established in an electrode melt before terminating the cell operation were retained in the microstructure at ambient temperature. Analysis of these gradients was complicated by the strong tendency of the polysulfide melt to supercool and form metastable polysulfide phases in addition to the equilibrium sodium polysulfides. Before a predictive model of sulfur electrode behavior can be developed, the compositions of these phases need to be established. Five recurring metastable phases were identified using polarized-light microscopy and x-ray diffraction.

Scanning electron microscopy and energy-dispersive spectroscopy (SEM-EDS) were the primary tools used to determine the composition of these metastable phases. For a number of reasons (including use of the software program ZAP to derive the initial estimates), the sodium content was consistently

Table 2-6. Summary of Sodium/Sulfur Posttest Examinations

Cell	Description	Major Findings
LL190	Mark-II cell voluntarily terminated after 1453 cycles	• Extensive sodium chromium sulfide deposits on the electrolyte • Cell hardware in fine condition
LL199	Mark-IID cell voluntarily terminated after 1551 cycles	• Extensive sodium chromium sulfide deposits • Electrolyte fracture on cooldown • Nonuniform corrosion of the chromium-plated container
LMA01	Modified Mark-IA cell terminated due to electrolyte fracture after 334 cycles	• Fracture throughout the seal assembly • Sodium monosulfide layer adjacent to the molybdenum container
VA661	EV cell terminated due to electrolyte fracture after 15 cycles	• Symmetrical container bulge near base • Axial compositional gradient in the sulfur electrode
VDQ16	EV cell failed due to electrolyte fracture on heat-up	• Multiple container bulges near base • Axial compositional gradient in the sulfur electrode
ADA23	Modified EV-type cell terminated due to electrolyte fracture after 3316 cycles	• Extensive sodium chromium sulfide deposits • Sodium polysulfides in sodium annulus

underestimated. The calibration curve shown in Figure 2-15 was generated by an analysis of specially prepared polysulfide standards. With this curve, the SEM-EDS-ZAP values were corrected for more accurate compositional estimates of the binary metastable phases. For example, samples of the metastable M-phase taken from Cell LL199 have corrected sodium contents within the range of 36 to 38 at%. This compositional range is higher in sodium than the nearest equilibrium phase, sodium tetrasulfide (Na_2S_4). For samples of A-phase, the compositional range bracketed the sodium pentasulfide (Na_2S_5) standard, which indicated that this phase is a crystallographic variant of the equilibrium phase. This technique also proved sensitive enough to confirm that the sodium monosulfide that formed because of electrolyte failure in Cell VDQ16 was not stoichiometric. The ratio of sodium to sulfur was approximately 2.05 to 1. To date, the compositions of three metastable phases were established by this method. Work continues to isolate sufficiently pure samples of the two remaining metastable phases.
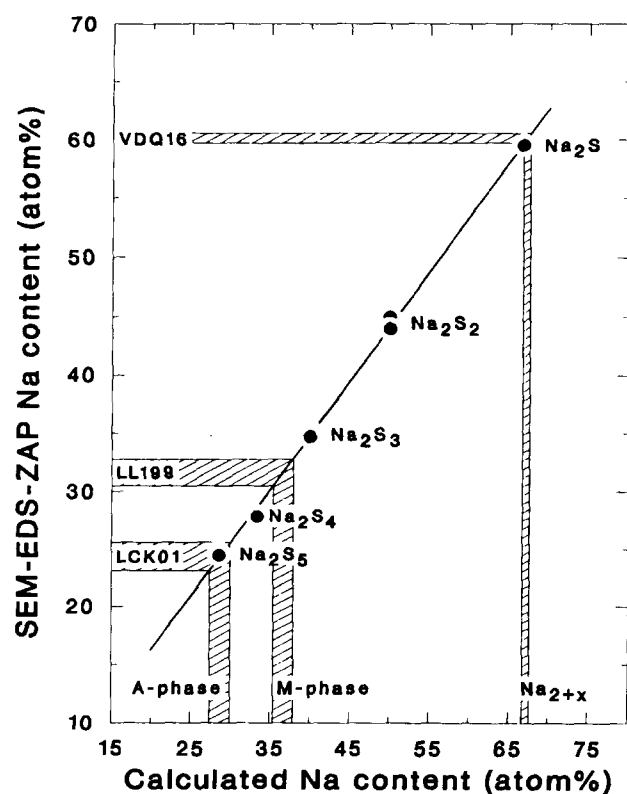
Figure 2-15. Calibration Curve for Determining Na_2S_x Phase Compositions

The electrode microstructures observed for four of the six cells were influenced by the electrolyte fractures that these cells experienced. The location of lower polysulfides indicated where most of the direct reaction between sodium and sulfur occurred. For Cells VA661 and VDQ16, nonstoichiometric sodium monosulfide ($Na_{2.05}S$) predominated at the bottom of the electrodes, where bulges in the containers developed. Although the mechanism responsible for these bulges has not been fully elucidated, the formation of sodium monosulfide, which is solid at normal operating temperatures and up to 978°C, was undoubtedly an instrumental factor. In Cell VA661, the smooth contours of the expanded container circumference suggested that the bulging process was a single continuous event. The irregular expansion of the VDQ16 container, however, suggested that this process could also occur in smaller multiple stages. In both cells the full electrode thickness was composed of sodium disulfide above the area of container bulging. This phase field gradually gave way to sodium tetrasulfide near the center of the cell. A more abrupt transition to higher polysulfide phases, such as A-phase, was noted closer to the top of each cell. The axial gradients in electrode compositions reflected the charged condition of these electrodes prior to electrolyte failure.

In Cells ADA23 and LMA01, most of the lower polysulfides were located in the upper half of the cell. The fractured electrolytes were encased in a sodium monosulfide, but this phase field did not extend the full electrode thickness. In addition, this compound was present in the sodium annulus (the space between the electrolyte and the safety tube) because of the inflow of polysulfides after the fracture. In Cell LMA01, the safety tube was indented in two areas where sodium monosulfide formed. In Cell ADA23, the positive electrode was compressed to as little as 70% of its nominal thickness by the outward pressure applied to the beta-alumina fragments when the lower polysulfides formed in the annulus. These findings further substantiated the mechanical forces generated within these cells when electrolyte failure results in solid polysulfide formation.

One additional feature of the sulfur electrode from Cell LMA01 was the development of a continuous white band of polysulfides along the molybdenum container. This band was rich in stoichiometric sodium monosulfide and averaged 60 μm in thickness over the lower three-quarters of the container. Cell LMA01 was the only cell examined in which sodium monosulfide was found at the container interface.

This interfacial layer could not be readily explained as a consequence of the electrolyte fracture or as a condition that existed before failure.

In long-lived cells such as LL190, LL199, and ADA23, the electrode microstructure was altered by the formation of a migratory corrosion product, sodium chromium sulfide ($NaCrS_2$). The sodium chromium sulfide initially formed as a scale on the chromium-plated container. The scale spalled when a maximum thickness of ~ 15 μm was reached. These fragments gradually dissolved during charge cycles, and the chromium migrated toward the electrolyte as a result of potential or concentration gradients. Eventually, an enriched concentration developed near the electrolyte. The ternary compound reformed as a precipitate on the electrolyte surface or nearby graphite fibers when the solubility limit was exceeded. Repeated occurrences of scale formation, spallation, dissolution, and precipitation led to extensive deposits on the electrolytes from these three cells. The deposits adhered more tenaciously to irregularities in the electrolyte surface (Figure 2-16).
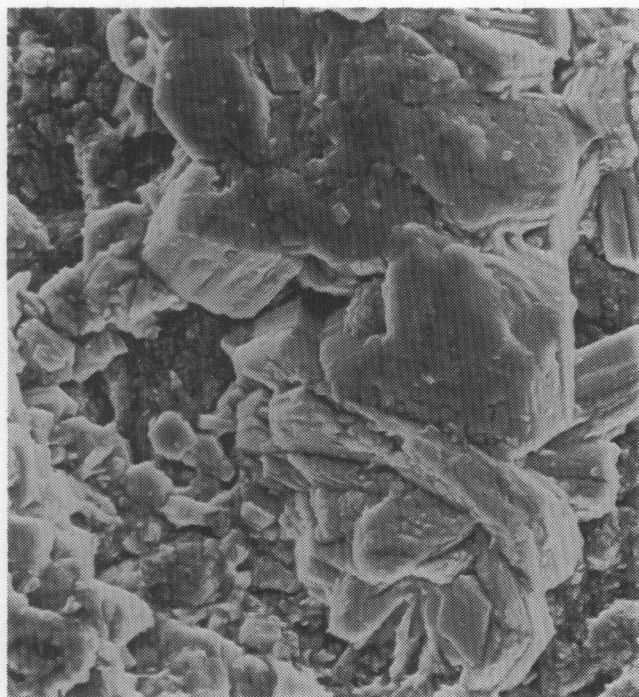
Figure 2-16. Adherence of $NaCrS_2$ Crystals to Irregularities in Outer Electrolyte Surface

The amount of deposition was dependent on operating temperature and cycle life. Limited data for cells tested at 350°C included three cells of moderate cycle life (587 to 727 cycles). In these cells the deposits coated less than 10% of the electrolyte surface and averaged no more than 50 μm in thickness. Lower temperatures promoted more deposition (apparently because of decreased chromium solubility in the electrode melt) and increased coverage of the electrolyte surface. Roughly 90% of the active electrolyte surfaces were covered with thick deposits for three vertically operated cells tested at 325°C. The data for these cells are shown in Figure 2-17 and illustrate that the deposit thickness was linearly dependent on cycle life. Since this group of cells had long cycle lives, these deposits may not have been detrimental to the life of the electrolyte. The effect on cell performance, if any, has not been ascertained.
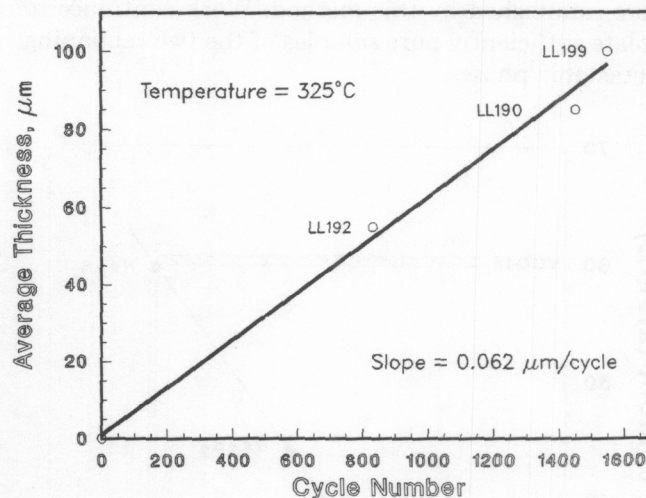
Figure 2-17. Thickness of $NaCrS_2$ Deposits on Electrolyte Surface Showing a Linear Dependence on Cycle Life for this Group of Load-Leveling Cells

As the preceding discussion suggests, the reliability of the beta″-alumina electrolyte continues to be an important concern. The severe fragmentation of the four electrolytes that failed in operation made determination of the source of electrolyte failure infeasible. However, the failure of the electrolyte from Cell LL199 during cooldown offered key insights into the causes of freeze-thaw failures. The fracture pattern

consisted of eight axial cracks that extended the full length of the tube. Five of these cracks, such as those shown in Figure 2-18, initiated at the outer (sulfur) electrode surface and were concentrated along the two separations between the electrode halves. These separations were devoid of active material. The other three cracks were roughly centered with respect to the electrode halves and initiated at the inner surface.
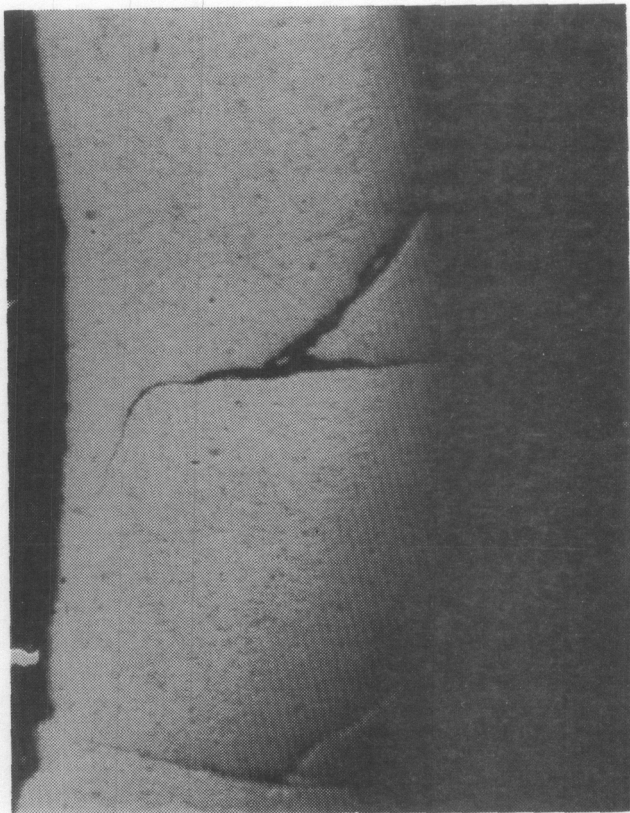
Figure 2-18. Fractures in the Beta″-Alumina That Initiated on the Outer Surface Adjacent to the Separation Between the Two Positive Electrode Halves

These findings are consistent with the hypothesis that the failure initiated on the outer electrolyte surface because of sheer stresses that developed at this surface. The tube was placed under compression when the electrode melt solidified around the electrolyte. The melt-free separations between electrode halves introduced discontinuities in this compressive stress field. Eventually, the shear stresses became large enough to induce fractures at defects aligned with electrode separations. Once a primary crack propagated the length and thickness of the tube, the stress pattern was altered. The stresses on the inner surface became tensile rather than compressive, and initiation of secondary cracks from the sodium side occurred. Previous fractographic examinations at SNL also identified fractures in which crack initiation occurred at the outer surface between electrode halves. Elimination of the electrode separations should minimize this form of failure.

The electrolyte fracture in the Mark I Cell LMA01 led to subsequent fractures through the glass seal and into the insulating collar. This failure triggered leakage of polysulfide melt. A failure of this type was not observed in the other cells that suffered electrolyte failures. The seals of these newer cells used more massive insulating collars that were more resistant to fracture. The newer seal design also had a simpler joint geometry, with closer tolerances and increased bonding area for a stronger seal joint. These design changes appear to have eliminated this problem.

The lower surface of the aluminum gasket used to form the radial compression seal for Cell LL199 showed a moderate degree of corrosion. Subsequent corrosion of the stainless steel container occurred in the unprotected area where a ledge was machined to support this gasket. The wall thickness in the corroded area was reduced by a relatively minor 20% to 25%. The same corrosion mechanism resulted in container breaches for two previously examined cells. Cells of more recent vintage (such as ADA23) used an improved seal design that eliminated this deficiency. The interior of the container is plated with chromium after the machining step rather than before it.

Conclusion

In general, these examinations revealed that the plating technology used provided a chromium layer of sufficient quality to prevent significant corrosion of the stainless steel substrate. Although cracks existed in the chromium layers, most were blunted at the stainless steel interface. The final plating thickness remained more than adequate even for the cells with extensive sodium/chromium sulfide formation. Only Cell LL199 showed extreme variability in the plating thickness. The areas of high plating loss were location-dependent. Sections of the plated container adjacent to the separations between the positive electrode halves were the primary areas of reduced coating thickness. The low polysulfide concentration observed in these separations suggests that a vapor species was involved in localized acceleration of the corrosion process.

Chapter 3. Battery Technology Evaluation

Introduction

Rechargeable cell and battery evaluations were conducted by the Battery Technology Evaluation element during 1985. Five major tasks were in progress during the year. Standard testing of improved cells and batteries continued at the National Battery Test Laboratory (NBTL) at Argonne National Laboratory. Parametric evaluations of advanced prototype cells and batteries also continued at SNL. Battery field experiments with solar generation systems were in progress under Sandia's direction, at three locations. Testing of improved lead-acid, load-leveling batteries was completed at Exide Management and Technology Company under a Sandia contract. Also under contract, sodium/sulfur cells and modules were tested at FACC.

The objectives of the ANL and SNL laboratory and field test activities were to provide carefully controlled cell and battery evaluations of improved and advanced technologies being developed by DOE contractors and by independent organizations. Data were obtained that described the performance, cycle life, and operating characteristics of many different electrochemical technologies and cell designs. These data were used by DOE contract managers and decision makers in evaluating the progress of the development contract, in identifying problem areas for development emphasis, and in determining allocation of DOE funding and resources. The data were also used by battery developers to guide program direction and cell design efforts for specific application goals.

Activities at NBTL continued in 1985 with the testing of improved lead-acid, nickel/cadmium, and nickel/iron batteries for EV applications under standardized test regimes. During the year evaluation of advanced technologies, such as the Exxon zinc/bromine batteries and the FACC sodium/sulfur cells, was initiated using standardized test conditions. Evaluation of an Energy Development Associates (EDA) zinc/chloride battery continued. The manager of the NBTL was the major organizer of a successful International Workshop on Battery Testing, held in Heidelberg, West Germany, in October.

Testing activities at NBTL were generally completed on schedule. Performance characterization was completed, and life testing continued for four FACC sodium/sulfur load-leveling cells. Cycle life for these units ranged from 659 to 1030 cycles. An Exide lead-acid, load-leveling battery completed 1860 cycles at 50°C in continuing tests. Characterization of an experimental JCI flow-by lead-acid cell yielded 48.8 Wh/kg and a life of 116 cycles. Initial tests of a 30-kWh Exxon zinc/bromine battery were delayed by maintenance and system troubleshooting.

Sandia's evaluation of advanced prototype technologies under parametric and solar application-specific test regimes continued. The goals of these tests were to identify key performance and life limitations during the early stages of development of advanced technologies, when standardized tests would not be practical. Evaluation continued on zinc/bromine, sodium/sulfur, zinc/ferricyanide, and nickel/hydrogen cells and batteries. Also, as a continuing effort from prior years, an improved lead-acid battery was evaluated under solar application-specific test modes in support of the solar/battery field experimental work. The goal of the battery and solar field experiments was to determine the performance of batteries in stand-alone and grid-connected photovoltaic and wind turbine generator systems. Data for determining battery size, predicting load satisfaction, and evaluating system maintenance requirements were obtained. One wind turbine generator and battery experiment was conducted using a sealed lead-acid battery similar to the type developed in 1982 under Sandia contract. Also, an Exxon zinc/bromine 20-kWh battery was delivered and prepared for evaluation with a photovoltaic (PV) array at a Sandia test facility.

Tests at SNL proceeded according to schedule. Five different flow batteries were tested. One Exxon battery surpassed 1500 cycles. Life-cycle tests of a nickel/hydrogen cell were completed after 1106 cycles. Anomalous charging characteristics were observed on a FACC sodium/sulfur cell using constant-current charging. The cell was accepting full charge, using a more time-consuming current-limited constant voltage charge. Good performance was obtained in the initial evaluation of a 20-kWh Exxon zinc/bromine battery, and a parametric test regime was completed. Tests of this battery with a PV array were planned for early 1986.

The objective of the FACC evaluation contract was to continue and complete cell and module tests begun under development contracts. More than 100 cells were evaluated under several test regimes. Cell component studies, cycle-life tests, and freeze/thaw survivability evaluations were conducted.

A battery evaluation project was completed at Exide. Load-leveling, lead-acid batteries developed and built by Exide under other DOE contracts were tested either until failure or to the end of the contract. Two batteries that did not fail in these tests were shipped to ANL for continued testing. The effect of elevated operating temperature on cycle life was determined and quantified.

Progess of the individual evaluation activities will be detailed in this chapter. Work at NBTL will be covered first, followed by SNL's laboratory results. Data for SNL's solar/battery field test work will be presented. Finally, results from the FACC and Exide battery evaluation contracts will be described.

Battery Evaluation at NBTL

The National Battery Test Laboratory at Argonne National Laboratory was established to provide a facility for the independent testing and evaluation of batteries. The laboratory has played a leading role in this endeavor. Working with other national laboratories, industry, academic institutions, and professional societies, NBTL has developed and applied test methods, procedures, and instruments that yield meaningful characterizations of batteries for various applications.

Both cells and batteries developed within DOE-sponsored programs and by private funds are tested at NBTL. The laboratory is capable of the simultaneous and independent testing of 91 modules and four full-size (30- to 40-kWh) batteries under both simulated driving conditions and normal test conditions. Eight test stations in the Battery Components Technology (BCT) element of the laboratory are dedicated to specialized tests involving charge optimization studies and specific discharge studies. Twenty test stations are dedicated to high-temperature cell and module testing. During 1985, the NBTL operated for an average of 99% of the scheduled time around-the-clock, seven days a week, weekends and holidays included.

NBTL is made up of four major components:

- The control room and main test area, where ambient and elevated temperature tests are conducted
- The environmental annex, where low-temperature chambers and a zinc-chloride test facility (with halogen scrubber) exist
- The BCT laboratory, where refined instrumentation and software are installed to allow systematic parametric variation and optimization and other special studies
- The high-temperature test area, where lithium/sulfur and sodium/sulfur cells are evaluated.

Performance-characterization assessments are conducted under a series of charge/discharge cycles with constant current, constant power, peak power, and computer-simulated dynamic-load profile conditions. Flexible charging algorithms are provided to accommodate the specific needs of each battery under test. Within the BCT component, special studies are conducted to explore and optimize charge procedures, to investigate the impact of unique load demands (such as thyristor chopper-controlled discharges) on battery performance, and to analyze the thermal management requirements of battery systems.

Scaling and normalization techniques developed and practiced at NBTL permit full-size battery performance to be projected on the basis of tests conducted on three- to six-cell modules. As a technology under development matures, however, larger units (including full-size battery packs) can be tested to evaluate system performance and reliability in a well-instrumented and controlled environment. For example, prior to in-vehicle installation, batteries may be tested with the simulated, anticipated load requirements to ensure system integrity and expected performance before the batteries are subjected to more expensive and visible, but less controllable, tests in a vehicle.

At NBTL, test voltages and currents are controlled and data are recorded and formatted by computers located in the control room. Display systems conveniently provide graphs or tabulations of the prevailing status or of the performance history of a battery.

A normalization technique developed and practiced at NBTL allows aging effects on batteries, generally implicit in all test results, to be made explicit and separated from the results. The plots and graphs contained in this report have been subjected to this technique. Generally, data are normalized to the rated capacity of a battery; however, if the maximum capacity exhibited by a battery is less than rated, then the results are normalized to that value so that performance data are not reported that represent a capability beyond that which the battery exhibited or could exhibit.

Highlights of Battery Testing and Evaluation at NBTL

Following are the highlights of the battery testing and evaluation activities at the NBTL during 1985:

- Testing was initiated in the main component of the laboratory on the Lucas Chloride tubular lead-acid modules, SAFT nickel/iron modules, ERC nickel/cadmium modules, an Exxon 1-kWh zinc/bromine module, and the Exxon 30-kWh zinc/bromine battery. In the high-temperature test facility, testing was initiated on the FACC sodium/sulfur EV cells.

- Testing continued on cells representing several technologies from many manufacturers. These included ISOA lead-acid EV cells (Globe/JCI), advanced lead-acid EV cells (Globe/JCI), advanced lead-acid load-leveling modules (Exide), nickel/iron EV modules (Eagle-Picher), nickel/zinc EV modules (Electrochimica), and sodium/sulfur load-leveling cells (FACC).

- Tests were completed to determine the impact of depth of discharge (DOD) on the cycle life of ISOA lead-acid batteries.

- Under EPRI support, tests were completed to determine the impact of peak power and of extended rest periods after discharge on the cycle life of JCI EV-2300 lead-acid modules.

- The manager of NBTL as general chairman, with the help of technical chairman Dr. R. Knodler of Brown, Boveri, and Cie, organized and conducted the first International Workshop on Battery Testing (Methodology) held in Heidelberg, Germany, September 30 through October 2, 1985.

Summary of Tests Conducted at NBTL

The tests conducted at NBTL fell into three categories: (1) standard performance characterization and life-cycle tests; (2) parametric variation tests; and (3) special studies. Each of these categories is discussed below.

Standard Performance Characterization and Life-Cycle Test Procedures

The standard test procedures now in use have been described in detail in previous reports and are simply listed here.

- Capacity verification at $C_3/3$ rate
- Capacity and energy determination at 10, 30, 50, and up to 70 W/kg
- Sustained hill-climbing test
- Capacity and energy at low and elevated temperatures
- Peak power vs DOD
- Range on SAE J227aD/ETV-1, with and without regenerative braking
- Self-discharge rate
- Partial DOD test (to uncover "memory" effects)
- Life at 80% DOD.

The exploration of improved test procedures, analyses, and methodologies continues. In cooperation with the EHP Battery Test Working Task Force, we continued to determine the suitability of various versions of the Federal Urban Driving Schedule as a standard for testing EV batteries. Characteristics of several versions of the FUDS, including simplified and baseline variations, were applied, analyzed, and compared. The new methodology, described in last year's report, continues to be refined as a way to obtain battery discharge times (and vehicle ranges) for batteries discharged under varying load conditions (such as an EV battery operated under an urban driving schedule, a load-leveling battery operated under a peak-shaving mode, or a solar battery operated under transient cloud conditions). More advantages to this methodology are described later, under "Results of Standard Performance Characterization and Life-Cycle Testing."

Parametric Variation Tests

Parametric variation tests are an extension of the standard test procedures to measure the sensitivity of maturing battery technologies to variations of certain parameters. Tests in this classification include

- Cycle life vs temperature
- Cycle life vs DOD
- Cycle life vs peak power (or rate of discharge)
- Peak power vs cycle life
- Impact of regenerative braking on cycle life.

Special Studies

These research-oriented activities provide special insight into battery behavior as affected by application-oriented requirements. This classification includes the following activities:

- Impact of pulsed silicon-controlled rectifier (SCR chopper) discharges on battery performance
- Charge optimization vs temperature and life
- State-of-charge (SOC) algorithm determination
- Rapid charging
- Complex internal impedance measurements vs operating conditions and life
- Projected EV range, based upon generalized

battery parameters
* Analysis and evaluaticn of FUDS as a candidate for a standard driving profile in the battery testing program.

Summary of Test Results

The following sections describe the results of various tests conducted at NBTL in the three categories described above. Tests in the standard performance characterization and life-cycle categories were virtually all supported by the DOE Office of Energy Storage and Distribution; parametric variation tests and special studies were supported by both the Office of Energy Storage and Distribution and by the Electric and Hybrid Propulsion Division.

Results of Standard Performance Characterization and Life-Cycle Testing

Since the NBTL became operational in 1978, about 1400 cells (generally in the form of 4- to 6-cell modules, but up to 140-cell battery packs) have been evaluated under the Battery Test and Evaluation Program for DOE. These cells have been of various technologies, from nineteen battery developers. Table 3-1 lists the number, type, and capacity of the cells delivered to NBTL from contractors. Table 3-2 shows the ranges of specific energy, efficiency, and cycle life demonstrated in the standard performance characterization and life-cycle testing at NBTL.

Table 3-1. Cell Tests at NBTL, June 1978 Through December 1985

Source	System	Number of Cells*	Nominal Rated Cell Capacity (Ah)
Eltra	ISOA Lead-Acid	54	165
Exide	ISOA Lead-Acid	100	180
Globe/JCI	ISOA Lead-Acid	411	240/183
Globe/JCI	Advanced Lead-Acid	10	285/260
Globe/JCI	Advanced-II Lead-Acid	1	174
GE/Globe	IGCB[†] Lead-Acid	36	174
GE/Globe	Hybrid Lead-Acid	12	105
Exide	Advanced Lead-Acid (LL[‡])	12	3100
Lucas Chloride	Tubular Lead-Acid	24	184
ERC	Nickel/Cadmium	20	195
Eagle-Picher	Nickel/Iron	185	330/270/200
GM/Eagle-Picher	Nickel/Iron	10	160
Eagle-Picher	Hybrid Nickel/Iron	27	75
NIFE	Nickel/Iron	10	245
SAFT	Nickel/Iron	20	210
Westinghouse	Nickel/Iron	73	220
Eagle-Picher	Nickel/Zinc	20	225
Electrochimica	Nickel/Zinc	7	225
ERADCOM/ERC	Nickel/Zinc	24	128
ERC	Nickel/Zinc	56	240
Exide	Nickel/Zinc	4	290
Gould	Nickel/Zinc	49	400/225
GM/Delco Remy	Nickel/Zinc	16	144
Yardney	Nickel/Zinc	26	220
Eagle-Picher	Lithium/Iron Sulfide	9	390[¶]
Gould	Lithium/Iron Sulfide	19	239[¶]
Ford Aerospace	Sodium/Sulfur (LL[‡])	4	150
Ford Aerospace	Sodium/Sulfur (EV)	5	55
Exxon	Zinc/Bromine	132	80/190
EDA	Zinc/Chloride (LL[‡])	24	1050
		1400	

*These cells have been tested or are under test at NBTL
†Improved gell-cell, lead-acid battery
‡Load-leveling
¶Theoretical capacity

Table 3-2. Performance Data of Cells Tested at NBTL, December 31, 1985

	Specific Energy (Wh/kg)	Energetic Efficiency (%)	Cycle Life*
ISOA Lead-Acid			
Eltra	40	71	95
Exide	36	70	530
Globe/JCI	41	85	503
Advanced Lead-Acid			
Globe/JCI	47	74	185
Exide (LL)	26	78	>1866 Actual at 50°C (>5226 equivalent at 25°C)
Advanced-II Lead-Acid			
Globe/JCI	41	80	20
Tubular Lead-Acid			
Lucas Chloride[‡]	30	72	>144[†]
Nickel/Cadmium			
ERC	46	70	>254
Nickel/Iron			
Eagle-Picher I	47	65	1064
Eagle-Picher II	57	58	155
NIFE[‡]	38	48	189
SAFT[‡]	50	—	>22
Westinghouse	45	49	1329
Nickel/Zinc			
Eagle-Picher[‡]	50	70	38
Electrochimica	48	75	>352
ERC	46	73	76
Exide	42	48	35
Gould	68	72	200
GM/Delco Remy[¶]	52	81	280
Yardney	62	80	14
Lithium/Iron Sulfide			
Eagle-Picher	78	87	1093
Gould	79	86	522
Sodium/Sulfur			
Ford Aerospace (LL)	159	83	>1030
Ford Aerospace (EV)	147	89	>112
Zinc/Bromine			
Exxon	—	53	>60
Zinc/Chloride			
EDA (LL)	NA[§]	65**	>40

*>Indicates tests are continuing
[†]For programmatic reasons, test was terminated at 144 cycles while modules were still at ~100% of rated capacity
[‡]Direct purchase
[¶]Developed entirely by corporate funds; on loan to NBTL for testing
[§]Not measured; load-leveling design with extensive auxiliary equipment
**At the battery terminals, neglecting energy for all appurtenances

For EV battery testing, specific energies in lead-acid cells of up to 47 Wh/kg and in nickel/iron modules of up to 57 Wh/kg have been measured. Cycle life of over 600 cycles have been demonstrated for some lead-acid modules, and over 1300 cycles for some nickel/iron modules. In general, though, these same modules have not attained the highest specific energies. Specific energies, based upon naked cell weight, have been exhibited in nickel/zinc modules of up to 68 Wh/kg and in sodium/sulfur cells of up to 147 Wh/kg. Cycle life up to 280 cycles has been obtained for the nickel/zinc cells and over 112 cycles for the sodium/sulfur cells that continue under test at NBTL.

In an accelerated life test program, an Exide advanced lead-acid load-leveling module, still under test, has achieved >1860 actual cycles at 50°C, which translates to >5200 equivalent cycles at 25°C. In addition, FACC's sodium/sulfur load-leveling cells, placed under test in mid-1984, have accrued from 659 to 1030 test cycles.

Testing of a 50-kWh zinc/chloride load-leveling battery was continued through 1985 into 1986. In tests at NBTL, the battery has exhibited its rated capacity of 48 kWh and rated electrochemical efficiency (neglecting accessory energy) of 60% to 65%. The battery has accumulated 40 cycles, some of which were achieved in unattended around-the-clock operation. Although successes have been realized in the operation of this battery, time and labor were required to replace the gas pump a number of times, to repair leaks, to purify the electrolyte, and to adjust the hydrate-forming system. EDA was most helpful in responding to these needs.

Another halogen battery system, shown in Figure 3-1, was delivered and operated in mid-1985. The Exxon zinc/bromine 30-kWh 124-cell EV battery provided preliminary test information indicating that the specific energy of this unit may be power-limited between 25 and 40 W/kg, and that the thermal management system may be marginal. The battery is experiencing start-up and operational problems. Once the system is operating satisfactorily, additional data will be obtained to refine these preliminary results.
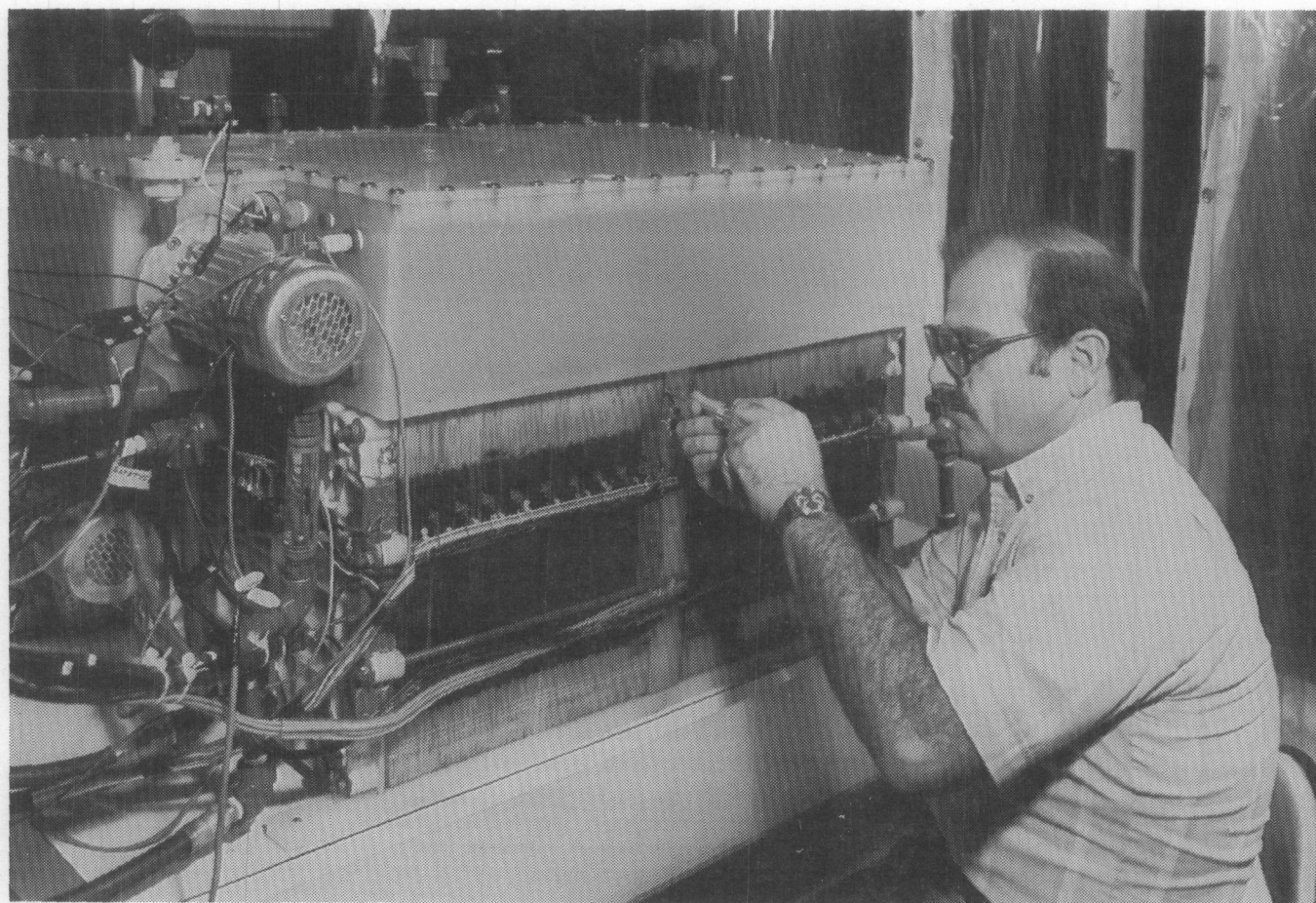

Figure 3-1. An Exxon 30-kWh Zinc/Bromine EV Battery Under Test at the NBTL. This battery is typical of the many advanced battery types that are routinely characterized in this computer-automated facility.

Two advanced EV technologies from JCI were tested. Experimental flow-by proof of concept and flow-through lead-acid cells were characterized and yielded specific energies of 48.8 and 41.2 Wh/kg, respectively. As a result of the successful demonstration of increased utilization, JCI is now working to improve the cycle life on future versions beyond the 116 and 20 cycles, respectively.

Additional EV technologies placed under test at NBTL in 1985 included four ERC nickel/cadmium five-cell modules, four SAFT nickel/iron five-cell modules, two Eagle-Picher nickel/iron 1985-technology five-cell modules, four Lucas Chloride tubular lead-acid three-cell modules, and five FACC sodium/sulfur cells.

The ERC nickel/cadmium modules are undergoing performance characterization and life tests (80% DOD) with results that indicate specific energies of 46 Wh/kg and a cycle life of ~254 cycles.

The SAFT nickel/iron modules were placed under test in November 1985 and have accumulated 22 cycles to date. A preliminary specific-energy measurement of 50 Wh/kg places these modules within the range of specific energy measured at NBTL for other nickel/iron technologies.

The tests performed on the Lucas Chloride EV-5T tubular lead-acid modules revealed specific energies equivalent to the Exide EV-106, a standard golf-cart battery with rubber separators (see Figure 3-2). Because of program priorities, the EV-5T module's life test program was terminated at 144 cycles, whereas the modules were in excellent operating condition, exhibiting ~100% of rated capacity.

The FACC sodium/sulfur EV cells were placed under performance and life tests in May 1985. Their specific energy (based on naked weight) exceeds 145 Wh/kg. Four of these cells have accrued >100 cycles. A fifth cell failed at 57 cycles. The specific energy of these cells, as expected, exceeded those of all other technologies. They were more rate-sensitive, however, and it should be kept in mind that this specific energy is based on the naked cell weight and does not include the burden of battery system hardware and insulating enclosures.

A conclusion drawn from the test program on both the FACC EV and LL sodium/sulfur cells is that these cells may suffer permanent damage if specific voltage/current relationships are exceeded near the end of their discharge. Another observation is that constant-current/constant-voltage (CI/CV) charging can extend considerably the useful life of these cells. Preliminary evidence suggests that eventually sodium/sulfur cells become charge-acceptance-limited, and CI/CV charging allows them to charge fully with an extended charge time.

In contrast to previous technology, Eagle-Picher's 1985 nickel/iron technology has shown an increase in specific energy as a function of specific power, but a decrease in specific peak power as a function of DOD.

Testing of a 1-kWh zinc/bromine module manufactured by Exxon began in July 1985. The module is performing in accordance with the manufacturer's specifications. A total of 60 cycles have been accumulated on the module, and during this period the capacity of the module has declined from an initial 75 to 65 Ah with 100-Ah charges. The loss of bromine by absorption into the module container is believed to be the cause for the capacity loss. Preliminary tests were conducted to determine the module's available discharge capacity as a function of charge ampere-hour level. A discharge capacity of 75 Ah was achieved with a 100-Ah charge, and 84 Ah was obtained with a 120-Ah charge. With an 80-Ah charge, module capacity was reduced to 62 Ah. These data indicate that the charge acceptance of the zinc/bromine system is similar to that of the nickel/iron system. A difficulty with the nickel/iron system was knowing the overcharge level needed to achieve a desired state of charge, especially from partial DOD levels. A similar problem is anticipated on the zinc/bromine system and the module's test plan includes a study of this matter. An open-circuit-after-charge (OCAC) test was also conducted to measure the capacity loss at full charge as a result of self-discharge with the electrolyte circulation pumps in continuous operation. OCAC times from 0 to 8 h were examined. A module capacity loss of ~14% was measured after a 4-h OCAC time, and a 24% loss resulted after 8 h. This test was to be repeated with the circulation pumps off during the OCAC times, but pump failures have caused delays.

A 30-kWh zinc/bromine battery was assembled and interfaced to the NBTL test system in September 1985. Fully automated cycling began in October using the NBTL computer system. Only about 19 cycles have been accumulated on this battery because of a number of shutdowns caused by pump and indicator malfunctions. Preliminary tests were conducted to measure the effects of discharge rate on the battery's available energy. Constant-current discharges at the 2-, 3-, and 5-h rates and constant-power discharges at 10-, 25-, and 40-W/kg rates were examined. These preliminary data are unconfirmed because of testing delays caused by the repair shutdowns. Table 3-3 shows the preliminary test data (data have not been reproduced).

Table 3-3. Preliminary Test Data on 30-kWh Zinc/Bromine Battery

Battery Weight: 547.3 kg
Number of Cells: 248 (124 cells/stack, with two stacks in parallel)

Specific Power Level of Discharge (W/kg)	Specific Energy (Wh/kg)	Energy Efficiency (%)
10	48.10	53.6
25	48.33	53.9
40	36.69	40.9

As stated in previous reports, one of the most useful tests performed at NBTL is the mapping of the specific energy available from a battery as a function of the specific power level at which it is discharged. This map is defined as a Ragone plot. An updated Ragone plot for several EV batteries tested at NBTL is shown in Figure 3-2.
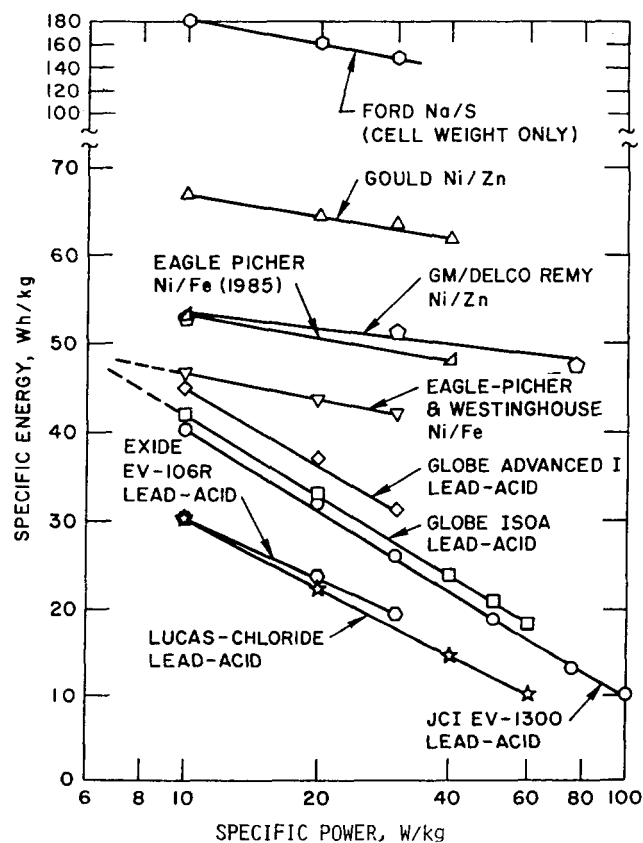
Figure 3-2. NBTL-Derived Ragone Plot Showing Specific Energy as a Function of Specific Power Level of Discharge for Several Types of EV Batteries

The Ragone plot shows that except for the naked sodium/sulfur cell, the nickel/zinc batteries manifest the highest specific energies. The nickel/zinc and nickel/iron batteries show the lowest sensitivity to power demands. The plot also shows the increased specific energy of the Eagle-Picher 1985 nickel/iron battery; however, as will be shown, the specific peak power of the Eagle-Picher 1985 battery is lower.

Figure 3-3 depicts specific peak power as a function of DOD for several of the EV batteries in Figure 3-2. Examination of the peak-power curves, as reported in 1984, shows that for the EV application the nickel/zinc system exhibits the highest specific peak power, followed by nickel/iron and then lead-acid. The figure also shows the higher peak-power capabilities of the lead-acid and nickel/iron systems for the hybrid vehicle application expected from their designs. This observation supports the contention that peak-power capability is not necessarily an intrinsic property of a technology, but is dependent on the design and construction of the battery.
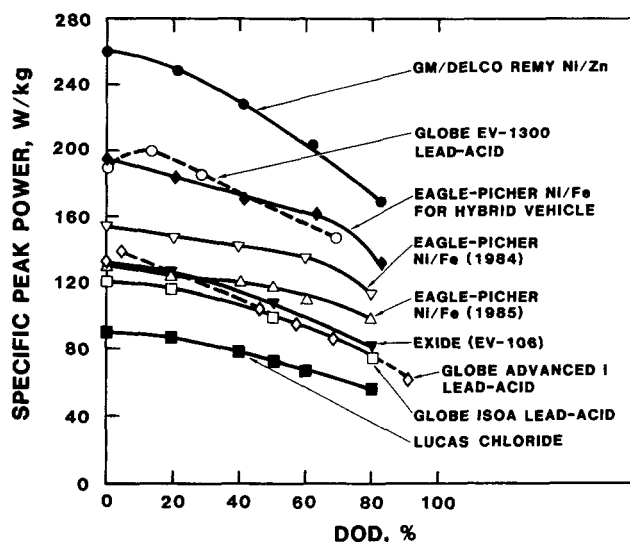
Figure 3-3. Specific Peak Power as a Function of DOD for Several Types of Aqueous Mobile Batteries Measured at NBTL

In 1985, the methodology that combined the Ragone plots with the peak-power plots to estimate battery discharge times (and vehicle ranges) for arbitrarily structured load profiles continued to be developed and refined. If the Ragone and peak-power information, such as that illustrated in Figures 3-2 and 3-3, are known, then only the average and peak-power demands on the battery are required of the application load profile; the detailed structure of the load profile is not essential. Several benefits accrue by using this methodology:

68

- Discharge times can be estimated for a host of application requirements without having to apply specific discharge profiles to the battery. Testing costs can be avoided, and discharge times for specific applications can be assessed, even though applying such discharges may be inconvenient or impossible.

- If a specific discharge profile is applied, a consistency check can be applied. If the results of this test do not agree with the estimate obtained by the methodology, reasons for the variance can be explored immediately.

- A convenient tool is provided for sensitivity analyses in determining the impact on battery discharge times of load profiles having various peak and average power demands on the battery. Trade-offs become quickly evident, and a beneficial insight into the relationship between peak and average power characteristics of a battery is provided.

Results of Parametric Variation Tests

Tests to determine the impact of DOD on cycle life for ISOA lead-acid batteries were completed. In these tests, two modules were discharged a fixed relative number of ampere-hours (30% of the ampere-hours achieved on a room-temperature capacity measurement at 100% DOD). End-of-life criterion was defined as the time at which the capacity of the modules declined to <75% of their original capacity. Cycle lives of 1507 and 1648 were achieved. This result compares to a cycle life of about 503 cycles achieved in previous tests when 80% discharges were used. Thus, indications are that the use of this battery technology at lower DOD offers only a slight benefit to the total ampere-hours throughput of the battery; in other words, cycle life appears to increase roughly in inverse proportion to the DOD, at least for DODs up to 80%.

In a program supported by EPRI, the effects of different peak-power demands on the cycle life of the EV-2300 lead-acid modules fabricated by JCI were evaluated. Six 12-V modules were used in this evaluation. Two modules were cycled under a simulated EV driving profile having a peak power of 57 W/kg; a second pair was cycled with a profile having a much lower peak power, 35 W/kg. Both profiles had an average power requirement of 15 W/kg. A third pair of modules was cycled using constant-current discharge at the $C_3/3$ h rate for comparison. The impact of an 8-h open-circuit period after charge and discharge was also evaluated. The following observations resulted.

Under the simulated driving profiles, the module capacity decreased as the peak-power demand in-

creased, even though the average power required remained constant. The degree to which the capacity decreased was in good agreement with that obtained by applying the methodology described in the previous section. In other words, the available capacity under the driving profile was limited by the modules' decline in power capability at high DODs. In addition, the number of charge/discharge cycles attained by the EV-2300 module before it failed to deliver 80% of the initial projected vehicle range under the driving profile declined significantly as the peak-power demand of the profile was increased. When the failure criterion of a 20% loss of projected vehicle range on the driving profile was reached, the modules still retained the capability to deliver nearly their initial capacity under constant-current discharges at the $C_3/3$ h rate. Thus, a loss of peak-power capability was indicated, with no loss of capacity at nominal discharge rates. The 8-h open-circuit periods imposed after discharge and after charge had no significant effect on cycle life.

Results of Special Studies

Special charge and discharge studies were conducted to quantify inherent characteristics and to identify operational factors that affect the available capacity and efficiency of EV batteries. This type of information is needed to design battery chargers and vehicle propulsion systems that will provide maximum battery performance and life and minimize maintenance.

During 1985 we completed tests to quantify the relationship among available capacity, applied overcharge, and depth of discharge for an EV-3000 lead-acid battery. The data show that the charge acceptance of a lead-acid battery rapidly declines to zero as a 100% SOC level is approached. Figure 3-4 shows the SOC (measured 100% DOD capacity divided by maximum available capacity) achieved by an ISOA EV-3000 lead-acid module as a function of the applied recharge factor (RF) (RF = charge Ah divided by discharge Ah) when operated at DOD levels of 25%, 75%, and 100%. As the DOD level is increased, a greater overcharge is needed to attain maximum capacity. About 8% overcharge is needed for 75% and 100% DOD operation, but only about 4% is needed for 25% and 50% DOD operation. In practice, applying an 8% overcharge (9.6 Ah) for 50% DOD operation instead of the minimal 4% (4.8 Ah) results in an extra 4.8 Ah of electrolysis, which consumes ~1.6 mL of water in each battery cell during each charge. For each charge of a 200-V lead-acid battery, 160 mL of electrolyte water would be needlessly consumed and an extra 216 L (7.7 ft^3) of hydrogen gas would be generated. We found also that the ISOA EV-3000

battery achieved a reproducible 99.2% SOC from 75% and 100% DOD with a 6% overcharge and a SOC of >99% from 25% and 50% DOD with only a 3% overcharge. Based on these EV-3000 data, it would be inefficient and cause increased battery maintenance to (1) always recharge the battery to a full 100% SOC condition or (2) accumulate partial discharges to recharge from a deeper discharge condition. Extended operation at slightly reduced SOC levels was not examined during this study, but we believe that such operation may eventually result in an irreversible capacity loss. However, we also expect that periodic 8% overcharges should retain maximum capacity while minimizing the maintenance requirements of the EV-3000 battery. The acquired data—which relate capacity, overcharge, and DOD level—permit definition of an optimum charge algorithm that ensures the achievement of full capacity without excessive overcharge. Applying only the minimum overcharge level needed for full capacity offers advantages of (1) reduced generation of gases, (2) reduced water consumption, (3) cleaner battery containers, (4) reduced maintenance, and (5) increased battery life. A smart charger that furnishes the miminum overcharge correlated with the initial DOD of the battery can realize a significant reduction in the hydrogen gas management and maintenance requirements of an EV-3000 battery. Regardless of the method used to ascertain battery DOD data, a charger is needed that would terminate the charge based on those data.

NBTL also completed studies on the internal impedance of nickel/iron batteries. Test data show that the battery's internal resistance is almost constant during discharge, regardless of the discharge rate or battery age (number of cycles applied). A constant resistance allows the determination of an internal current times cell resistance-free (IR-free) voltage during discharge, from the equation

$$V_B = V_A + I_A R_B ,$$

where V_B is the IR-free voltage, V_A is the battery terminal voltage, I_A is the load current, and R_B is the internal resistance. The values of V_A for a 6-V, 270-Ah nickel/iron module measured at constant-current dis-

charge rates of 90-, 180-, and 270-A are plotted in Figure 3-5 as a function of Ah-DOD level. Also plotted are the computed values for V_B at the three discharge rates. The plots show that V_B is essentially independent of discharge current. Only after ~90% DOD (>200 Ah) is there an apparent increase in internal resistance, which causes the IR-free voltage curves at the different discharge rates to separate slightly. These results indicate that the battery's internal IR-free voltage may be usefully employed as a DOD measure, which could serve as an accurate and reliable "fuel" gauge for electric vehicles equipped with nickel/iron batteries.
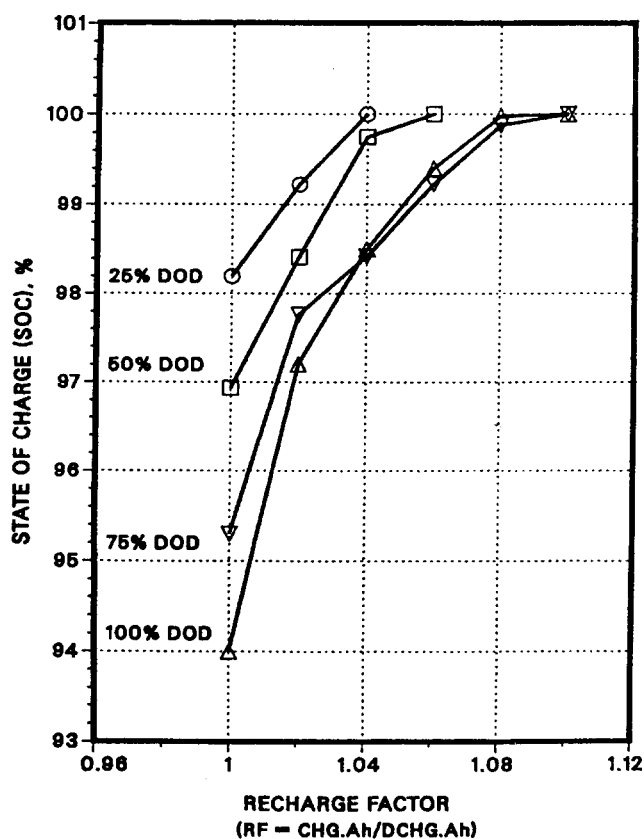
Figure 3-4. State of Charge Achieved by ISOA EV-3000 Lead-Acid Module as a Function of Applied Recharge Factor

BID: 70 TESTS: 10 NI/FE VOLTAGE @ 90,180,270A DCHG.RATES   04-NOV-85
TCT NAME: DRT90T270   10:29:38
STATION NAME: 43
TIME SETS: 23

CYCLES
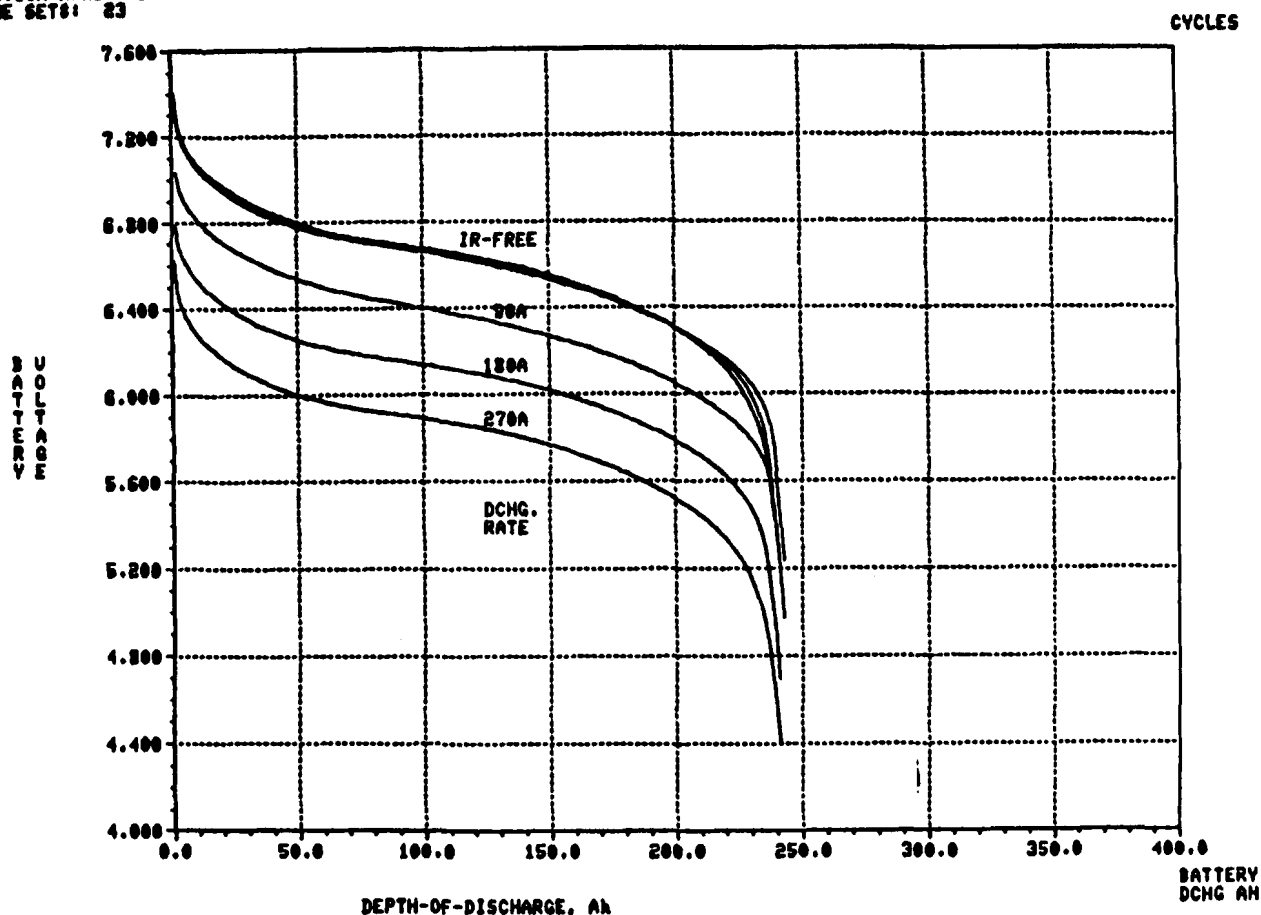
Figure 3-5. Discharge Voltages and Calculated IR-Free Voltages vs DOD for EPI Nickel/Iron Battery

The effects of temperature on the characteristics of a 200-Ah nickel/iron battery from Eagle-Picher Industries (EPI) were also examined in 1985. The results showed that the discharge capacity of a nickel/iron battery is directly related to its operating temperature, but its charge acceptance is maximal near 25°C. Battery charge acceptance was decreased by 6% at 0°C and 50°C from that obtained at 25°C. It was also determined that the self-discharge losses of the nickel/iron system are virtually the same at 0°C and 25°C, but are increased significantly at 50°C. The ampere-hour capacity loss for a 4-h OCAC period was increased from 7.5% to 13% as the temperature was increased from 25°C to 50°C (9% to 15% increase in watt-hour loss). In the first 0.5 h after charge, the ampere-hour self-discharge loss was doubled at 50°C (~6%) from that measured at 0°C and 25°C (~3%).

This corresponds to an increase in self-discharge rate from 8 to 16 A. It is believed that this increased self-discharge rate occurs in the latter portion of charge and, thereby, causes the 6% decrease in battery charge acceptance at 50°C. Supporting effects include a 6% decline in battery ampere-hour efficiency (4% Wh efficiency loss) as the charge rate is reduced from 50 to 25 A at 50°C. At temperatures of 0°C and 25°C, this decrease in charging rate had no effect on energy efficiency and only a 1% decline in ampere-hour efficiency.

Low temperatures were found to have a greater impact on the battery's internal resistance and IR-free voltage than that caused by high temperatures. For a 25°C increase in ambient temperture (from 25°C to 50°C), battery IR-free voltage increased <1% and battery resistance decreased by only 3%. However, a

71

25°C decrease in ambient temperature (from 25°C to 0°C) resulted in a 2.3% decrease in the IR-free voltage and ~22% increase in resistance.

For these reasons, the available capacity and operating efficiency of a nickel/iron battery are maximal near 25°C. Plots of measured discharge capacity at 100% DOD of a 6-V, 200-Ah nickel/iron module vs the applied recharge factor at 0°C, 25°C, and 50°C are given in Figure 3-6. In these tests, the module was charged at a constant current of 50 A for 50 to 250 Ah and discharged at this same current to 100% DOD. The measured capacities were normalized to those obtained with 200-Ah charges at 25°C. Using a fixed overcharge level of 30%, the available discharge capacity of the nickel/iron battery is decreased from that obtained at 25°C by 10% at 50°C and by 20% at 0°C. Similarly, to maintain the same available Ah capacity achieved at 25°C with an overcharge of 20%, the overcharge level must be doubled at 50°C (to 42%) and tripled at 0°C (to 60%). The plots indicate that the performance of the nickel/iron battery is optimal near 25°C. This optimum is the result of increased self-discharge losses at elevated temperatures (50°C) and a decreased charge acceptance and available energy at reduced temperatures (0°C).

RECHARGE FACTOR = CHG AH / DCHG AH
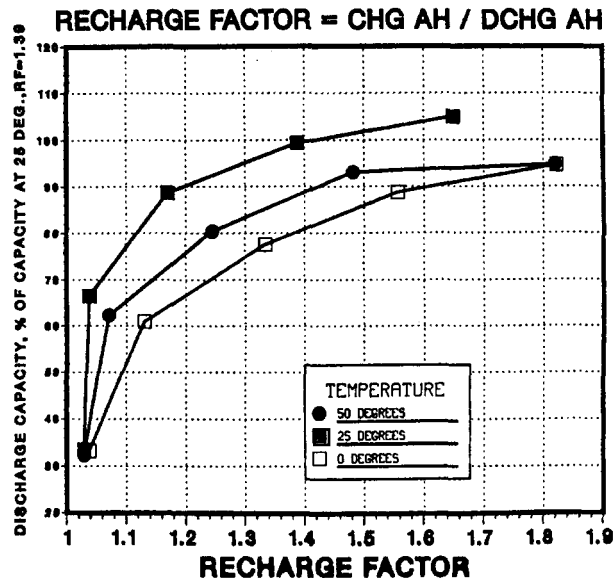
Figure 3-6. Nickel/Iron Discharge Capacity as a Function of Applied Recharge Factor

Advanced Lead-Acid Batteries for Electric Utility Load Leveling

ANL, with the cooperation of SNL, has worked on the development of lead-acid batteries for load-leveling applications since 1979. The goal of this program has been to advance the lead-acid technology to meet the cost and performance requirements of this application. Key objectives were to increase battery life from 2000 to 4000 cycles while maintaining low initial battery cost. Until April 1985, ANL directed two cost-shared R&D contracts awarded to Exide and to C&D Batteries. Under the Exide contract, a prototype design was developed and three modules were delivered to NBTL in April 1982 and one in mid-1985 as contract deliverables for testing and evaluation. One module delivered in 1982 contained six cells with a rated capacity of 3100 Ah and 36 kWh at the 5-h discharge rate. The other two units delivered in 1982 were three-cell, 18-kWh modules. The unit delivered in 1985 was also a six-cell module with a rated capacity of 3100 Ah and 36 kWh. It will be placed on test in 1986.

The test program for these load-leveling modules includes performance characterization tests and accelerated life-cycle (80% DOD) tests. The results of parametric performance evaluation and simulated application tests were described in previous reports. In 1985, life-cycle tests were continued as planned on all three 1982-delivered modules. The six-cell, 36.0-kWh module was life-cycled at a temperature of 50°C; each cycle at 50°C is assumed to be equivalent to 2.8 cycles at 25°C. To date, over 1865 actual cycles (5200 equivalent cycles) have been obtained on this module. Life cycling of both three-cell modules connected in series was also continued through 1985 at 60°C, where an acceleration factor of 4.1 was assumed. To date, over 3925 equivalent 25°C cycles have been obtained on one module and over 1875 on the other. The three-cell module with 3925 equivalent 25°C cycles experienced an electrolyte leak due to a cell case failure in one cell in November 1985 and in another in December 1985. As a result, the decision was made to remove this module from the test program, even though the capacity was still 111% of rated. With life-cycle tests completed by Exide on other cells at 40°C, and future tests at ANL starting in 1986, these tests will provide a measurement of cycle life at different temperatures

and thereby permit an assessment of the feasibility and projected economics for load-leveling applications. In testing to date at NBTL, the Exide lead-acid load-leveling modules have operated reliably, with performance exceeding the 4000-cycle design goals. Life-cycle testing will be continued to failure on the remaining two modules delivered in 1982, and will be started in 1986 on the module delivered in 1985.

Battery Information Notebook

The NBTL Battery Information Notebook provides a vehicle for disseminating test information in a standard format to DOE battery users. As each battery technology completes the test program at NBTL, an information packet is issued to holders of the notebook. Information packets were distributed for the following batteries: (1) performance characterization testing of Globe/JCI EV-2300 and EV-3000 lead-acid modules, and the Eagle-Picher nickel/iron hybrid module; (2) life-cycle testing of GM/Delco Remy nickel/zinc modules; and (3) a composite Ragone plot, a composite projected EV range chart, and a composite peak-power chart. Battery users indicate that the information in the notebook is most useful, and its contents are being considered for a computerized database.

NBTL Advances in Testing Capability

Advances were made in facility improvements and software development to meet the needs of the battery test program in 1985.

The testing capabilities at NBTL were expanded to include 91 independent, fully instrumented, computer-controlled test stations (described in the 1982 report), with the additional conversion of ten high-temperature test stations to sodium/sulfur from lithium-aluminum/iron-sulfide cells in anticipation of the delivery of sodium/sulfur cells from CSPL.

Several major additions were made to both the hardware and software components of the NBTL computer-automated data acquisition and process control systems. The following hardware upgrades were accomplished in 1985:

- The aging and no-longer-maintainable 300-Mbyte removable disk drive was replaced by a 456-Mbyte Winchester-type drive.

- System memory was expanded to 1.5 Mbyte.

- An Ethernet interface was added to increase our DECnet throughput and to decrease system loading for data transfer to the division's VAX 11/780. The link to the PDP 11/34 development system was also improved.

- A new magnetic tape controller was installed to replace a unit that was no longer maintainable.

The operating system for our PDP 11/44 was upgraded from RSX-11M V4.0 to RSX-11M+ V2.1 to make more effective use of the new Winchester disk drive and the DECnet Ethernet interface.

The development of the NBTL application software system continued in order to meet additional program requirements. Some of the more important software additions are summarized below.

- The graphics system software was expanded to allow plotting of the pressure transducer data for the zinc-chloride battery. A major rewrite of the entire graphics subsystem has decreased system overhead and increased system utility.

- Special software was developed, supported by EPRI, to interface to a charger/equalizer (designed by the Battery Component Test group) that was used for bulk and equalized charging of two lithium-aluminum/iron-sulfide modules.

- Special software was required to directly control pumps and valves of the Exxon zinc/bromine battery currently under test. Software was also needed to accommodate its unique discharge requirements and to monitor various alarm conditions.

- Further refinements were made in the software associated with the EDA zinc/chloride battery system in order to handle overpressure conditions. Data-sampling rates were increased during certain critical phases of its operation so as to be more responsive to rapidly changing conditions.

- Several unique charging algorithms were implemented, including "step charges," "charge, rest, and charge," and a "multistep charge" with a temperature-compensated voltage used as a terminating condition.

- Several special tasks were written to handle the test requirements of the sodium/sulfur cells. This included one task that dynamically calculates a discharge terminating cell voltage. All tasks related to sodium/sulfur cell tests feature a variable data-sampling rate that speeds up near the end of charge or discharge (for state termination checks) to fully protect cells against overcharging or overdischarging.

- Two new profiles were developed, under EPRI support, for a VW Electrotransporter bus using the SAE J227a "C" cycle—one a base version and the other a more simplified version.

• A program was developed to calculate peak power as a function of DOD from any driving profile discharge cycle.

Laboratory Evaluations at SNL

SNL battery evaluation activities were divided into two catagories:

1. *Prototype Battery Evaluation.* Sodium/sulfur cells, flowing electrolyte cells and batteries, nickel/hydrogen cells and batteries, and an improved lead-acid battery were tested under individualized parametric evaluation regimes. Computer-controlled test facilities completed in 1982 were used to perform these activities. Laboratory maintenance and calibration procedures were completed. Test control and data acquisition software were enhanced during the year to provide increased test regime flexibility. A 132-Mbyte disk drive and magnetic tape drive were added to the Hewlett-Packard 1000 central control computer to provide increased data reduction and archive facilities. One additional test bench under construction will provide more fume hood and temperature chamber test facilities when completed in 1986. Hardware was assembled for testing CSPL sodium/sulfur cells.

2. *Battery Field Tests for Solar Applications.* Two battery/solar energy system experiments were in progress at remote sites, while another was in progress at SNL's Photovoltaic Advanced Systems Test Facility (PASTF). Individually designed computer-controlled data acquisition systems were used at these sites. Another remote site experiment was planned, and a sealed lead-acid battery was purchased in 1985. A 20-kWh Exxon zinc/bromine battery was installed in May 1985 at SNL's PASTF.

The battery successfully completed characterization tests prior to its evaluation with a PV array, planned for 1986.

Flow Battery Test Results

Five flowing electrolyte systems were tested electrically, chemically, and mechanically during 1985. These units represented two technologies and three developers. Table 3-4 describes these cells and batteries.

The Exxon batteries were tested using "standard" electrolyte consisting of ~3 molar zinc bromide (discharged state) and ~1 molar quarternary ammonium compounds (bromine complexing agents). Two ammonium compounds were used, in equal ratios: N-ethyl, N-methyl morpholinium bromide and N-ethyl, N-methyl pyrollidinium bromide. The discharged electrolyte in the GEL, Inc. zinc/bromine battery comprised ~1.6 molar zinc bromide and ~2 molar ammonium chloride. In the zinc/ferricyanide system, each electrode required a specific electrolyte. The discharged zinc electrolyte consisted of a saturated solution of zinc oxide in 2N sodium hydroxide. The discharged ferricyanide electrolyte was a saturated solution of sodium ferrocyanide in 2N sodium hydroxide.

Both Exxon batteries continued life-cycle testing in 1985. The twenty-cell battery demonstrated declining performance, particularly near the end of the year, but the eight-cell battery performed well. Both Lockheed cells were removed from test. Multiple, nonrepairable cell case leaks caused one cell to fail. The other cell failed because of a nonfunctional zinc electrode and cell case leaks. The GEL zinc/bromine battery completed a factorial test matrix and was placed on a life-cycle test. By year's end this battery showed indications of declining capacity.

A summary of flow battery test results is presented in Table 3-5.

Table 3-4. Flow Cells and Batteries Tested at SNL During 1985

SNL ID No.		Developer (ID No.)	Start of Test	No. of Cells	Capacity (Ah)	System Weight (kg)
300	Zinc/Bromine	Exxon (PAM-18)	10/82	20	40 @ C/3	65
301	Zinc/Bromine	Exxon (S8-2)	10/82	8	40 @ C/3	46
345	Zinc/Ferricyanide	Lockheed	9/83	1	3.5 @ C/2	—
380	Zinc/Ferricyanide	Lockheed	4/84	1	3.5 @ C/2	—
394	Zinc/Bromine	GEL (DP-71)	12/84	17	130 @ C/4	118

Table 3-5. Flow Battery Data Summary, December 1985

SNL ID No.	Mean Coulombic Efficiency (%)	Mean Voltaic Efficiency (%)	Mean Energy Efficiency (%)	Total Cycles	No. of Cycles in 1985	Status
300	68.7 ± 0.4	67.6 ± 0.3	46.5 ± 0.4	727	324	On test
301	87.5 ± 0.2	77.9 ± 0.1	68.1 ± 0.2	1521	667	On test
345*	83 ± 1	76.3 ± 0.2	63.2 ± 0.8	520	274	Failed
380	82 ± 2	82.8 ± 0.4	68 ± 1	451	45	Failed
394	80 ± 2	81.4 ± 0.5	65 ± 2	193	171	On test

Uncertainties are 95% confidence limits.
*Data for improved polysulfone membrane only.

These efficiency values represent averages over the life of each unit while at SNL. One of the goals of these investigations was to evaluate these cells and batteries using meaningful and comparable test regimes. Individual design limitations were considered during test planning; test regimes for each cell or battery were different and involved various charge and discharge rates, zinc loading, and temperatures. Thus, individual test conditions must be considered when interpreting these data.

The key conclusions from these results are that long life is possible in the case of the Exxon technology, but identification of the exact characteristics of Battery 301 is necessary in order to understand why this battery has demonstrated long life. Degradation mechanisms such as elevated electrolyte pH and declining efficiencies observed in Battery 300 need a thorough investigation. For the GEL zinc/bromine battery, early performance was good but the battery deteriorated after <200 cycles. The reason for this decline needs to be defined. The GEL battery also exhibited decreased efficiency and capacity caused by elevated zinc loading. Further, the battery demonstrated charge and discharge rate limitations. The zinc/ferricyanide cell evaluations identified several problems with system design and materials durability. These design problems included the preparation of functional zinc electrodes, the imbalance of ferricyanide electrolyte, and the loss of electrical contact in the felt ferricyanide electrode. Materials problems included the degradation of cell case and plumbing components and membrane stability and function.

Flow Battery Evaluation Procedures Used at SNL

The evaluation procedure used on all these units consisted of electrical charge and discharge using various rates and states of charge. In addition, electrolyte chemical analyses were conducted. These were considered necessary for system maintenance and for evaluation of system problems. Data were collected on pump and plumbing longevity and maintenance requirements. Failure analyses were conducted on the units that failed during the year.

A typical electrical cycle for these systems consisted of a timed, constant-current charge related to a theoretical zinc loading. After a 1- to 5-min open-circuit wait following charge, a constant-current discharge was imposed until the cell or battery voltage fell below a cutoff level, typically 1.0 V per cell. Periodically, it was necessary to discharge these units to the completely discharged condition (0 V). This is a maintenance requirement of the zinc flow technology. The frequency of this deep discharge depends on the cell design and varies from every three to forty cycles. This frequency is a variable in the operation of these systems.

Baseline cycles were defined for each of the units tested. The cycles were based on developer guidelines and design information. These regimes and corresponding battery electrolyte characteristics are specified in Tables 3-6 and 3-7, respectively.

Table 3-6. Baseline Cycle Regimes for Flowing Electrolyte Systems

SNL ID No.	Electrode Area (cm²)	Charge Current Density (mA/cm²)	Discharge Current Density (mA/cm²)	Nominal Zinc Loading (mAh/cm²)
300	600	20	20	60
301	600	20	20	60
345	60	35	35	70
380	60	35	35	70
394	1936	10	10	62

Table 3-7. Electrolyte Characteristics for Baseline Cycles

SNL ID No.	Anolyte Pressure (psi)	Catholyte Pressure (psi)	Total Volume (L)	Operating Temperature (°C)	Utilization (%)
300	3	3	10	20	50
301	3	3	4	20	50
345	3	6	3	40	~20
380	3	6	3	40	~20
394	2.5*	2.5*	44*	25-45	54

*This battery contained only one electrolyte stream, and the pump operated for 12 s in 3 min. Pumps in the other systems operated continuously.

Other electrical tests were conducted in addition to baseline cycles. Self-discharge rate and internal resistance were determined. Once stable operation of a system was confirmed with baseline cycles, a factorial test regime was imposed on the Exxon and GEL batteries. This plan systematically varied charge and discharge rates, zinc loading, and in some cases temperature; the effect of such variations on efficiency and performance was determined. Typically, after this plan was completed, a qualified life-cycle test was begun. While not strictly a life test because of the previous treatment, these tests age the units and provide additional information about the system's longevity. The failure criteria for these tests was battery performance of <40% average energy efficiency for five consecutive cycles using the baseline test.

Failure was also declared if the cell or battery became unserviceable because of leakage or component failures.

The electrolyte chemical was analyzed using traditional wet methods and instrumental techniques. Bromine, ferricyanide, and trace metal concentrations were determined. Electrolyte pH was monitored and adjusted with hydrobromic acid to maintain a value of <3.0 in the Exxon batteries. Specific gravity and viscosity were measured for the GEL battery. These analyses were used to evaluate chemical changes during electrical tests.

Required and preventive maintenance was carried out. Problems with plumbing components, electrolyte pumps, thermal management systems, and cell case leaks were encountered, documented, and resolved.

Exxon 1.2-kWh Zinc/Bromine Battery (SNL ID No. 300)

Evaluation of the Exxon "controller" battery continued during 1985. A qualified life-cycle regime was used following the completion of the factorial test plan in 1984. Baseline cycles were run in sets of five cycles with intervening complete discharge operations.

Performance was stable early in 1985 but declined rapidly to below the failure limit (energy efficiency <40%) in August. Figure 3-7 illustrates electrochemical efficiencies for all cycles, cycles run in March 1985, and cycles run in August 1985, the last month of normal operation. Coulomic and voltaic efficiencies decreased during August, and energy efficiency declined to <10% on cycles run after August. No evidence was found of any weak individual cells in the battery during these last cycles.

added as hydrobromic acid resulted in high bromine concentrations in the anolyte and a significant amount of brominated complexing agent present at all times in both electrolytes. Bromine in large quantities in contact with the zinc deposit resulted in high self-discharge rates and poor coulombic efficiency.

Poor voltaic efficiency can be related to increased internal resistance. Polarization tests were run periodically during the life of the battery. Figure 3-8 shows the results of the tests plotted vs cycle life. The initial battery resistance was higher than a comparable eight-cell Exxon battery (ID No. 301) by ~300 mΩ. The resistance gradually increased during testing until, between Cycles 600 and 700, it increased by almost an order of magnitude. Attempts were made to run cycles following Cycle 727, but because of the high resistance very little energy could be discharged from the battery and the cycles were aborted.

Figure 3-7. Electrochemical Efficiencies for All Cycles, Cycles Run in March 1985, and Cycles Run in August 1985 (Battery 300)
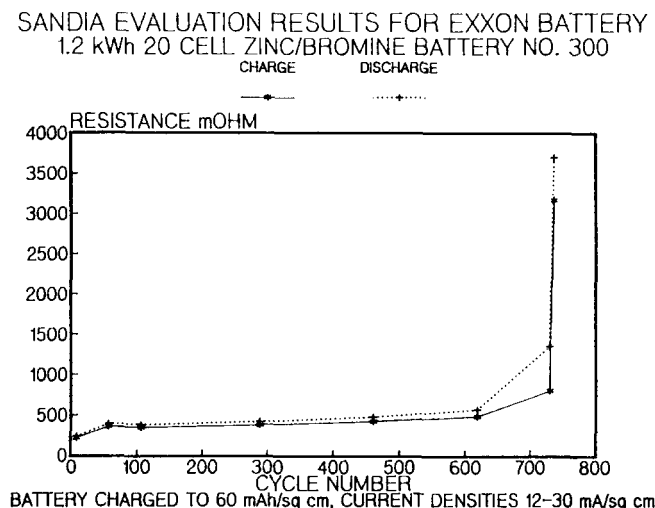
Figure 3-8. Battery Resistance vs Cycle Number (Battery 300)

Decline in coulombic efficiency can in part be attributed to the large quantities of hydrobromic acid (HBr) added to the electrolyte to maintain a pH of <3.0. Early in life (between Cycles 74 and 117), the battery required 0.3 mL hydrobromic acid/cycle to maintain the specified pH. Electrolyte pH gradually increased during the cycle testing and more hydrobromic acid was added as necessary. Between Cycles 543 and 585, 5.8 mL hydrobromic acid/cycle was added to the battery electrolyte for pH maintenance. If the pH was allowed to rise above 3.0, a gray floating precipitate formed in the electrolyte. This material blocked flow channels and caused very poor battery performance. However, the large quantities of bromine

In addition to pH maintenance, several other maintenance procedures were performed. The anolyte pump motor was replaced once and the catholyte pump motor was replaced twice. The plastic tubing used for a heat exchanger in the anolyte reservoir became brittle and broke, flooding the reservoir with distilled water. This problem was corrected by replacing the tubing and 4 L of electrolyte.

Following suspension of the electrical tests, several chemical analyses were initiated to characterize the observed behavior. This work was coordinated with SNL's organic chemists already involved with studies of the materials used in Exxon batteries. A preliminary analysis of the high electrolyte pH

precipitate mentioned above indicated it might be a degraded form of the bromine complexing agent. Further results from these activities will be available in early 1986. The battery will be disassembled in 1986 to determine the cause of failure and to complete the evaluation process.

Exxon 500-Wh Zinc/Bromine Battery (SNL ID No. 301)

Evaluation of an Exxon eight-cell battery continued through its third full year in 1985. A qualified life-cycle test, begun in 1984, continued using primarily baseline cycles. At the beginning of the year, a complete discharge was performed between each set of five cycles. After problems were encountered with one weak cell, a complete discharge was performed between each set of three cycles. This latter mode provided stable battery performance during the year.

Electrochemical efficiency performance declined while adjustments were made to the complete discharge schedule because of the weak cell. Figure 3-9 shows average efficiencies for each month of the year. A slight downward trend was observed during the year. Average monthly efficiencies by the end of 1985 were down approximately 4% coulombic and 2% voltaic when compared with those at the start of the year. By the end of 1985 the electrochemical energy efficiency exceeded 65%, still within nominal performance for the Exxon design.

SANDIA EVALUATION RESULTS FOR EXXON BATTERY
500 Wh 8 CELL ZINC/BROMINE BATTERY NO. 301
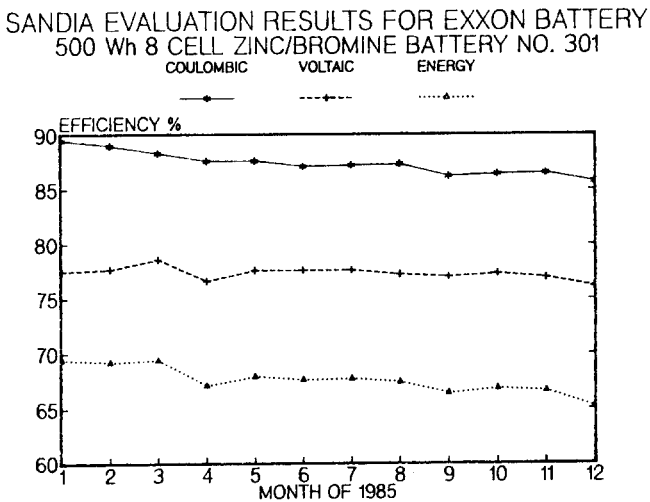
Figure 3-9. Monthly Efficiencies of Battery 301

Two factors contributed to the decline in performance. The primary cause was the weakening of one cell in the stack. A weak cell is one with a smaller capacity (zinc loading) compared to the other cells in the stack. It is easily observed when the battery voltage decreases by 1.5 V during discharge and then stabilizes for a time before the 1.0-V/cell cutoff is reached. The decrease in battery voltage can be described as cell dropout. It was first observed on this battery late in 1984 during a set of ten consecutive cycles without an intervening complete discharge. After returning to the standard mode of five cycles between complete discharge operations, the problem did not recur until Cycle 946 in March 1985. It occurred inconsistently at first, but steadily increased in frequency (see Figure 3-10). Once complete discharge operations were conducted every three cycles, the weak cell was rarely observed.

SANDIA EVALUATION RESULTS FOR EXXON BATTERY
500 Wh 8 CELL ZINC/BROMINE BATTERY NO. 301
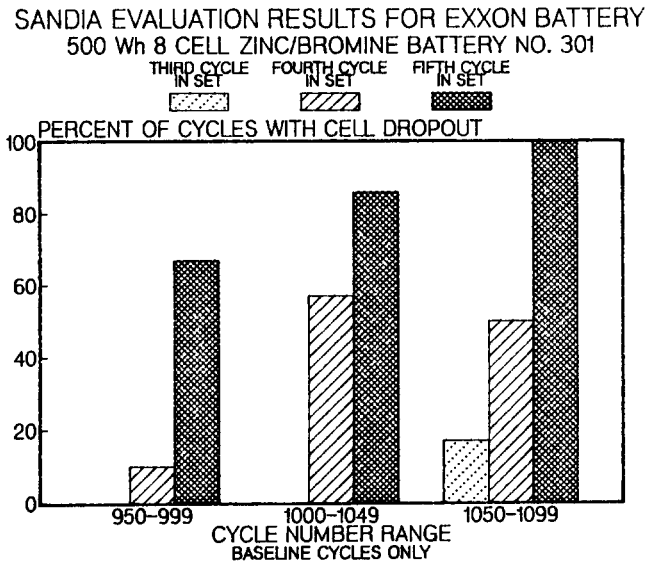
Figure 3-10. Percent of Third, Fourth, and Fifth Cycles in a Set With Cell Dropout for Three Ranges (Battery 301)

To further characterize the weak cell's behavior, parametric variations using increased electrolyte flow rates, increased charge and discharge current densities, and decreased zinc loading during cycle operation were conducted. Increasing the electrolyte pump's output from the nominal 3.0 psi to 3.6 psi reduced the incidence of cell dropout on the fifth cycle of a set by 80%. Higher current densities tended to increase the frequency of cell dropout, whereas decreased zinc

loading reduced the frequency by ~20%. These data indicate that the weak cell may be caused by the partial obstruction of a flow channel. The uniformity and thickness of the zinc deposit may be a factor. Some data indicate that, in addition to the frequency of the complete discharge operations to control the weak cell problem, the duration of the complete discharge may also be a factor. This behavior will be studied further in 1986.

Performing complete discharge operations more frequently also contributed to the decrease in efficiency. There is an approximate 5% coulombic efficiency penalty in this battery for cycles run immediately after the complete discharge, compared to those cycles run without a preceding complete discharge. Therefore, performing a complete discharge every three cycles instead of every five cycles leads to more cycles that suffer the efficiency penalty and thus a lower average efficiency.

Apart from these changes, operation of the battery was stable. Battery resistance did not increase noticeably during the year. Average battery resistance at 60 mAh/cm² of charge between 12 and 30 mA/cm² as measured periodically during the year, was 110 mΩ on charge and 120 mΩ on discharge. These measurements have a lack of reproducibility of ~10%.

Maintenance consisted of electrolyte pH measurements and adjustments. The battery required 0.36 mL of hydrobromic acid per cycle to maintain the pH at <3.0. This value was calculated between Cycles 1196 and 1251. Electrolyte pH did not tend to increase during the year, and no precipitates were observed. One catholyte pump motor was replaced following Cycle 957. Both plastic reservoirs were replaced because of brittleness. The electrolyte plastic cooling tube broke and flooded the reservoirs with distilled water during Cycle 1492. The tubing was replaced, new electrolyte was installed, and cycling was resumed. The old electrolyte had been in the battery since Cycle 228; it had accumulated 1265 cycles. Approximately 25% of its volume had been replaced in small increments between Cycles 228 and 1492. These additions were necessary because electrolyte was lost during sampling, maintenance, and because of minor leaks. Also during this interval, a cumulative amount of hydrobromic acid equal to ~6% of the total volume had been added. This resulted in a bromine-rich electrolyte that may have slightly decreased coulombic efficiency. These results have implications regarding

maintenance of large batteries: reducing pH by the simple addition of hydrobromic acid over long periods may result in reduced coulombic efficiency and increased materials degradation caused by high bromine concentrations.

The evaluation of this battery will continue in 1986. It remains the longest-lived example of the Exxon zinc/bromine battery technology.

GEL Zinc/Bromine Battery (SNL ID No. 394)

Evaluation of the GEL battery, begun in late 1984, continued in 1985. This battery was designated by GEL as a Duke Power design type. After stable baseline performance was established early in the year, a factorial test regime was imposed. The three factors and their levels are listed in Table 3-8.

Table 3-8. Factorial Test Plan for GEL Zinc/Bromine Battery

| | Levels | | |
Factors	Low Point	Center Point	High Point
Charge rate (mA/cm²)	5	10	15
Discharge rate (mA/cm²)	5	10	15
Zinc loading (mAh/cm²)	46	62	77

The main effects from this regime were calculated for coulombic, voltaic, and energy efficiencies. These results are plotted in Figure 3-11. The pattern of this response is similar to that of the Exxon zinc/bromine batteries under a comparable test regime except for the large negative effect of high zinc loading. This difference is probably due to the lack of a separator in the GEL design. Without a separator, increased zinc loading permits higher coulombic losses due to the chemical self-discharge reaction of zinc with free bromine. The magnitude of the negative effects of high charge and discharge rates on voltaic efficiency is significant. Compared to the Exxon and ERC designs, this design has a lower current capability. The energy efficiency of this battery decreases as these factors increase.
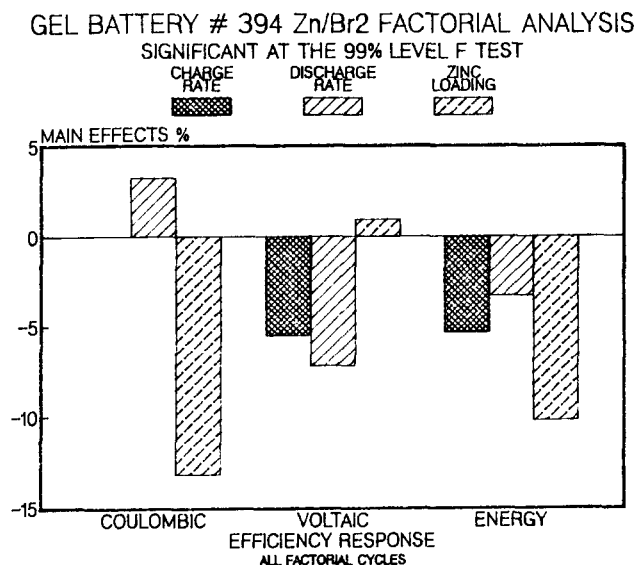
Figure 3-11. Main Effects of Three Factors on Battery Efficiency (Battery 394)

Figure 3-12. GEL Zinc/Bromine Battery Performance in 1985. Legend: C, coulombic efficiency; E, energy efficiency; S, complete discharge performed. Vertical lines at Cycles 130, 145, and 171 indicate that the battery was charged in reverse following a complete discharge. Vertical line at Cycle 153 indicates the addition of zinc to the electrolyte following a complete discharge.

An attempt was made to fit these data to a simple linear model. Statistical tests of the validity of the model indicated that it did not accurately predict battery performance. Quadratic models will be necessary for this technology.

Following the factorial test regime, an open-circuit stand test was performed. The pump was left on and operated normally with 12 s of run time in three min. Baseline cycles were run with a 48-h open-circuit rest between charge and discharge. Five such cycles were run consecutively. The efficiencies of these cycles were compared with those of baseline cycles run without the open-circuit stand. The average decrease in efficiency during the stand time, in percent per hour, was coulombic, 0.7; voltaic, 0.07; and energy, 0.6. Although the voltaic efficiency was relatively unaffectived, average coulombic efficiency was reduced by 33% in 48 h because of the chemical self-discharge of bromine and zinc.

A life-cycle test was begun following the open-circuit tests at Cycle 100. Performance remained stable for only a short time. While early in life a complete discharge operation was necessary every 20 cycles, this procedure became necessary more frequently after Cycle 118. In accordance with GEL guidelines, a complete discharge was performed when coulombic efficiency or capacity began to decline rapidly. This situation increased in frequency during the year. By year's end, at Cycle 193, complete discharge operations were necessary every three cycles. Immediately after a complete discharge, coulombic efficiency had also declined about 12% compared with early cycles. Figure 3-12 illustrates this performance.

Based on discussions with GEL, several rejuvenation procedures were conducted. As one will note in Figure 3-12, the battery was charged in reverse after Cycles 130, 145, and 171. These operations provided improvements, but their effects had diminished by year's end. Also, zinc was added in the form of zinc bromide to increase the active material concentration in the battery to 1.9 molar. Subsequent chemical analysis revealed a nonreversible loss of zinc somewhere in the battery. According to GEL personnel, this may have been caused by a design problem in the battery's flow system.

Little routine maintenance was necessary on this battery. The specific gravity of the electrolyte was monitored once a month, and distilled water was added twice during the year to replace evaporative losses. No other maintenance was performed.

Evaluation of this battery will continue in 1986. The performance will be studied to determine the nature of the decline in efficiency. Failure analysis will be performed as necessary.

Lockheed Zinc/Ferricyanide Cell (SNL ID No. 345)

This cell was placed on test in November 1983. Six different membranes were evaluated using baseline electrical cycles. The last membrane to be tested was an SNL-fabricated sulfonated polysulfone type. This membrane was a second generation of this class to be synthesized at SNL and was thicker than a previous polysulfone membrane tested in this cell in 1984.

Evaluation of this cell was terminated in April 1985 because of an irreparable cell case leak and a pump failure. The cell had completed 852 cycles at SNL, with six different membranes. It had exhibited several problems, which were discussed in earlier reports. The primary cause of failure was deterioration of the glued joints that hold the cell case parts together. This led to severe electrolyte leakage. Other problems identified were poor electrical contact at the ferricyanide felt electrode, ferri- and ferrocyanide species imbalance, and deterioration of pumps and tubing components. This cell did not exhibit poor zinc electrode performance.

The improved polysulfone membrane completed 520 baseline cycles in this cell. Performance was relatively stable and the membrane was still functional when the cell test was terminated. Figure 3-13 illustrates the average electrochemical efficiencies observed with this membrane. These data must be interpreted carefully as the above-mentioned problems caused significant variation in performance and may have biased the results. Compared with the standard Nafion N-117 membrane, the polysulfone membrane demonstrated promising performance and stability. The membrane was removed from the cell and delivered to SNL's organic chemists for posttest analysis.
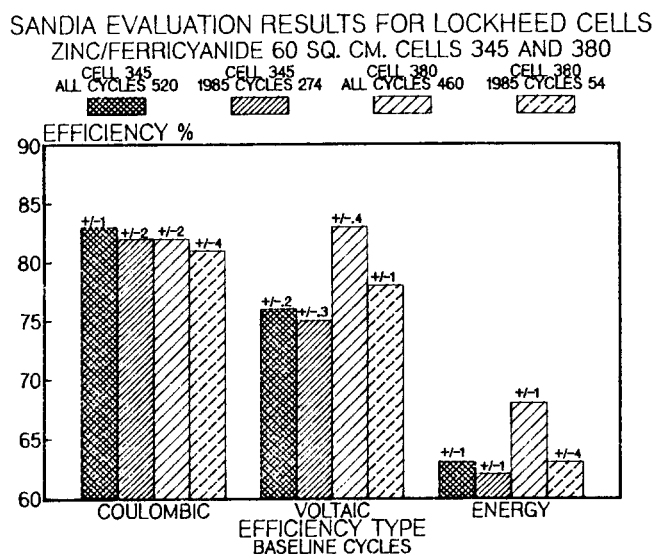
Figure 3-13. Efficiencies for Cells 345 and 380 for All Cycles and for 1985 Cycles. Cell 345 contained a polysulfone membrane. Cell 380 contained a Nafion N-117 membrane.

During the 274 cycles run in 1985, six maintenance operations were performed. The cell was disassembled twice for ferricyanide felt electrode cleaning and replacement; three plumbing fittings failed and were replaced; a zinc electrolyte filter became clogged

and was replaced; and the zinc electrolyte pump was replaced. A total of 460 g of sodium ferrocyanide was added to the electrolyte during the year. This was necessary to minimize ferricyanide electrode polarization and to replace active material lost from leaks and maintenance procedures. The material was added in 10- to 50-g increments and amounted to 1.67 g per cycle.

Lockheed Zinc/Ferricyanide Cell (SNL ID No. 380)

Evaluation of a cell with the standard Nafion N-117 membrane was continued using a new zinc electrode in February 1985. Earlier cell operation with several zinc electrodes had been poor because of non-adherent zinc deposition and subsequent flow channel blockage with zinc particles. Lockheed provided the electrode used in 1985 with the understanding that it was properly prepared. The key preparation step to ensure proper zinc deposition was apparently cadmium-plating the steel substrate.

The cell completed 54 cycles in 1985, for a total of 460 cycles. It was removed from test because of cell case leakage. Performance of the new zinc electrode was not significantly better than with previous units. It was necessary to perform complete discharge operations every two cycles to prevent flow blockage caused by nonadherent zinc deposition. The other zinc/ferricyanide cell (SNL ID 345), using a nominal zinc electrode, routinely operated for ten or more cycles between complete discharges.

Cell efficiencies with the Nafion membrane are plotted in Figure 3-13 along with results for the cell containing the polysulfone membrane. Because of operational problems such as electrolyte leakage, ferricyanide species imbalance, and frequent maintenance, the data must be carefully interpreted. It can be concluded, however, that the Nafion membrane provides good performance for this technology.

Controlled potential coulometry was used to quantify the imbalance problem in the ferri- and ferrocyanide species. During charge, ferrocyanide is converted to ferricyanide at a higher efficiency than zincate is converted to zinc metal, because of the higher redox electrode efficiency relative to that of the zinc electrode. Consequently, an excess of ferricyanide is present at the end of charge relative to the quantity of zinc metal. During discharge, the zinc is converted to zincate but not all the ferricyanide is converted to ferrocyanide.

In these experiments, ferrocyanide concentration was determined after a complete discharge, and this concentration was used as a basis for the subsequent

analyses. After a set of eight baseline cycles, the ferrocyanide concentration decreased an average of 1% per cycle when measured at the end of the discharge of the eighth cycle. Following a complete discharge, which completely converted any remaining zinc metal to zincate, additional ferricyanide was converted to ferrocyanide. However, after the cell had been completely discharged to 0 V for 12 h, there remained an incomplete conversion of ferri- to ferrocyanide. The net loss of ferrocyanide averaged 0.1% per cycle after complete discharge. Further chemical analyses of active electrolyte species should be performed in future evaluations of this technology so that this performance can be characterized more accurately.

This cell required frequent maintenance during the 54 cycles run in 1985. Six maintenance operations were performed, including the replacement of the zinc electrode. Two plumbing fittings failed and were replaced; the ferricyanide electrolyte filter housing developed a leak and was replaced; and the ferricyanide felt electrode was cleaned twice with hydrochloric acid to remove a resistive coating. One addition of 20 g of sodium ferrocyanide was made during the cycles run in 1985. At the end of testing, the ferricyanide electrode exhibited high resistance.

Testing of FACC Sodium/Sulfur Cells at SNL

SNL has been testing three FACC Mark IID sodium/sulfur load-leveling cells since January 1985 and three ETX electric vehicle cells since August 1985. Table 3-9 shows the design data from FACC for these cells. The internal design of all six cells is similar, but the overall physical dimensions are different between the LL cells and the EV cells. The open-circuit voltage is 2.07 V, but the rated capacity of the LL cell is considerably greater at 155 Ah vs 55 Ah for the EV cell.

Table 3-9. FACC Cell Design Data

	Mark-IID Cell	ETX Cell
Weight		
Sodium (g)	170 ± 5	70
Sulfur (g)	345 ± 10	116
Total cell	2.0 kg	750 g
Dimensions		
Diameter (mm)	55.75	38.0
Length (mm)	427.0	320.0
Capacity		
Thermal (Ah)	190	64.7
Rated @ 350°C	155 Ah @ C/5	55 Ah @ C/3
Average open circuit (V) at 350°C	2.071	2.074

The nominal discharge voltage limits were consistent with the full-capacity cutoff algorithm for each type of cell, and are shown below.

LL cell: $V_{DL} = 1.80 - (0.01)I$

EV cell: $V_{DL} = 1.76 - (0.008)I$

where V_{DL} is the discharge voltage limit in volts, and I is the cell current in amperes.

The six cells were first instrumented with thermocouples and placed into individual furnaces in a vertical position with the negative terminal down (LL cells only). They were then slowly heated to 350°C, and initial tests were run to verify their capacity. Each cell was placed on its own test plan, shown in Table 3-10. Also shown in this table is the FACC and SNL identification numbers assigned to each cell, the number of cycles completed on each, and the nominal and end-of-1985 capacity of each cell.

Table 3-10. Status of FACC Cells on Test at SNL

Ford ID No.	SNL ID No.	No. of Cycles	Nominal Capacity (Ah)	Present Capacity (Ah)	Test Regime
LL971	389	174	155	155*	Capacity
LL972	390	312	155	158	80% DOD
LL973	391	193	155	156	Parametric/Capacity
VB007	407	32	55	55	Capacity @ C/1, C/2
VB003	410	25	55	60	Capacity @ C/1, C/2
VB006	411	23	55	64	Capacity @ C/1, C/2

*At 15-A charge rate

The capacity tests for all three LL cells were the same using a 30-A discharge current to a 1.5-V cutoff value and recharging the cell at 18 A to 2.5 V. Initially, all three cells performed well under these conditions; however, after a few cycles, Cell 389 developed difficulties on recharge and was unable to maintain a capacity of 155 Ah at the 18-A charge rate. The charge current was then varied from 10 to 16 A on this cell, and it performed reasonably well at currents up to 15 A.

FACC Cell 389 has demonstrated anomolous charge acceptance while maintaining full capacity and nominal coulombic efficiency. Figure 3-14 illustrates voltage and current profiles for Cycle 1, which was run at reduced currents per FACC instructions. The voltage plot displays the characteristic two-phase and single-phase transitions. On subsequent cycles, using nominal and constant 30-A discharge and 18-A charge currents, recharge acceptance was ~75% of full-rated capacity. Using a lower constant current of 10 A or a taper charge at 2.5 V resulted in nominal recharge and subsequent full-discharge capacity. Between Cycles 52 and 118, a systematic charge acceptance study was conducted. Starting at 10 A constant-charge current, sets of cycles were run with successively higher charge currents (1-A increments). The results are plotted in Figure 3-15. Nominal recharge (and subsequent discharge) capacity was obtained using charge currents up to 15 A. Upon stepping to 16 A, recharge acceptance first dropped to 75% of nominal. On subsequent cycles, recharge acceptance gradually increased and finally reached nominal levels. The last cycle using a 15-A charge current (Cycle 108) and the first cycle using a 16-A charge current (Cycle 109) are plotted in Figures 3-16 and 3-17, respectively. The voltage profile near the end of charge is distinctly different in Cycle 109, compared with Cycles 1 or 108. Temperature variations did not correlate with this behavior.
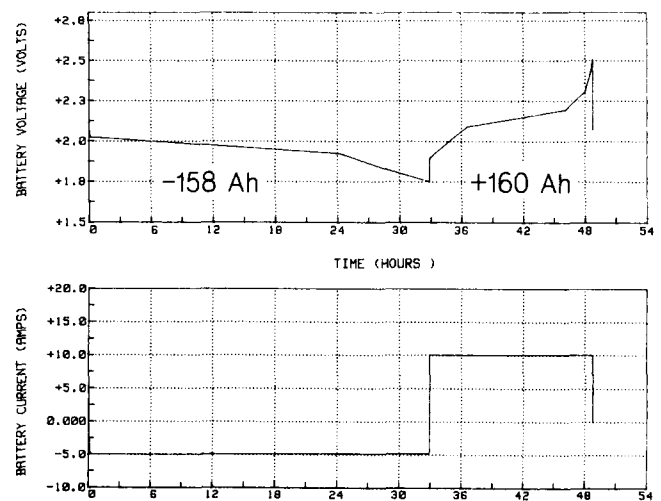
Figure 3-14. Voltage and Current Data for Cycle 1, FACC Cell 389
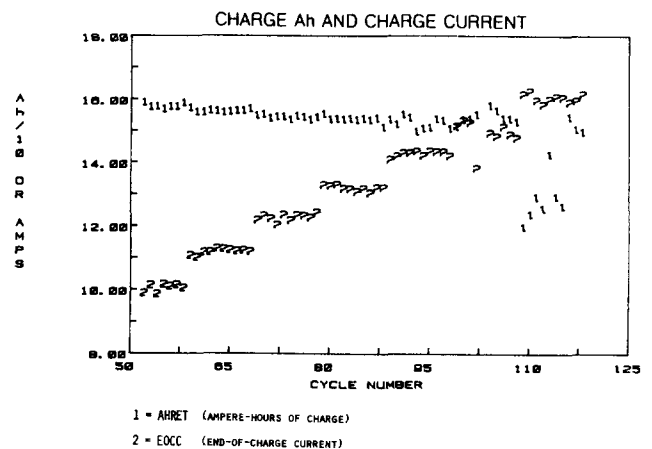
Figure 3-15. Charge Acceptance Data, FACC Cell 389

83
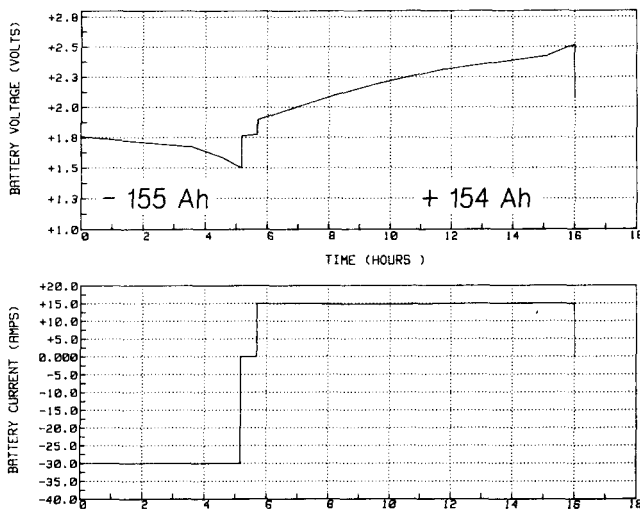
Figure 3-16. Voltage and Current Profiles for Cycle 108, FACC Cell 389
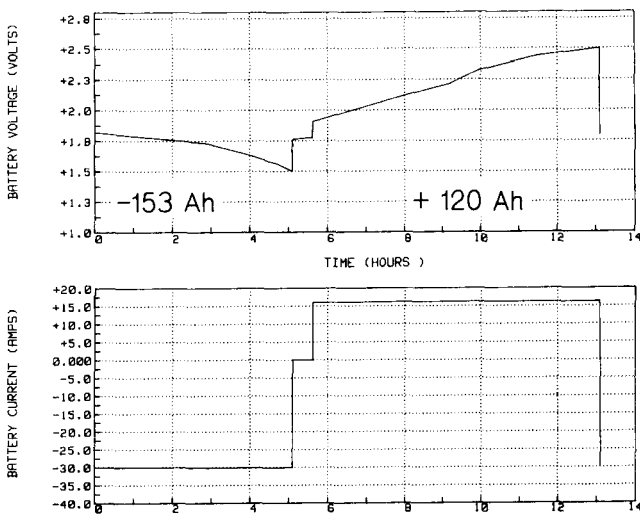
Figure 3-17. Voltage and Current Profiles for Cycle 109, FACC Cell 389

This behavior was repeated in tests performed near the end of 1985. Figure 3-18 illustrates Cycles 153 and 154. Cycle 153 was the fourth cycle of a set using a 16-A constant-current charge. The first cycle of the set demonstrated 75% of nominal recharge acceptance. The recharge acceptance increased to 87% at Cycle 153, and was 100% at Cycle 154. No significant difference was observable in the voltage profiles of the two cycles, although neither cycle was similar to the profile observed at lower charge currents. This appeared to be a cathode-related problem, and further investigation will continue in 1986.
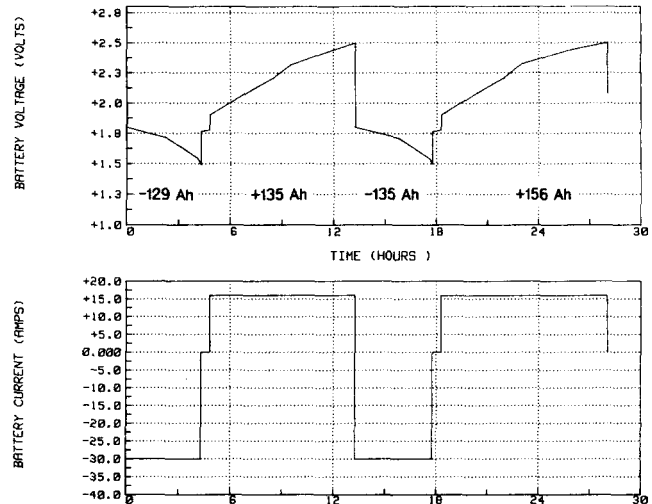
Figure 3-18. Voltage and Current Data for Cycles 153 and 154, FACC Cell 389

After completing several capacity cycles on Cell 390, the cell was placed on an 80% DOD life-cycle test regime. This test consisted of a set of 20 cycles at a discharge current of 30 A to the 80% DOD value and then recharged at the 18-A rate to 2.5 V. Between each 20-cycle set, two full-capacity cycles were run. To date, Cell 390 has completed 13 sets of 80% DOD cycle tests and continues to maintain a capacity >156 Ah.

When the initial capacity tests were completed on Cell 391, the cell was evaluated under a factorial test regime. The purpose was to quantify the effect of temperature, charge rate, and discharge rate on cell performance over an expected operating range. Table 3-11 illustrates the three factors, each at two levels, of the test plan.

Table 3-11. FACC Factorial Test Regime

Factor	Low Level	Center Point	High Level
Temperature (°C)	325	337	350
Charge rate (A)	10	14	18
Discharge rate (A)	20	25	30

Each of the eight factorial cycle regimes was run five consecutive times. The run order was random. The center point regime was run at the beginning and end of the factorial cycles. Baseline capacity cycles were run between each set of five cycles. These tests were run between Cycles 13 and 88 during the life of this cell.

The results of these tests are summarized in Figure 3-19. Illustrated are the main effects of each of the three factors on discharge and recharge energy. These effects are expressed as percent of rated cell capacity. The data show that increasing the cell operating temperature from 325°C to 350°C increases both the discharge and recharge energy. Increasing the charge rate has a negative effect on discharge and recharge; increasing the discharge rate causes a strong negative effect on the watt-hours discharged from the cell. The sensitivity of the cell to relatively small temperature and charge-rate changes is clear.
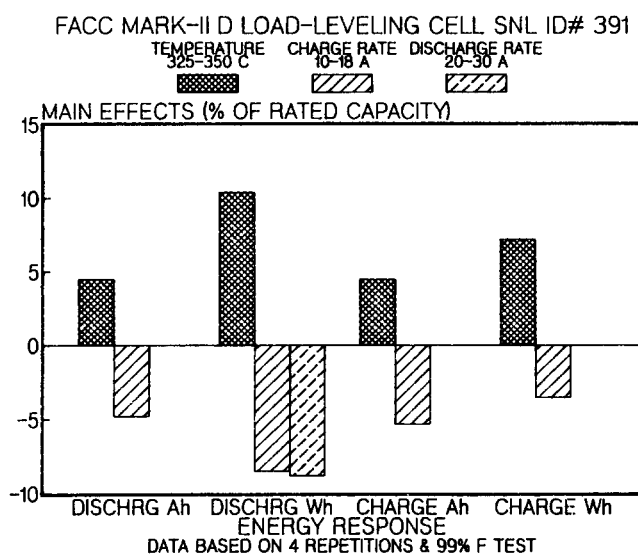
Figure 3-19. SNL Factorial Test Results for FACC Sodium/Sulfur Cell

While some interactions were statistically significant, their magnitude was <1%. There was consistent interaction between temperature and discharge rate.

Using these data, a simple linear cell performance model was developed and checked against the center point data. The model did not accurately predict performance according to confidence limit tests. A quadratic model will be required to predict the performance of this cell design.

Once these tests were completed, the cell was placed on a 100% DOD life-cycle test regime at the 30-A discharge rate to a cutoff voltage of 1.5 V and then recharged at the 18-A rate to 2.5 V.

Capacity tests began in August 1985 on one of the ETX electric vehicle cells (No. 407) but the end-of-discharge voltage cutoff limit was set 0.2 V too high and the capacity of the cell was only 44 Ah. This cutoff value was readjusted and testing was started on all three cells toward the end of October. The capacity

tests on these cells consisted of an 18-A discharge with the end-of-discharge cutoff voltage set to 1.6 V. A two-step recharge consisted of 9 A to a voltage limit of 2.3 V, and then a 3-A charge to 2.3 V.

The capacity of Cell 407 was 55 Ah, which is the nominal capacity for these cells. This value, however, is 5 to 9 Ah below the capacity of the other two ETX cells. The capacity of Cell 410 is 60 Ah whereas Cell 411 is running 64 Ah.

Higher discharge rate tests up to 55 A were started on Cell 410 and will be performed on the other two cells in the near future. Using the EV cell algorithm shown previously, the discharge voltage limit was adjusted for each discharge current value. The results to date indicate that the capacity remained above 60 Ah for Cell 410, even at the maximum discharge current of 55 A. The cell temperature initially increased above 380°C on discharge at the higher current levels but cooled down later in the cycle. Once these tests have been completed, the cells will undergo a set of parametric tests.

Testing of Hydrogen/Nickel Oxide Batteries at SNL

The hydrogen/nickel oxide cells and batteries on test at SNL are a prismatic configuration designed for terrestrial solar applications. They were received as contract deliverables from COMSAT Laboratories, and were described in a previous section of this report. Four cells and one 6-cell battery were on test at the beginning of 1985, six additional cells and one battery were put on test during the year, and four cells were removed from test. Thus, at the end of 1985, six cells and two batteries were on test.

Both cycling and characterization tests were conducted. The cycling regime consisted of a set of 50 cycles to 80% DOD and, later in the year, to 1.0 V/cell (100% DOD). Charging was terminated when the pressure-time slope dropped to 50% of the linear value. This was followed by two capacity tests to 1.0 V/cell with the charge to 25% of the linear slope.

Characterization tests included the continued development of a method to terminate charging when the pressure-time slope reaches a preselected fraction of the linear slope; investigating methods of charging to maximize coulombic efficiency; studying the effects of precharge pressure and coolant temperature on performance; and determining stand-loss characteristics.

Included in the contract deliverables in 1985 were Battery 02 and Cells 15, 16, and 17. All had a nickel wire screen substrate in the negative, replacing the

more expensive, expanded metal current collector. To reduce costs, Cell 17 did not have the Gortex backing on the negative. Also received and put on test were Cells 18, 19, and 20. All were assembled with the thick (0.068 vs 0.030 in.) positive electrodes. Considerable cost reductions are possible here, since there is a significant increase in capacity with the same volume and about half the number of cell components. The thick positives in Cells 18 and 20 were formed in potassium hydroxide electrolyte with a lithium additive to improve performance at higher temperatures. Cell 20 had negatives without the Gortex backing.

Cell 12 and Battery 02 represent the baseline design at the beginning of 1985; the modifications discussed above are summarized in Table 3-12. Also in Table 3-12 are the total cycles accumulated by the end of the year, and the end-of-year capacity using the coolant temperature indicated. As noted, four cells were removed from test during the year. The capacity of Cell 03 was declining after about 1000 cycles, and it was noted upon its removal from the pressure vessel that the unrestrained cell case had bulged considerably; later cells were restrained with plastic or metal plates. Cells 15, 16, and 17 all exhibited capacity decline early in life; a bad lot of catalyst in the negative is suspected. All four cells are being returned to COMSAT for posttest analysis.

Of the units still on test, Cell 12 and Battery 02 are doing very well after about 700 deep cycles (Table 3-12). The cells with the thick positives have demonstrated capacities >125 Ah and Cells 18 and 20, which contain the lithium additive, are doing particularly well.

Sealed Lead-Acid Battery Testing

Testing of sealed lead-acid batteries received as contract deliverables from Gould and Eagle-Picher was completed in December 1984. A revised report updating the test results was issued in May 1985. As a result of this development effort, GNB Batteries (a spin-off from Gould) is marketing a version of the sealed lead-acid battery under the trade name of Absolyte. SNL purchased a nominal 6-V 125-Ah battery (with Type 35A09 cells) and placed it on cycle test in March 1985.

The battery is discharged by removing 80% of its nominal capacity; it is charged by returning 110% of the amp-hours removed, both with a current of 25 A. The initial capacity was 137 Ah; by December 1985 its capacity was 113 Ah after 509 cycles.

Table 3-12. COMSAT Nickel/Hydrogen Test Summary—1985

S/N	Variations	Rating (V)	Rating (Ah)	Coolant (°C)	Cycles	Capacity (Ah)
Batteries						
02		7.50	100	10	743	91.5
03	Screen substrate in negative	7.50	100	20	345	87.0
Cells						
03		1.25	90	RT	1106	69.6*
09		1.25	90	RT	754	75.1
10	Thick positive	1.25	120	10	352	113.2
12		1.25	90	20	666	102.6
15	Screen substrate in negative	1.25	90	RT	263	59.1*
16	Screen substrate in negative	1.25	90	RT	142	69.3*
17	Screen substrate in negative[†]	1.25	90	RT	180	66.3*
18	Thick positive with lithium additive	1.25	125	10	98	137.1
19	Thick positive	1.25	125	10	27	125.8
20	Thick positive with lithium additive[†]	1.25	125	10	27	133.8

*Removed from test
†No Gortex backing on negative

Battery Field Tests at SNL

Four battery field test programs were conducted by SNL during 1985. Three of these involved photovoltaic arrays, the other a wind turbine. Two of the tests were terminated during 1985; the other two are still in progress. Their goals were to evaluate batteries associated with PV arrays or wind turbines and to determine battery performance and life under field conditions.

The first field experiment involved a lead-acid battery that had been deep-cycle-tested over 230 times using a standard charger and resistive load. The test results from these experiments were discussed in SNL's *Exploratory Battery Technology Development and Testing Report for 1984*. This battery and one of SNL's small tracking arrays were then used to perform the initial tests on an Abacus Controller, a unit designed to interface a battery to a photovoltaic array and a utility grid. The experience gained from these tests will allow us to interface this controller to Exxon's PV-20 zinc/bromine battery and a larger flat-plate array. Software will also be needed to handle data collected from the array, battery, and load. The lead-acid battery was removed from test after the field experiments were completed.

The second field experiment to be concluded during 1985 was the monitoring of the Public Health Service (PHS) stand-alone PV/battery system located on the Jicarilla Apache Indian Reservation in northwest New Mexico. This system consisted of a 490-W PV array connected in parallel to an Exide 12.5-kWh, 24-V conventional lead-acid battery. The array supplied power to a residential load and charged the battery. If additional power was required by the load, the battery made up the difference. The load consisted of a 1/2-hp pump motor (used to pump well water to the house) and five fluorescent light fixtures. A battery-operated data acquisition system monitored various parameters such as array voltage and current, battery voltage and current, battery temperature, and solar radiation.

Our goal was to evaluate battery system-load interactions. The results showed that the system was reasonably well-designed and the load was being met by the array or battery over 99% of the time; during the winter months the PV/battery system was unable to meet the load on a few occasions. The cause was a combination of cloudy weather (thus, no array output) and cold temperatures (which prevented the battery from accepting a full charge). The problem with battery temperature could have been avoided by placing the battery on the south side of the house to obtain

more daytime exposure to the sun. The battery should also have been placed deeper in the ground (below the frost line).

Another design problem was the depth of the water pipes. These lines were also not placed below the frost line and, in the winter months, they would freeze and crack. This caused the water pump to run continuously and changed the load profile so that a greater percentage of the load occurred at night. Since the battery supplied this nighttime load it experienced greater DOD cycles, which will probably shorten its life. Figure 3-20 shows the load satisfaction differences before and after this problem occurred.
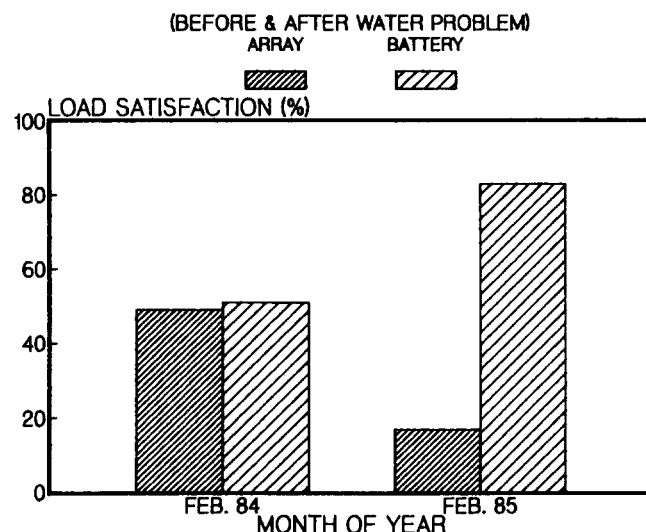
Figure 3-20. Load Satisfaction Data on PHS Battery and Photovoltaic Array

Finally, a well-designed controller is very important for these small stand-alone systems. If the controller fails, more than likely the array output will be placed across the battery and the battery will overcharge. In many cases, the user is not aware of a controller failure until the battery has gone dry and the damage has been done. This problem did occur on the system we monitored and we were able to save the battery. Ideally, a controller should be designed to charge a battery properly, according to the manufacturer's specifications, and to have the proper cutoff adjustments so as to prevent overcharge damage.

Another field experiment involved the evaluation of Exxon's 20-kWh (PV-20) zinc/bromine flowing electrolyte battery. This battery was delivered to SNL in April 1985 and preliminary cycle tests were started in May, using a commercial battery cycler made by Firing Circuits. Long delays were encountered due to

voltage filtering problems on the battery's electrolyte pump motors and failure of an electrolyte heat exchanger. Once these problems were corrected, several baseline-capacity tests were run. A baseline-capacity test occurs when the battery is charged at the 70-A rate for 3 h and then discharged at the 70-A rate to a 72-V cutoff.

Next, a factorial test regime was used to evaluate the performance of PV-20. Three factors were chosen for these tests, each at two levels. They are presented in Table 3-13.

Table 3-13. Factorial Test Plan for PV-20

Factor	Low Level	High Level
Charge rate (A)	48	70
Discharge rate (A)	48	70
Zinc loading (mAh/cm²)	60	90

In addition, center point values of these factors were selected approximately midway between the low and high levels; therefore, this led to nine different cycle types for the complete test regime. Because of constraints in the battery test plan, only one repetition was possible for eight of the nine cycle types; one type was run twice. These cycles were run in random sequence between Cycles 48 and 57 of battery life.

The response variables were coulombic, voltaic, and energy efficiencies. These efficiencies included losses to the shunt current protection system but not for pump power, thermal management system power, or any other auxiliary system.

Because we lacked multiple-data samples, it was not possible to calculate confidence limits or other statistical characteristics to quantify the reproducibility of the results; therefore, only effects with a magnitude >1% will be reported. To estimate the reproducibility of the results, Table 3-14 describes the efficiencies for the cycle type that was run twice.

Table 3-14. Results of Factorial Test for Cycle Run Twice

Response Efficiency	First Trial (%)	Second Trial (%)	Mean (%)	95% Confidence Limits
Coulombic	82.3	81.8	82.0	± 0.5
Voltaic	75.1	76.0	75.5	± 1
Energy	61.8	62.2	62.0	± 0.3

These data indicate that an efficiency change >1% may represent a significant difference in battery performance.

Figure 3-21 illustrates the main effects for the three factors evaluated. Zinc loading showed no significant effect on efficiency, whereas small negative effects on voltaic and energy efficiencies were observed for increased charge and discharge rates. These effects are similar to performance observed on smaller batteries tested at SNL. The magnitude of these effects are smaller than those observed in the other tests. Therefore, a scale-up of this design from 0.5 to 20 kWh appears insensitive to these performance characteristics.
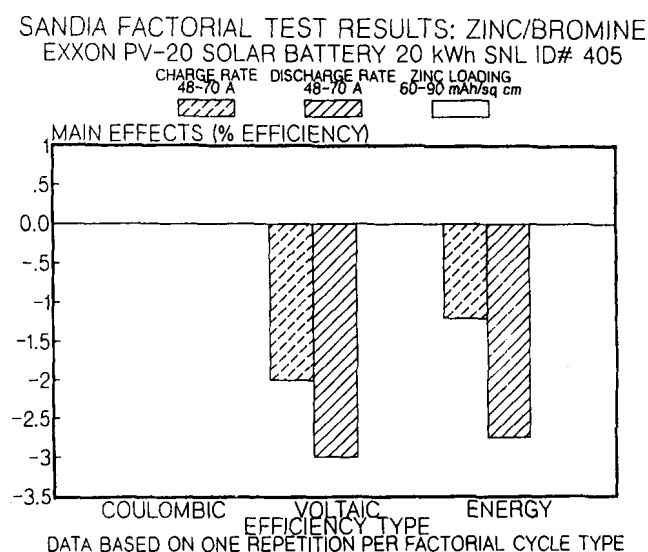
Figure 3-21. SNL Factorial Test Results for PV-20

A performance prediction equation was derived from these data:

$$Y = b0 + x1b1 + x2b2 + x3b3$$

where Y is the efficiency response (coulobmic, voltaic, or energy) and the b-values are given in Table 3-15.

Table 3-15. Prediction Equation Parameters for PV-20

	Response			
	b0	b1	b2	b3
Coulombic	82.0	0.3	−0.2	−0.2
Voltaic	78.4	−1.0	−1.5	−0.3
Energy	64.2	−0.6	−1.4	−0.4

The x-values are related to the three factors as follows:

$x1 = [\text{charge current (A)} - 59]/11$
$x2 = [\text{discharge current (A)} - 59]/11$
$x3 = [\text{zinc loading (mAh/cm}^2) - 75]/15.$

This equation was checked against the center point cycle type experimental data. The equation predicted coulombic and energy efficiencies that were ~1% low compared to the experimental results, whereas it predicted the observed voltaic efficiency exactly. While additional experimental data would provide increased confidence in the prediction equation, it does provide an estimate of performance for the 20-kWh prototype battery.

Several cleanout-stand tests were performed on the battery. First, it was charged, then the cleanout portion of the test was performed by shorting the battery across a strip resistor. This was done to lower the open-circuit voltage of the battery and to keep the shunt currents under 1/2 A. The battery was then allowed to stand with the electrolyte pumps off for a period of time, which varied from a few hours to as long as three days. Table 3-16 compares the battery efficiencies after 1- and 3-day stands to the values obtained on a baseline-capacity test.

Table 3-16. Comparison of Battery Efficiencies for PV-20

Efficiencies	1-Day Stand (%)	3-Day Stand (%)	Baseline Capacity (%)
Coulombic	68.9	70.8	80.9
Voltaic	73.7	72.6	75.0
Energy	50.8	51.4	60.7

These data indicate that the larger share of the losses were caused by cleanout, and this means that even for short stand periods the losses will be relatively large.

Modification problems with SNL's PV array have delayed interfacing this battery to the array and utility grid. The battery has nevertheless completed 35 cycles at Exxon and 31 cycles at SNL. A plot of the coulombic, voltaic, and energy efficiencies along with the energy output for all the cycles run on this battery is shown in Figure 3-22. Exxon started testing the battery at a low-energy output value and reached the 20-kWh value toward the end of its testing activity (Cycles 31 to 34). When one compares their efficien-

cies at full capacity with SNL's results, one will note that SNL's coulombic efficiency was ~8% higher, whereas SNL's voltaic efficiency was 5% lower than Exxon's result. The energy efficiency at both locations was ~60%. The reason for the differences in efficiency was because SNL operated the battery at a lower temperature.
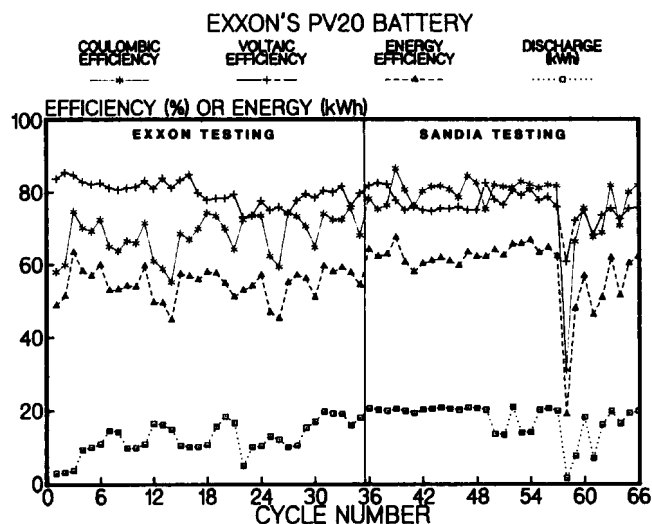
Figure 3-22. Cycle Efficiencies and Energy Output for PV-20

The last field test was the wind/battery experiment performed by the Solar Energy Research Institute (SERI) at Rocky Flats in Colorado. This experiment was a continuation of work that started three years ago using an Exide 25-kWh, 24-V conventional lead-acid battery tied to a 2-kW wind turbine generator (WTG) and operated in a stand-alone mode. A typical daily residential load profile using water heating as a demand determinant was first satisfied by the wind turbine output, if available, or by battery energy, if necessary. Key performance measures were load satisfaction by the wind turbine and battery and energy flow.

The system was changed and extensive software was written as a result of data acquisition problems during much of the conventional lead-acid battery testing. Testing of a 22.5-kWh sealed lead-acid battery from GNB, Inc. was initiated in May 1985, and seven months of data were collected. The battery performed extremely well, and only minor problems were encountered with the wind turbine. The system configuration remained the same as in previous experiments with a total daily load of 2.8 kWh. Figure 3-23 is a bar graph showing the average monthly load and how this load was met by the battery and wind turbine. During June and July, when the average wind

speed was low, 80% of the load was met by the battery, and during the 7-mo testirg period 73.2% of the load was met by the battery. The wind turbine was required in order to keep the battery charged, however, and there were times when it produced large amounts of excess energy. This information is displayed on a pie chart (Figure 3-24), and shows how the wind turbine's total energy output was distributed for the 7-mo period. The system was down twice during this period because the battery and wind turbine could not meet the load. This experiment will continue until June 1986 so as to obtain one full year of data.

Figure 3-23. Load Satisfaction Data on Rocky Flats Wind/Battery Experiment

WTG ENERGY IN kWh

Figure 3-24. Wind Turbine Generator/Battery Experiment at Rocky Flats

In addition to these field test activities, SNL also worked with the New Mexico Solar Energy Institute on a PV/battery experiment. The institute operates the Southwest Residence (SWRES) photovoltaic evaluation facility. SNL purchased a GNB 17-kWh, 24-V sealed le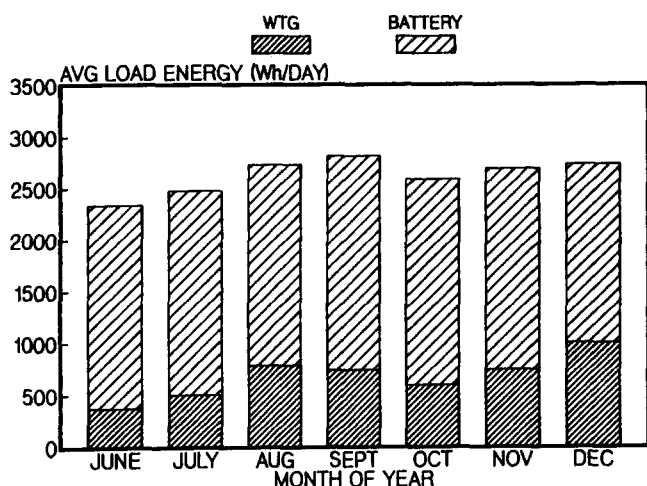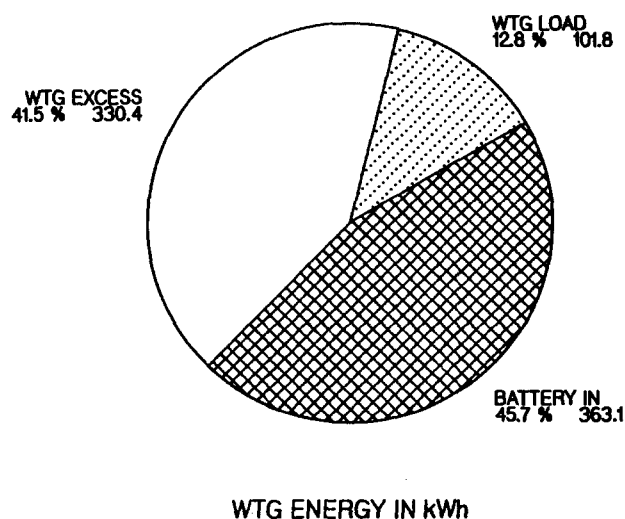ad-acid battery for SWRES and performed the preliminary capacity tests. The battery was then delivered to SWRES and interfaced to a 1.7-kW flat-plate array. A "real" electrical load (including lights, fans, a refrigerator, and a radio) was used to complete the system. SWRES plans to collect data on the experiment and provide us with their results.

SNL was also involved in capacity tests for the 750-kWh conventional lead-acid battery at Natural Bridges National Monument (NBNM). This was part of a project sponsored by the Department of Energy in collaboration with the National Park Service and the Department of Interior. The intent of the project was to demonstrate that a PV/battery system could provide the energy needed for the Visitor's Center and several park service homes, which until now have relied on diesel generator power. This work was requested by the National Park Service and the contract monitor of the PV/battery system (SNL Division 6221). Before accepting the system from DOE, the National Park Service inquired about the status of the battery that had been in operation since June 7, 1980. The results of the tests indicate that the capacity is still 91% ± 3% of the original value. SNL also provided NBNM with a battery maintenance procedure that could be used by the site personnel.

Sodium/Sulfur Cell and Module Testing at FACC

FACC was funded by SNL to continue testing selected cells and modules under test at the conclusion of Phase VB of the Sodium/Sulfur Battery Development Program. This work covered the period from March 1, 1985, through December 31, 1985.

At the start of the program this included more than 100 EV-type cells being evaluated in various tests to determine durability, freeze/thaw survivability, and performance. Of these, 24 cells contained developmental components (coatings for corrosion protection of the cathode container, or electrolytes made by the slurry-solution spray-drying process). Also on test were cells for stationary energy storage (SES) applications including high-energy cells being tested singly and in pairs and an original Mark-II cell that had already reached 2300 cycles.

Tests of two 96-cell SES modules also continued from Phase VB. These modules were being tested to evaluate an interconnection strategy based on short strings, and had been assembled using Mark-II cells taken from a previous 100-kWh battery after operating for ~675 cycles.

At the conclusion of the technical effort under the EV Battery Technology Development Program (SNL Contract No. 51-9391) in November 1985, tests of cells fabricated in that program were also continued in this Cell and Module Testing Program.

Highlights of these evaluations included

- An average life of 924 cycles for a group of 46 ETX-type cells with only one failure after 900 cycles

- More than 200 cycles on a group of four Electric Vehicle Engineering Model-1 (EVEM-1) cells operated in a vertical orientation

- More than 40 successful freeze/thaw cycles for a group of 24 ETX-type cells when either fully charged or half-charged

- Excellent performance by high-energy cells under weekly cycling conditions for test periods approaching 1 yr

- More than 2500 cycles in 5 yr with good performance by a Mark-II cell

- Continued good performance by cells with alternative, lower-cost electrodes for test times up to 889 days

- Good performance for up to 1852 cycles by cells with cathode corrosion protection provided by conductive glass coatings

- Good performance for cells with improved chromium plate (independent of substrate type) for up to 1426 cycles

- More than 2000 cycles in 25 mo with good performance by EVEM-1 size cells with slurry-solution spray-dried (S^3D) electrolytes, and 1075 cycles in 30 mo by Mark-II size cells with S^3D electrolytes, also with good performance

- Demonstration of the benefits of short strings in eliminating charge control requirements during normal operations.

Cell Tests at FACC

Categories of cells on test at the beginning of this program are shown in Table 3-17. Tests in progress at the conclusion of the EV Battery Technology Development Program were also continued in this Cell and Module Testing Program.

Table 3-17. Units of Test

Description	No. on Test March 1, 1985
Electric Vehicle Cells	
ETX*	
• Exploratory	
–Durability	4
–Accelerated corrosion	8
• Prototype	
–Durability	20
–Freeze/thaw survivability	10
• Alternative	
–Durability	8
–Performance and special tests	10
• Preproduction	8
EVEM-1†	4
High-Energy Cells	
Single-cell tests	5
Two-cell pairs	10
SES Cell (original Mark-IID)	1
Alternative Electrodes	
Mark-IID	1
EV	2
Alternative Sulfur Containers	
Conductive glass-coated	5
FACC chromium-electroplated	7
SNL chromium-electroplated	4
Alternative Electrolyte Evaluation	
Mark-IID, slurry solution spray-dried	3
EV, slurry solution spray-dried	5
Total	115

*Cell for a battery developed in the DOE/Ford Experimental Transaxle Program
†Electric Vehicle Engineering Model-1

Electric Vehicle Cells

Sixty-eight ETX cells and four EVEM-1 cells, fabricated in the previous DOE-funded Phase VB Sodium/Sulfur Battery Development Program, were continued on test, mostly for evaluation of cycle life and freeze/thaw response (Table 3-17). Several cell groups were reassigned for special testing after their initial test sequence, including 20 ETX cells fabricated in an associated (ETX battery) program. The results of these tests are presented by function in the following sections.

The EVEM-1 cell is designed for horizontal operation and high-performance duty cycles. The ETX cell is designed for vertical operation. Table 3-18 gives the ratings for both cells. The larger capacity of the ETX cell reduces the number of cells required for an EV battery, and its vertical orientation improves its thermal-cycling characteristics.

The developmental ETX cells tested in this program reflect several stages of manufacture, which incorporated various aspects of the overall design as components became available. The salient features of these cells are summarized in Table 3-19. For additional information on the design and development of these EV cells, please refer to the Final Report for Phase VB of the Sodium/Sulfur Battery Development Program (Contract No. DE-AMO4-79CH10012).

Table 3-18. Electric Vehicle Cell Design

	EVEM-1	ETX
Size and Weight		
Diameter (cm)	3.6	3.8
Length (cm)	25.2	33.1
Volume (cm^3)	260	380
Weight (g)	529	750
Ratings		
Resistance (mΩ)		
Steady	9.3	7.8
Pulse	<8	<6.7
Capacity at C/3 (Ah)	41.5	55.0
Energy at C/3 (Wh)	77	102
30-s pulse power (W)		
0 – 50% DOD	140	—
at 80% DOD	114	135
Specific energy at C/3 (Wh/kg)	145	136
Power density at 80% (W/L)	420	355

Table 3-19. Developmental ETX Cells

Series Designation	No. of Cells	Sulfur Electrode Length	Conductive Shunt	Ceramic Spacer	Other
Exploratory					
A	6	2 segments	No	No	Floating sodium reservoir
B	9	2 segments	No	No	Flexible sodium reservoir (FLEX)
C	30	2 segments	No	No	FLEX; shortened container
Prototype					
D	55	Continuous	Flame-sprayed	Yes	FLEX; design length
Preproduction					
E	25	Continuous	Flame-sprayed	Yes	FLEX; reduced length
Alternate					
F	23	Continuous	Bimetal	Yes	FLEX; reduced length

92

Cell Durability

The largest test category consisted of developmental ETX cells being evaluated for cycle-life durability under continuous cycling conditions representing a 3-h discharge rate and a 6-h recharge rate. Except for the 12 exploratory cells, test conditions were standardized to those listed in Table 3-20 by the second month of the program. The conditions reflect a fixed-capacity cycle (80% DOD) in a 2.4-h discharge at a C/3 rate in contrast to the fixed-voltage limits (variable capacity) previously employed.

Table 3-20. Standardized Test Conditions

Discharge: 18 A for 2.4 h, or until voltage drops to 1.70 V; 0.3 h idle

Charge: 9 A for 5.3 h, or until voltage reaches 2.30 V

3 cycles/day

$350°C \pm 5°C$

Since the purpose of the 12 exploratory cells was to establish the sensitivity of cycle life and the corrosion rate of chromium plate to the DOD (cutoff voltage), test conditions for these cells were continued as before, with four cells operating to 1.70 V and eight

cells being extended to 1.60 V. These tests yielded about two cycles per day.

With the change to the standardized conditions for the other cells, several small effects were noted in the computerized data reduction. The short idle-after-discharge period limited the open-circuit voltage (OCV_D) recovery to values less than would have been obtained at equilibrium. This was interpreted by the analysis code as a lower state of charge after discharge than was actually the case. In turn, this directly underestimated the cell chargeability (SOC after charge) and indirectly overestimated the resistance during charge, $R_C = (\overline{V}_C - \overline{OCV})/I$, where R_C is the cell resistance during charge, $\overline{V}_C$ is the average charge voltage, $\overline{OCV}$ is the average open-circuit voltage, and I is the charge current. This also underestimated the resistance during discharge, $R_D = (\overline{OCV} - \overline{V}_D)/I$, where R_D is the cell resistance during discharge and V_D is the discharge voltage, since a low value of $\overline{OCV}$ was calculated from the erroneous OCV_D. During a brief calibration test, cycles with an extended idle period after discharge were used to determine that the magnitude of the effect was small ($\Delta R_D < 4\%$, $\Delta C = 1\%$ of capacity) and generally uniform. The principal effect was to invalidate the early cycle data when correlating the small changes in cell resistance or change in capacity with cycle life.

A summary of the test results is given in Table 3-21 based on linear regression analysis. The

---

Table 3-21. Durability Test Results

Cells/ Conditions	Status, October 6, 1985 — 46 Cells, 871 Cycles (734 Avg.), 0 Failures					Status, December 31, 1985 — 45 Cells, 772 – 1027 Cycles (924 Avg.), 1 Failure	
	Avg. Cycles	R_D (mΩ)	(dR/R)/N	Capacity (Ah)	(dC/C)/N	No. of Cells	Avg. Cycles
10 Exploratory 3 @ 88% DOD, 1.7 V 7 @ 108% DOD, 1.6 V	824	8.98	46×10^{-6}	56.21	-22×10^{-6}	10	980
20 Prototype 80% DOD, C/3	795	7.87	149×10^{-6}	54.74	-26×10^{-6}	19	998
8 Alternate prototype 80% DOD, C/3	574	8.50	67×10^{-6}	58.92	-33×10^{-6}	8	775
8 Preproduction 80% DOD, C/3	631	8.48	99×10^{-6}	58.36	-8×10^{-6}	8	827

extrapolated "initial" values for resistance during discharge and capacity are given, along with the rate-of-resistance rise and capacity declines for each of the classes of cells. Excellent cycle life (exceeding 3000 cycles) with good performance is predicted by these linear rates of change.

Of equal importance, only a single cell of the 46-cell test group failed (at over 900 cycles) during this test, indicating major improvements in reduction of early mortality and improved failure statistics for the ETX cell design compared with previous designs. At the end of this testing period the average cycle life for the 46 cells had reached 924 cycles, with the longest at 1027 cycles.

The data from most cells are well fitted to a linear regression analysis, although the resistance of a few shows an upturn at higher cycle life. Prolonged testing would be valuable in establishing the practical life for these cells.

Four EVEM-1 cells were initially put on test to evaluate the effect of orientation on performance. Both continuous cycle performance and pulse response (30-s loads to ~100 A) indicated lower resistance when horizontal (~9% for continuous, 5% for pulse) attributed to more complete area coverage of the electrolyte. Durability tests continued in the vertical orientation. After ~1400 cycles, the pulse response was again measured and found to be reduced by only 10% to 15% from the initial value, even though the continuous cycle resistance had risen by about 30%. The tests were voluntarily terminated at just beyond 2000 cycles. Figure 3-25 shows the pulse characteristics comparing effects of orientation and life and showing the power behavior to be nearly independent of DOD.
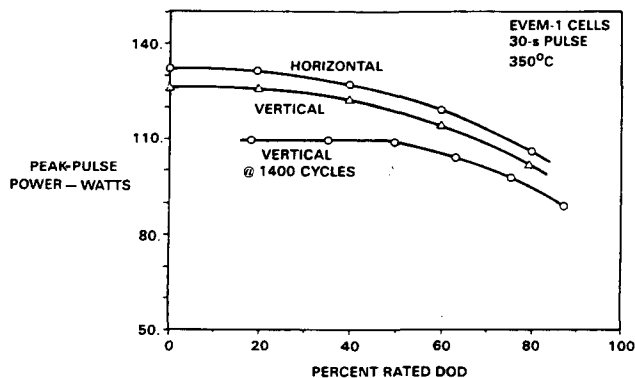

Figure 3-25. Effect of Orientation and Age on Pulse Power

Thermal Cycle Tests

An important contribution to the poor reliability of the EVEM-1 cell was its failure during freeze/thaw cycles when oriented horizontally. The high failure rate was attributed principally to the nonsymmetrical cantilever forces developed during phase change in the cathode. The vertical ETX cell design provided symmetry and included improvements in component clearances and other stress-reducing modifications.

The success of the ETX cell design is shown in the test summary in Table 3-22. No electrolyte failures occurred in any freeze/thaw testing of 24 cells fully charged or half-charged at the time of freezing, and a number of cells exceeded 40 freeze/thaw cycles. In contrast with cells fully discharged, however, five of ten cells failed within six freeze/thaw cycles. Additional testing is required to establish the SOC threshold and precise cause for the increased failure sensitivity.

Table 3-22. Freeze/Thaw Test Results for ETX Cells

Test Method
- Reference electrical cycles
- Several freeze/thaw cycles
- Repeat

Results
- 24 Cells (frozen when charged)
  - –14 to 40 thermal cycles (25 average)
  - –No failures
  - –Capacity retention (98% average, 94% worst)
  - –Resistance rise (5% average, 13% worst)

- 5 Cells (frozen when half-discharged)
  - –5 Thermal cycles
  - –No failure
  - –No change in capacity or resistance

Another effect that frequently occurred with freeze/thaw cycles was deterioration of electrical performance (resistance rise and capacity decline). Two main hypotheses for these effects are (1) spalling of the protective chromium polysulfide layer from the chromium plate due to mismatch of thermal expansion coefficients, and (2) unfavorable precipitation of corrosion products throughout the cathode.

Because of the unusual thermal characteristics of the sodium polysulfides, test procedures are especially important in establishing the cells' freeze/thaw characteristics. In addition to the average rates of heating or cooling, the roles of supercooling and crystallization must be considered. Effects similar to zone refining with associated thermal shock can be observed, depending on the relationship between electrical and thermal cycle sequences. Figure 3-26 shows the development of a larger and sharper exotherm in the second thermal cycle following an electrical cycle. The onset temperature of the exotherm in the first thermal cycle indicates substantial supercooling below all equilibrium liquid-solid transitions; in the second (and subsequent) cycle it is initiated at a temperature nearly corresponding to the sodium trisulfide eutectic. Cell failure, when discharged, was frequently associated with such events.
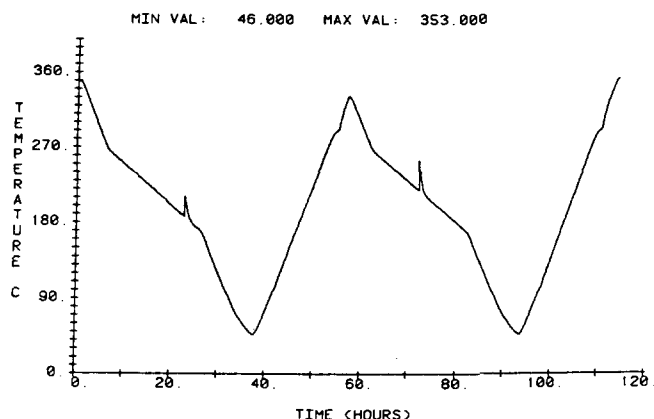

MIN VAL: 46.000   MAX VAL: 353.000

Figure 3-26. Temperature-Time Relationships for Freeze/Thaw Cycles

Special Tests

In other programs, high failure rates have resulted from extreme overdischarge and from maintenance operations on a battery at room temperature. A number of cells were used to investigate the rule of small currents that could circulate within battery circuits during the maintenance interval at ambient temperature.

Exploratory tests were performed, but they were only marginally successful in establishing crude thresholds of damage for charging while frozen, for discharging while frozen, and for unbalanced strings at ambient temperature.

The test matrices in Table 3-23 involve various times of exposure, current densities, and reverse voltages. No failures were induced during charge while frozen or while in the shorted-cell test.

Table 3-23. Damage Threshold Test and Procedures

Test A: Charge while frozen (10 cells)
(Maximum voltage limited to 5 V by Zener diode)

Group I   – 4 cells I = 200 µA
Group II – 4 cells I =   2 mA
Group III – 2 cells I = 20 mA

1. Charge each group for 1 h.
2. If no apparent failure, set aside one cell from each group. Continue charging to 3 h total.
3. Reheat and perform reference electrical cycle.
4. Repeat Steps 1 and 2 for 10 and 30 h.
5. Repeat Step 3, then repeat Step 1 for 100 h.

Test B: Discharge while frozen (8 cells)

Group I   – 4 cells V = 0.0 V
Group II – 4 cells V = −2.0 V

1. Apply voltage for 1 h for two cells, 3 h for two cells, for each group.
2. Reheat and perform reference electrical cycle.
3. Repeat Step 1 for 10 and 30 h.
4. Repeat Step 2.

Test C: Interconnected strings (20 cells)

1. Reference electrical cycles as 20-cell string.
2. Two freeze/thaw cycles as 20-cell string.
3. Repeat Step 1.
4. Two freeze/thaw cycles as balanced (10-10 or 9-9) strings in parallel.
5. Repeat Step 1.
6. Two freeze/thaw cycles as unbalanced (10-9, 9-8, or 10-8) strings in parallel.
7. Repeat Step 1.

Twenty cells that survived a previous extreme overdischarge to the sodium trisulfide during a module test were subjected to freeze/thaw cycles as a 20-cell string and as balanced and unbalanced short strings outlined Test C in Table 3-23. Except for one initial cell failure, no other cells were damaged. During the unbalanced-string test, one cell in the shorter string developed and successfully withstood high voltage, thereby restricting the level of circulating current and protecting other cells.

These special tests confirmed the ruggedness of the ETX cell design, but the cause of increased failures observed during maintenance of modules remains unresolved.

High-Energy Cells

Five high-energy cells with a theoretical capacity of ~675 Ah were on test at the beginning of the program. These cells had accumulated test times of 2 to 4 mo and were demonstrating excellent performance. Also on test were ten 2-cell pairs of similar cells.

In October 1985, testing on three single cells was discontinued voluntarily to accommodate tests of cells fabricated in the EV Battery Technology Development Program. The three cells had operated for 157, 152, and 135 cycles, respectively, in ~335 days. Performance under weekly cycling conditions remained excellent throughout the test. At its conclusion the mean reactant utilization was 73.3% of theoretical and the mean resistance was 9.8 mΩ. Earlier in the test period a similar cell had become nonfaradaic after 118 days on test (21 cycles), and another after 166 days (60 cycles).

Four of the ten 2-cell pairs on test at the beginning of the program contained one failed cell each. Testing of these pairs was continued in order to evaluate the effects of voltage abuse on the remaining good cells. During July 1985, after ~90 cycles in 150 days, two more pairs developed one failed cell each. By the end of the program all ten strings had been on test ~300 days and for >175 cycles. The mean capacity of the four strings with two good cells each was 72.6% of theoretical; the mean resistance of these two-cell pairs was 21.7 mΩ. The tolerance of cells to voltage abuse following failure of their "partner" cells is encouraging with respect to the short-string interconnection approach.

Mark-II Cell

Test of an early Mark-II cell were continued until voluntary termination after more than 2500 cycles in 5 yr. Performance was still acceptable at the end of the test (reactant utilization of 64.2% of theoretical and resistance of 14.3 mΩ). Figure 3-27 compares the charge and discharge curves for Cycle 2515 with a similar cycle in early life.

Since this test represented the achievement of a major milestone, the cell was sent to Dr. James E. Battles of Argonne National Laboratory for dissection and dissemination of component samples to appropriate laboratories for independent analyses.
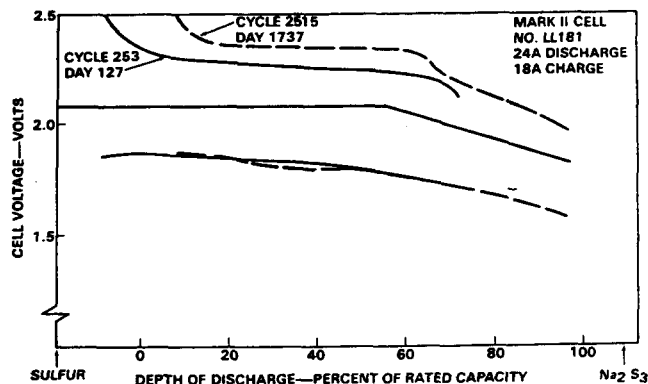

Figure 3-27. Performance Stability of Mark-II Cell

Alternative Electrodes

Three cells were being tested at the start of the program to evaluate and qualify lower-cost electrode materials. One of these was a Mark-II size and two were EVEM-1 size.

Testing of the Mark-II cell was discontinued after 1012 cycles in 889 days following development of a leak in the area of the seal between the ceramic header and the cathode container. The leak was most likely due to a previously identified failure mechanism in some cells of that time period (loss of corrosion protection related to machining of the chromium plate during fabrication). Performance had been excellent throughout the life of this cell, lending optimism for the use of the lower-cost material.

One of the EVEM-1 size cells exhibited a gradual loss of performance thought to be indicative of corrosion of the cathode container. Testing was discontinued after 1310 cycles in 505 days. The other EVEM-1 size cell failed after an equipment failure resulted in an uncontrolled freeze/thaw cycle. This cell had operated for 1229 cycles in 475 days with acceptable performance.

None of these cell failures appear to be directly attributable to the alternative electrode materials. Longer-term tests are still necessary however to establish the durability of cells fabricated with lower-cost electrodes.

Alternative Sulfur Containers

A population including five cells for the evaluation of proprietary glass coatings and twelve for the evaluation of improved chromium plate was carried over from the Phase VB program.

Conductive Glass Coatings

The cells being tested for conductive glass evaluation had already operated for more than 14 mo when this program began. Two of these cells were still on test at the end of the program, having reached 1596 and 1852 cycles, respectively. The mean reactant utilization was 57.1% of theoretical and the mean resistance was 14.7 mΩ.

The other three cells were unintentionally subjected to an uncontrolled freeze/thaw cycle because of a malfunction in the temperature controller after about 1225 cycles. Two of these cells became nonfaradaic; the third exhibited serious loss of capacity. The loss of capacity and the nonfaradaic behavior of one cell were related to reactant leakage near the cathode seal area. Posttest analysis of similar cells had shown the problem to be related to damage of the protective glass coating during seal fabrication. It appears that the conductive glass coating can offer good corrosion protection, but improvement is needed in the fabrication and assembly processes to ensure defect-free coatings.

Chromium Plate

The twelve cells used to evaluate chromium plate variations included four with E-Brite stainless steel containers plated by SNL and eight with chromium plates prepared by FACC according to procedures developed by the research staff at Ford Motor Company. Substrates (containers) included three made of E-Brite, two of 1006 steel, and three of Type 410 stainless steel. Testing on one cell was terminated in March 1985 after 650 cycles in more than 8 mo. The cell had developed low capacity. Visual observation of the cooled cell revealed a cathode container leak at or near the end-cap weld area. At the end of this program only three cells were still on test; the testing on eight of the cells had been discontinued at preplanned intervals to provide samples for posttest analysis. One of the three remaining cells (E-Brite container) had operated for 1426 cycles and the other two had operated for more than 1200 cycles (SNL's chromium plate on Type 410 stainless steel).

In addition to these eight test terminations, tests of two exploratory ETX cells were also discontinued voluntarily to provide posttest analysis samples. These cells had been discharged to a lower voltage than normal in an attempt to accelerate corrosion.

In preliminary posttest analysis the following observations were made:

- The crack-free chromium plates prepared by SNL appeared to corrode at about the same rate as FACC's crack-free chromium plates.
- The crack-free plates corroded more slowly than the microcracked plates.
- The substrate had no effect on the corrosion rate until the plate was penetrated locally.

In November 1985, at the conclusion of the EV Battery Technology Development Program, ten cells containing a developmental chromium plate on 1020 steel were continued on test in this Cell and Module Testing Program. These cells represented an effort to develop a low-cost coating for a low-cost steel while maintaining adequate cell performance and life. Three of the cells were equipped with chromium-plated containers that had been subjected to heat treatment to diffuse chromium into the steel (described in the Final Report for SNL Contract No. 51-9391). The other seven used the containers as plated, but with a hydrogen bakeout.

Based on these early results (up to ~90 cycles), these cells had a somewhat higher than expected resistance (9.9 vs ~8 mΩ). The cells contained electrolytes made by the seeded slurry-solution spray-drying (S^{4}D) process rather than by the standard Zeta process, but based on other experimental work in the EV Battery Technology Development Program, the higher resistance does not appear attributable to the S^{4}D electrolytes. Nine cells were still on test when the program ended. One cell with an as-plated container had become nonfaradaic at Cycle 41. Longer-term tests are necessary to define trends of resistance change with the number of cycles and/or time.

Alternative Electrolytes

At the beginning of this program eight cells were being tested to evaluate electrolytes made by the S^{3}D process. Five of these (EVEM-1 size) had already operated for more than 1300 cycles in 15 mo; the other three were of the Mark-II size and had accumulated ~675 cycles in 20 mo.

Three of the EVEM-1 size cells failed after similar test periods (1510, 1556, and 1596 cycles, respectively) because of loss of capacity associated with the sodium supply. Test data indicated that the electrolytes in these cells were still physically intact; performance had been good until the abrupt capacity loss. By the end of the program the other two EVEM-1 size cells had operated for 2000 cycles in 25 mo with good performance.

When the program ended, two of the three Mark-II size cells were also still on test, with a mean capacity of 63.1% of theoretical and a mean resistance of 13.8 mΩ after ~1075 cycles in 30 mo. Testing was discontinued on the third cell after an apparent sodium supply problem that developed at about Cycle 942. This cell had also demonstrated good performance throughout its life, until the last few cycles.

The S^3D process continues to hold promise for adequate life at a reduced electrolyte cost, but additional in-cell evaluation is required.

Stationary Energy Storage Modules at FACC

Two reconfigured modules, which consisted of Mark-IID cells recovered after 675 cycles in the 100-kWh battery, were continued on test. The cells in each module were connected in a 2×48 configuration to evaluate the charge control requirements of parallel short strings, each string having two cells and a fuse in series.

When this test period began, both modules were operating in series. The status of Module 1 after 240 cycles showed thirty-nine functional strings, and nine inoperable strings (eight strings with one failed cell and one good cell each, and one string with good cells but with a torn fuse). The eight partner cells (the remaining good cells in failed strings) were polarized to 4 V, and provided 100% coulombic efficiency for the module, as desired. The status of Module 2 after 40 cycles showed thirty-seven functional strings, nine inoperable strings, and two strings that were not initially installed.

During the testing program, occasional cell failures were followed by the polarization of the corresponding partner cells, so that the module maintained 100% coulombic efficiency. None of the partner cells failed, even though they were exposed to high voltages (4 V average, 5.2 V peak) for up to 18 mo.

The summary of each module's test history, showing the number of active strings and module coulombic efficiency, are given in Figures 3-28 and 3-29, along with an indication of the final exposure times to high voltage without partner cell failure. It is clear that the short-string configuration offers benefits for charge control.
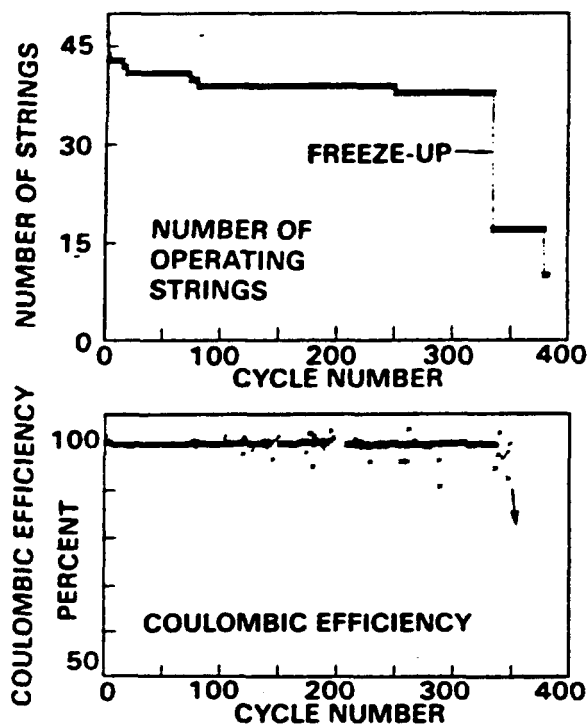
CONCLUSIONS

- 100% COULOMBIC EFFICIENCY RETAINED
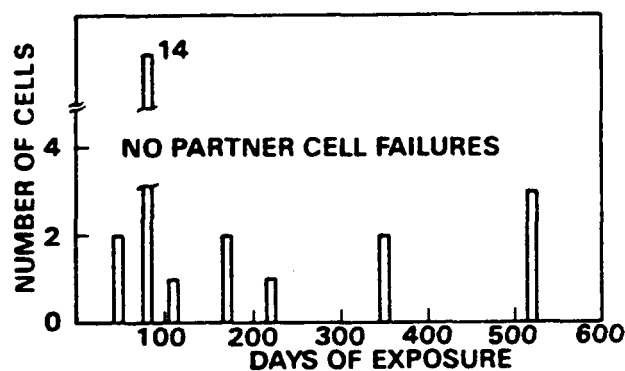- NO PARTNER-CELL FAILURES
- POOR FREEZE-THAW RELIABILITY

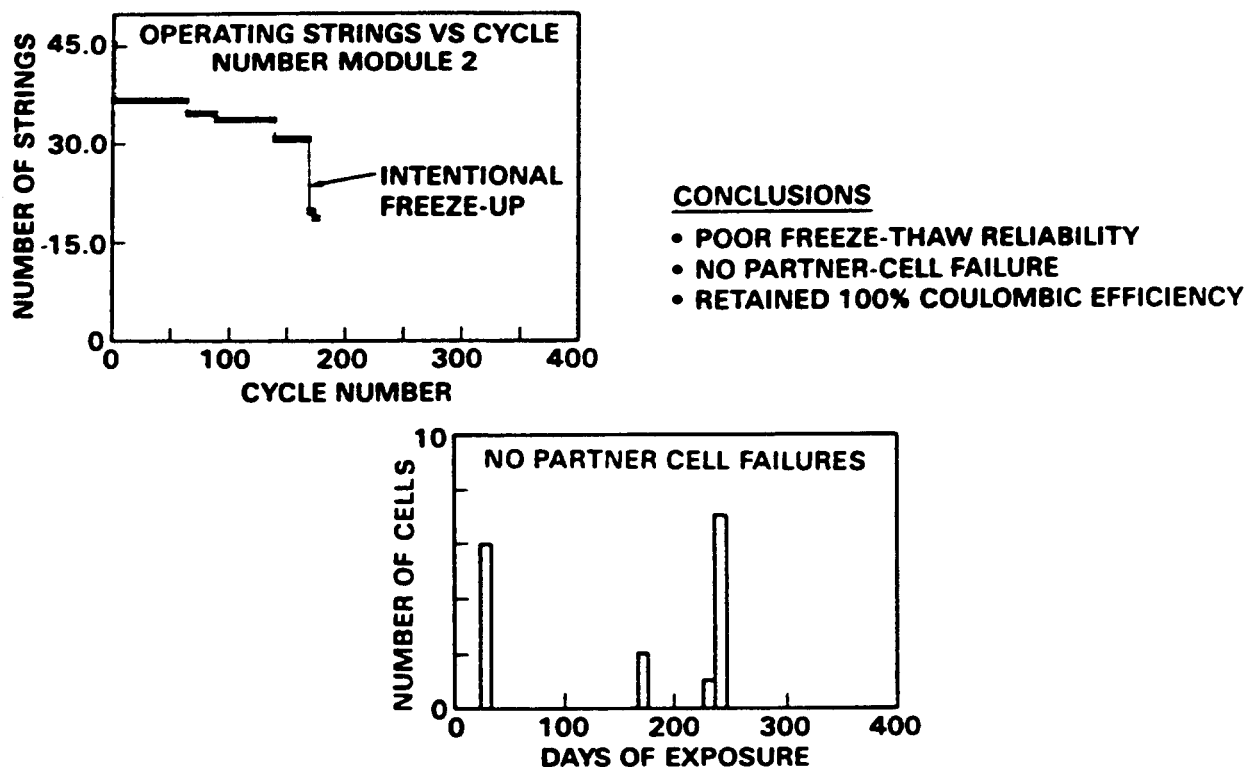Figure 3-28. Test Results of Module 1

Figure 3-29. Test Results of Module 2

However, three less favorable events occurred during the test. One string in Module 1 became erratic and appeared to draw current continuously. When the fault did not clear in several days, visual inspection was scheduled, and the module temperature was reduced to ~250°C. During cooling the fault cleared itself, as confirmed visually by inspection of the blown fuse. After the temperature was restored, the module continued to operate at 100% coulombic efficiency.

A weekend failure of the oven's circulating fan caused Module 1 to cool to 90°C. The bus voltage dropped to approximately zero, with many cells registering reverse voltages. Upon reheat, sixteen strings experienced failure of one cell and proper blockage by its partner cell. However, in four strings, double cell failures occurred, but the fuses did not blow until special module-charging routines were employed. Although unscheduled, the module cooldown fortunately occurred while the module was charged. The high failure rate was unexpected.

To explore the causes of failure during freeze/thaw, a test plan was prepared for intentionally cooling Module 2 while maintaining its bus voltage near the proper OCV. During cooldown to ~80°C performance was generally as expected. Several apparently

good strings developed unbalanced voltages (e.g., 1.8 and 2.3 V) during cooldown. Since the voltages did not stay balanced near their OCV, this observation was interpreted as one cell having a moderately conductive shunt due either to a very slight internal short or to an external cause. This could have been caused by the minor leakage of reactants near the seals that had been observed on some cells. As heating began, at least one double cell failed, pulling the bus voltage to 0.1 V despite the 5-A, 4-V power supply that had been attached to maintain module voltage. Many cells experienced reversed voltages from −0.2 to −0.5 V until the temperature reached ~240°C and the good strings could provide current to offset the losses. In summary, more than half the strings had failed and several strings continued to draw leakage current, requiring special charge control for Module 2.

After several diagnostic cycles, the tests were terminated and both modules were cooled down. At termination, Module 1 had completed 379 cycles and Module 2 had 174 cycles. This was in addition to the 675 previous cycles the cells had completed in their original configuration. The individual cells had been on test for ~4.5 yr. A large percentage of the cells still appeared functional.

The two-cell string appears to offer strong benefits in eliminating charge control requirements during normal operation. However, the sensitivity to cell failure during cooldown suggests that the module configuration must be developed further.

Conclusions and Recommendations of FACC Tests

This program provided a valuable extension of test time necessary to evaluate the durability of component and cell designs and materials, and to evaluate the short-string module design.

Although more test time is desirable, results to date appear promising for the ETX cell design and for lower-cost electrodes, electrolytes, and cathode containers. Testing should continue on the ETX cell design and lower-cost components should be incorporated as they become qualified.

Tests showed that short (two-cell) strings can eliminate module-charge control requirements during normal operation. Based on the limited tests in this program, however, the configuration appears sensitive to cell failures during cooldown, suggesting the need for additional development.

Improved Lead-Acid, Load-Leveling Batteries—Exide

During the first three quarters of 1985 final cycling of the 35-plate, 3100-Ah preprototype, load-leveling, lead-acid cells (developed on ANL Contract 31-109-38-4951) was completed, and the remaining cells that had not failed were shipped to ANL/NBTL for continued testing.

The design that delivered the highest energy output during the cycling test, meeting the cycle life goal at 40°C ± 5°C, consisted of the following:

- Low-density positive active material in a long-life lead antimony grid design
- High-density negative active material in lead-calcium negative grids
- 1.285 sp gr sulfuric acid electrolyte
- A perforated PVC, random glass mat, microporous rubber separator system.

Cells of this type were assembled in three- and six-cell modules for delivery to ANL/NBTL. Tests of two cycles per day were performed at 80% DOD on these batteries at 50°C ± 5°C and 60°C ± 5°C to extend the data on cycle life as a function of operating temperature.

Table 3-24 summarizes the cycle life at each temperature and includes the cycle life of half-size cells (full-size plates) at 70°C. From this data, the relationship between cycle life and cell electrolyte temperature was found to be

$$\ln F = \alpha \, (t_E - 25°C)$$

where $\ln F$ is the natural logarithm of the ratio of cycles projected at 25°C to actual cycles to failure at test temperature t_E. The initial value of α was estimated to be 0.03. Recent data analysis by Battelle, Columbus, now predicts an α of 0.04.

Table 3-24. Multitemperature Cycle Life of 6-kWh Prototype Cells

Test Temperature Target (°C)	Life Mean (°C)	No. of Cell Samples	No. of Cycles to Date or to Failure (F)	Cycle Life Goal	Percent of Goal	Equivalent 25°C Cycles (Calc.)
40	39	6	2324	2220	105	4190
50	50	6	1582	1495	106	4430
60	54	3	916	1250	73	2965
70	66	4	1012(F)	775	130	5220

This equation assumes a linear relation for log cycle life that declines with increasing operating temperature. Practical experience in cycling lead-acid EV batteries and other systems from frigid to hot temperature extremes predicts a maximum cycle life between 25°C and 45°C, with cycle life declining as either extreme is approached. The decline of cycle life between 40°C and 70°C is the result of energy decay as the negative plates become limited near end of life. Negative active material sulfation, positive grid corrosion, and moss accumulation on the top edges of the element assembly contributed to energy loss.

Figure 3-30 shows that the advanced load-leveling cells cycling at 40°C, 50°C, and 70°C had met or exceeded their cycle life goals at their respective temperatures. On a single 80% DOD cycle per day in a load-leveling regime, a conservative life of 3000 cycles to failure by energy decay appears to be an achievable goal for future energy plants.
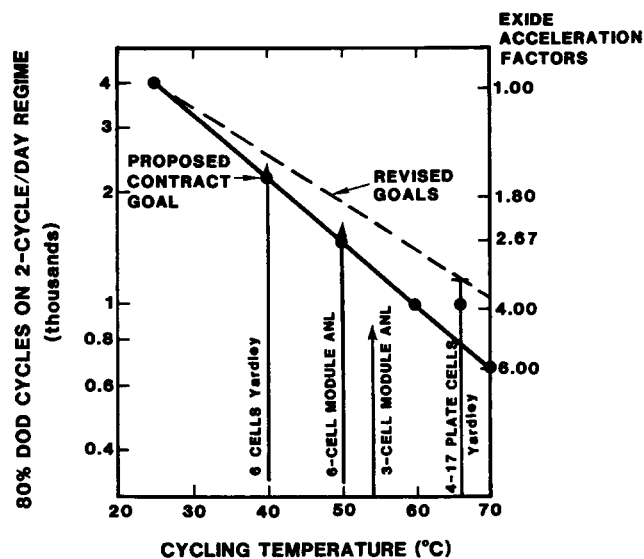
Figure 3-30. Cycle Life vs Operating Temperature

Chapter 4. Technology Improvement

The Technology Improvement element of the ETD Project was initiated in 1985. The purpose of this element is to investigate and often solve specific problems encountered in the development of advanced secondary batteries. Solutions to problems that will give a competitive advantage to a particular developer are not sought. Rather, in these cases, insight into causes of the problem are desired. During the past several years, it became increasingly apparent that some problems impeding the development of advanced batteries could be better addressed with resources not available at the principal developers. These desirable resources might be at SNL or elsewhere. In previous years, a number of such tasks were initiated under either the Aqueous or Nonaqueous Battery Development elements. With the creation of the Technology Improvement element, these efforts have been combined and several new activities initiated.

Seven active tasks were included in this element during 1985: two relate to aqueous batteries and five to nonaqueous batteries. Progress during 1985 for each of the seven tasks is outlined in the remainder of this chapter. One aqueous task is related to the zinc/bromine system, the other to the zinc/ferricyanide system. All five of the nonaqueous tasks pertain to the sodium/sulfur system. All but one of these were conducted in-house at SNL. The exception was an activity at Oak Ridge National Laboratory (ORNL) designed to explore new concepts for the ceramic electrolyte used in the sodium/sulfur system. Two of the nonaqueous tasks were initiated in 1985; the other five tasks were already underway during 1984 and were reported in *Exploratory Battery Technology Development and Testing Report for 1984* (SAND85-1446).

Membrane Research—SNL

The objective of this task is to develop a suitable low-cost membrane for the zinc/ferricyanide battery. In previous studies, a sulfonated polysulfone membrane (prepared at SNL) and a radiatively grafted membrane (prepared for SNL by RAI Research Corporation) performed well in the Lockheed cycling test cell. This year, efforts were focused on three areas:

- Optimization of sulfonated polysulfone membranes
- Analysis of the long-term aging behavior of a radiatively grafted membrane
- Evaluation of newly introduced commercial membranes.

Results

The highlights for the SNL membrane research program in 1985 include the following:

- Sulfonated Polysulfone Membranes
  - These membranes were optimized by a factorial study.
  - Asymmetric membranes were prepared.
- Radiatively Grafted Membrane
  - A postmortem analysis revealed severe graft degradation.
  - An accelerated aging study showed complete loss of ionic exchange capacity.
- Evaluation of Commercial Membranes
  - The millipore membrane was not selective.
  - The new version of Nafion® appeared promising.

Area resistivities of early sulfonated polysulfone membranes needed to be reduced in order for the battery to have reasonable voltaic efficiency. Initial efforts showed that the area resistivity could be reduced by an order of magnitude simply by increasing the molar ratio of SO_3/triethylphosphate(TEP)/polysulfone(PS) from 2/1/1 to 2.4/1/1, but this resulted in unacceptable permeation rates. To achieve a better balance of properties, a factorial study was carried out in which the effects of the following variables were determined: SO_3/TEP/PS ratio, concentration of sulfonated polysulfone in the casting solution, thickness of the cast solution, and degree of extraction with water. The results of the factorial study are shown in Table 4-1. Good selectivity and low area resistivity were achieved by a membrane cast from a 0.038-cm-thick 20% solution and extracting the membrane with water. If these procedural guidelines are followed, selective membranes can be made even with high SO_3/TEP/PS ratios. Samples of these membranes have been sent to Lockheed for cycle testing.

Table 4-1. Optimization of Sulfonated Polysulfone Membranes

| | Process Variable | | | Properties | |
SO$_3$/TEP/PS Mole Ratio	Polymer Conc. w/v%	Cast Sol'n Thickness (cm)	Extraction With H$_2$O	Area Resistivity ($\Omega \cdot$ cm^2)	Permeation (millimoles Fe/cm^2/h)
2.4/1/1	20	0.038	Y	0.62	1.3×10^{-4}
2.4/1/1	20	0.038	N	0.24	8.3×10^{-3}
2.4/1/1	20	0.013	Y	0.31	1.3×10^{-3}
2.4/1/1	20	0.013	Y	0.13	1.7×10^{-2}
2.4/1/1	10	0.038	Y	0.34	2.8×10^{-4}
2.4/1/1	10	0.038	N	0.24	1.1×10^{-2}
2.4/1/1	10	0.013	Y	0.16	1.4×10^{-2}
2.4/1/1	10	0.013	N	0.04	1.6×10^{-2}
2.2/1/1	20	0.038	Y	1.2	9.6×10^{-5}
2.2/1/1	20	0.038	Y	1.1	9.3×10^{-3}
2.2/1/1	10	0.013	Y	0.77	4.6×10^{-5}
2.2/1/1	10	0.013	Y	0.58	7.6×10^{-4}

Asymmetric membranes are expected to have improved electrochemical and mechanical properties. The asymmetric membranes were prepared by placing a formamide and tetrahydrofuran solution of the polysulfone polymer into the nonsolvent isopropyl alcohol. The resulting membranes were examined by scanning electron microscopy and found to have a 0.002-cm skin supported by a 0.008-cm porous substrate. Their resistance ranged from 0.4 to 1.0 Ω cm^2. Preliminary evaluation indicates that their selectivity is close to meeting the battery requirements. An accelerated aging test showed that the stability of the asymmetric membranes is comparable to that of the solid cast membranes.

A membrane from RAI Research Corporation has exhibited a 79.3% average energy efficiency for over 760 charge/discharge cycles in the Lockheed test cell. The membrane was prepared by radiatively grafting styrene and divinylbenzene onto a fluorocarbon substrate followed by sulfonation. The long-term stability of the membrane was a concern however, because short-term cycling indicated that the membrane lost a substantial amount of its ion exchange capacity with time. These concerns were realized when postmortem analysis of the cycled membrane indicated that no experimentally significant ion exchange capacity remained. The results from an accelerated aging test, shown in Figure 4-1, substantiated the membrane's loss of ion exchange capacity. These results would be extremely disappointing were it not for the fact that the membrane continued to perform well in the cycling test cell. The possibility is being investigated that the microporosity of a radiatively grafted membrane may have qualitatively different properties than that of several commercial microporous membranes that have been evaluated.
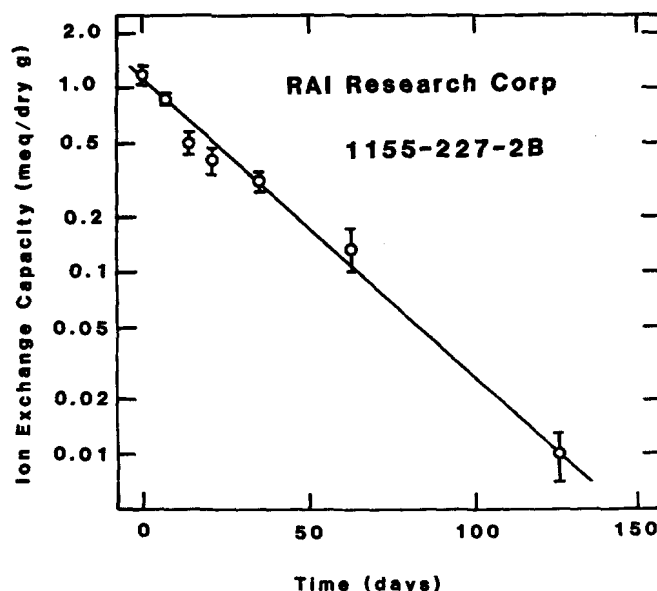

Figure 4-1. Accelerated Aging Test Showing Membrane's Loss of Ion Exchange Capacity

Millipore respresentatives requested that SNL evaluate an experimental membrane they developed for reverse osmosis applications. The membrane was a composite of a thin film of sulfonated polysulfone supported by a laminated layer of microporous polysulfone and a woven layer of polyethylene. Low area resistivity could be achieved only after a wetting process, which unfortunately caused an undesirable increase in the rate of iron permeation. DuPont recently developed a new version of Nafion® membrane that has a higher ion exchange capacity, is thinner, and will cost about 50% less than the previous Nafion. We found that the area resistivity was quite low and that the permeation of iron was negligible. This membrane was sent to Lockheed for efficiency and life tests.

Technical Challenges Remaining

The ability to scale up the production of sulfonated polysulfone membranes must be demonstrated. Commercial sources of sulfonated polysulfone and automated methods of solvent-casting membranes will be explored.

We will attempt to determine why the radiatively grafted membrane continues to perform well in the cycling test cell after its ion exchange capacity has been lost. It is possible that this membrane's unique microporosity may allow the membrane to perform well indefinitely. A contract will be placed with RAI Research Corporation to prepare membranes with grafts of enhanced stability.

We will continue to monitor the performance of existing commercial membranes that appear promising, and we plan to evaluate new membranes that are brought to our attention.

Durability of Polymeric Materials Used in Zinc/Bromine Battery

Carbon-plastic electrodes in zinc/bromine batteries have an advantage over metals in that they are not as susceptible to corrosion. Other advantages include low cost and ease of fabrication. However, plastic materials, which are used in the flow frames and storage containers as well as in electrodes, are not immune from attack by bromine-containing electrolytes. Previous studies have shown that incorporating bromine complexing agents, such as quaternary amine salts, reduces but does not eliminate such degradation reactions as bromination and oxidation. Several batteries have failed because of what are believed to be materials-related problems.

The purpose of this task was (1) to determine the cause of these materials-related failures, and (2) to further our understanding of the chemistry and physics involved in the degradation process. These goals were achieved by postmortem analyses on the carbon-plastic electrodes and electrolytes of two failed batteries (#143 and #169) manufactured under a previous contract with Exxon, and by characterization studies of degraded plastic materials that were subjected to accelerated aging tests.

Results

Battery 143 failed after 198 cycles. A description of this battery is given in previous annual reports. The bipolar electrode used in the battery became badly warped with use; this was considered a factor that contributed to the battery's failure. The following postmortem analyses were made on this electrode to determine what property changes accompanied warpage and to gain insight as to why warpage occurred:

- Scanning electron microscopy (SEM)
- Total bromine content
- Electron microprobe analysis
- Surface area (BET)
- Percent extractables
- X-ray diffraction
- Infrared analysis (IR).

SEM analysis of the electrode revealed the presence of microcracks on the cathode surface and a roughening of the anode surface. It is conceivable that microcracks could alter the pattern of electrolyte circulation, which might in turn adversely affect battery performance.

Figure 4-2 shows the electron microprobe analysis of the zinc and bromine contents of the electrode as a function of position across the thickness dimension. High concentrations of both zinc and bromine occur on either side of the interface of this bipolar electrode, resulting in a bimodel profile. Clearly, deep penetration of the zinc bromide into the electrode occurred from both the anode and cathode sides, but crossover at the interface was minimal. Extraction with deionized water removed most of the zinc, but not all of the bromine. One explanation for this is that the bromine is chemically bound to the electrode. If bromination of the polyolefin in the electrode occurred, the resulting brominated products would be difficult to remove by extraction. Because of the high carbon content of the electrode, this could not be verified by IR.
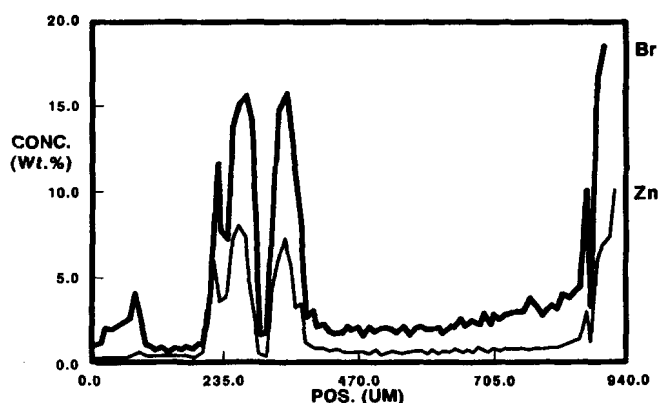
Figure 4-2. Bromine and Zinc Contents Across Thickness of Carbon-Plastic Electrode After 198 Cycles (Battery 143)

The polyolefins used were crystalline polymers. X-ray diffraction analyses revealed this morphology was not perturbed as a result of cycling.

The surface area of the electrode decreased considerably as a result of cycling. Thus, the virgin electrode had a surface area of 27.3 m^2/g; after cycling, the surface area was 10.9 m^2/g, a decrease of 60%.

The percentage of low-molecular-weight material extracted by consecutively recycling water and chloroform over the electrode using a Soxhlet extractor is shown in Table 4-2.

Table 4-2. Percent of Extractables Removed From Virgin vs Cycled Electrodes

	% Extractables	
Extracting Medium	Virgin Electrode	Cycled Electrode
H_2O	0	19.8
$CHCl_3$	6	4.7
Totals	6	24.5

One can see from this data that the electrode absorbed considerable quantities of the electrolyte. Since the flow frame that supports the electrode is thicker and more rigid than the electrode itself, it is proposed that warpage was caused by dimensional changes incurred as a result of electrolyte absorption.

On the basis of these findings, it is possible that Battery 143 failed because of the following looped chain of events:
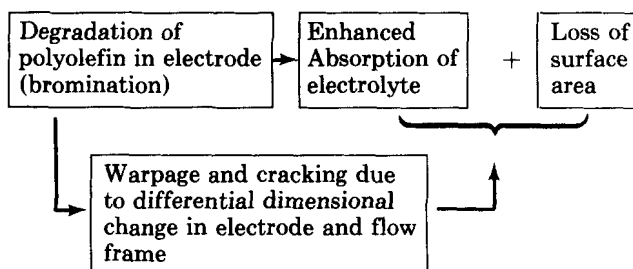
Battery 169 failed after 121 cycles. In this test, the pH of the electrolyte increased from 3 to ~5, and a precipitate formed that was less dense than the electrolyte. In later cycles, this precipitate redissolved. The electrode did not warp, but appeared to be contaminated by an impurity. In later tests, more precipitate was generated. This material had a lower density than the electrolyte and was easy to collect for analysis. The material was first separated into volatile and nonvolatile fractions. The volatile fraction, consisting primarily of bromine, was isolated by continuous pumping through a trap for ~10 days. The nonvolatile residue was identified by IR as a crude mixture of methyl ethyl morpholinium bromide and methyl ethyl piperidinyl bromide (i.e., the complexing agent and miscellaneous degradation products). The presence of enhanced absorption in the region of 1600 to 1700 cm^{-1} suggests that some of these degradation products contained carbonyl groups. Such products are typically formed by oxidative degradation reactions, and their presence, by some manner, caused the precipitate to float. The long time required to remove the bromine may be due to saturation of the complex with bromine. High bromine contents may have resulted from the fact that hydrogen bromide was frequently added to reduce the pH. The resultant loss of the complex by precipitation may have had an impact on the performance of this battery.

In summary, postmortem analysis of the carbon-plastic electrode taken from Battery 143 revealed

- A high degree of sorption of electrolyte (~20%)
- Complete penetration of the electrolyte into the electrode
- Chemically bound bromine
- Loss of surface area (~60%)
- Microcracks on the cathode.

106

The battery failure was probably caused by warpage of the electrode incurred by dimensional changes which, in turn, were brought about by electrolyte sorption and chemical degradation.

Accelerated Aging Studies

In the accelerated aging study, the effect of bromine and the presence or absence of other electrolyte ingredients on the absorption of electrolytes by polyolefins and polyolefin-containing materials became apparent. This effect is shown in Figure 4-3. Sorption of the anolyte, which contains no elemental bromine, was <2% for all the materials. In contrast, uptake by the catholyte, which differs from the anolyte in that it contains a small but finite amount of elemental bromine that is in equilibrium with complexed bromine, was significantly higher for all the materials (5% to 25%). Elimination of the complexing agent, which increased the equilibrium concentration of free bromine, resulted in much higher weight increases (up to 95%). These data, obtained at 55°C after 3 mo, were not entirely unexpected as bromine is soluble in, and capable of reacting with, polyolefins. What was surprising was the magnitude of this effect. Weight gains, upon exposure to the catholyte, were 20% to 80% lower at ambient temperatures. The average operating temperature of zinc/bromine batteries is intermediate between these two extremes (~35°C).
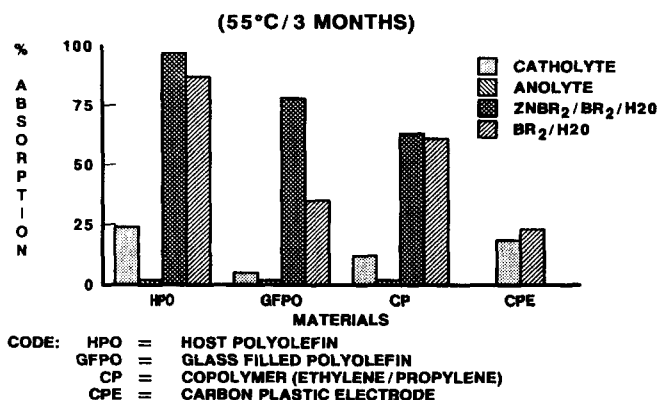

Figure 4-3. Absorption of Electrolytes

Since electrolyte sorption and/or reaction can incur dimensional changes, the length and thickness of a carbon-plastic electrode was determined after exposure to the catholyte for three months at ambient conditions. Sample thickness increased by 0.0025 cm (~3%); the length increased by 0.010 cm (~0.2%). As pointed out previously, dimensional changes will result in electrode warpage that adversely affects battery performance.

As reported, degradation of polyolefins by bromine-containing electrolytes is quite extensive at 55°C and 70°C. Under these conditions, polyolefins undergo bromination and oxidation. The question arises, do these reactions occur at ambient conditions and if so to what extent? Small amounts (0.1% to 0.8%) of chemically bound bromine were detected by ion chemotography in polyolefin samples that had been exposed to the catholyte at ambient conditions for 3 mo. Oxidation reactions generally result in chain cleavage, which results in a decrease in molecular weight. The average molecular weight of the polyolefin used in the flow frame decreased from 32,350 daltons to 23,750 daltons after exposure to the catholyte at ambient temperatures. Thus, oxidation seems to be occurring even at room temperature.

Electron microprobe analysis of samples exposed to the catholyte at 55°C indicated that the concentration of covalently bound bromine was high (~10% by weight). In addition, the bromine was fairly uniformly distributed as a function of sample depth. Whether this state was reached by rapid diffusion of bromine through the sample followed by slow consumption (reaction), or whether it occurred through extensive diffusion-limited heterogeneous degradation is not known. Profiling experiments are needed to enable us to distinguish between these two types of degradation.

The following stabilizers or combinations of stabilizers were blended into pure polypropylene: (1) 0.1% Irganox 1010, a phenolic antioxidant; (2) 0.1% Irganic + 0.1% B-255, a phosphite synergist; (3) 0.1% Irganox + 0.1% B-225 + 0.1% stearyl dithiopropionate; and (4) 0.1% Agerite, an amone antioxidant. As was observed with unstabilized polypropylene, the above "stabilized" samples lost mechanical integrity after exposure for 3 mo at 55°C in the catholyte.

In summary,

- Electrolyte sorption by carbon-plastic electodes and polyolefins scaled with the free bromine content in the electrolyte and, in the case of the electrodes, resulted in dimensional changes that could cause warpage.

- Bromination and oxidation of polyolefins occurred even at ambient conditions in the presence of the electrolyte over a time scale of three months.

- Covalently bound bromine was present in all polyolefin samples exposed to the catholyte for 3 mo at 55°C.

- Preliminary data indicate that incorporating stabilizers into the polyolefins had a neglible effect on durability.

Technical Challenges Remaining

- Improve the durability of inexpensive, easily processed plastic materials by the incorporation of unique stabilizers capable of countering the effect of bromine.

- Define the kinetics of bromine degradation in aqueous environments and determine whether the degradation is diffusion-limited and heterogeneous or homogeneous and nondiffusion-controlled.

Fracture Analysis of Beta"-Alumina Electrolyte

A significant number of sodium/sulfur cells have failed very early in life under circumstances that suggest mechanical failure of the solid electrolyte. In the 1984 annual report we described the analysis of a number of those failures in cells that had been fabricated by FACC. That analysis resulted in the identification of two previously unrecognized modes of failure produced by stresses generated in the electrolyte by the cathode.

A careful examination of the fracture surfaces in those electrolytes revealed that many of the fractures initiated at large grains or at combinations of large grains and large pores. The pores and the large grains usually contained impurities such as iron, copper, zinc, and silicon. Presumably, the impurities were introduced before the tubes were sintered and were responsible for the exaggerated grain growth.

As a supplement to the failure analysis study and as part of a general evaluation of the performance of electrolytes manufactured by Ceramatec, the strength and fracture toughness of production materials were measured. The goals were (1) to determine whether the defects responsible for failure in room-temperature testing were the same as those that produced failure in service; (2) to determine the uniformity of mechanical properties within a tube and the reproducibility from part to part within a production batch; and (3) to evaluate whether strength data obtained from ring specimens could be used to predict failure probabilities in tubes. Success with (3) would mean that the number of tubes required for an adequate statistical representation of tube failure could be reduced from thirty or more to one or two.

The mechanical properties experiment was conducted with four representative tubes taken from one production lot. Portions of these tubes were cut into ring sections 4 mm long, using a 220-grit diamond saw. The rings were tested at SRI International, using their ring tensile test apparatus. This apparatus uses a hydraulically loaded bladder to generate a nearly uniform circumferential tensile stress in the rings. To obtain fracture toughness values, well-defined flaws were introduced by indentation in some of the ring specimens prior to testing.

Ring Strength Data

The results of the ring tests are shown in Table 4-3. The number in parentheses next to the tube designator [e.g., A (13)] is the number of rings for which valid failure stresses were determined. The P-tube rings were reground after sawing to improve the finish on the cut surfaces. The results show that regrinding actually degraded the strength. The other three sets of rings show excellent agreement in the mean value of the failure stress, indicating good reproducibility from tube to tube. The standard deviation is typical for brittle fracture and reflects that failures were produced by defects, which vary in severity. As the footnote indicates, 17 of the 21 failure sources in the J-series were located and all were either large pores or large grains. Table 4-3 also shows the results of the Weibull statistical analysis, in which the failure probability, F, is related to the stress by the relationship

$$F(\sigma) = 1 - e^{-(\sigma/\sigma_o)^m}$$

where σ_0 is the stress at which the failure probability is $1-e$ and m is the "Weibull modulus." Because of the good agreement of the data obtained on the A, C, and J specimens, those data were pooled to obtain the plot shown in Figure 4-4. As indicated, the Weibull modulus for the pooled data was 7.6, whereas σ_0 was 140 MPa.

Table 4-3. Results of Ring Tensile Test

| Tube | Failure Stress (MPa) | | Weibull Analysis (MPa)* | |
	(mean)	(SD)	(m)	(σ_o)
A (13)	130	29.4	5.56	141
C (20)	134.4	14.6	9.53	141
J (21)[†]	129.6	29.4	7.85	142
P (18)[‡]	101.5	19.5	6.18	109

*$F(\sigma) = 1 - e^{-(\sigma/\sigma_o)^m}$

[†]Seventeen of the rings contained identifiable sources; all were internal flaws
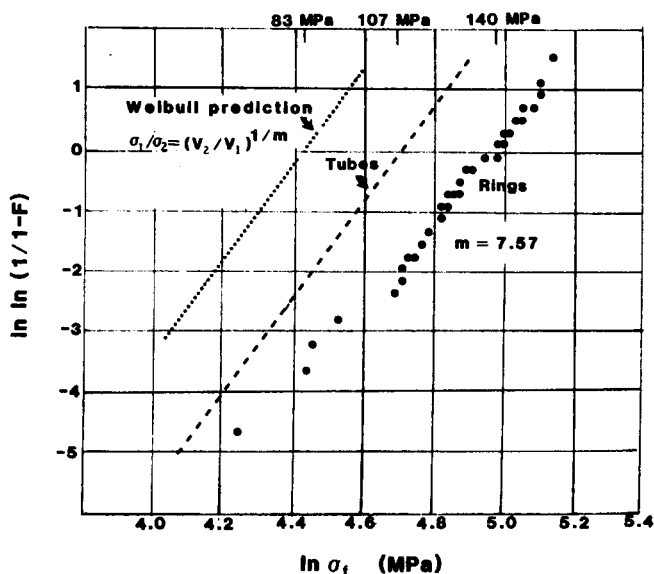
[‡]Reground

Figure 4-4. Weibull Modulus for Pooled Data From A, C, and J Specimens

Fracture Toughness

The calculation of fracture toughness, K_{1c}, is based on the Griffith relationship between the flaw size and the failure stress. A reliable value for K_{1c} depends on an accurate determination of the flaw size. For the indented ring specimens, the flaw size was determined by measurement of the length of the crack extending from the indentation before failure and by direct measurement on the fracture surface after the ring had fractured.

Figure 4-5 shows the fracture toughness data for the two methods of determining flaw size. The sketches show how the flaw dimensions were measured; the footnotes show the equations used in the calculations. The numbers in parentheses next to the mean fracture toughness values are the numbers of samples measured. It was difficult to obtain an accurate measure of crack length prior to testing, so the values obtained from measurement on the fracture surface are regarded as the more reliable ones.

		K_{1c} (MPa·m$^{\frac{1}{2}}$)	
		Mean	**S.D.**
Crack Length*		1.59 (17)	.26
Flaw dimensions**		1.84 (15)	.40

* $K = \sigma \sqrt{b\pi}$

** $K = \sigma \sqrt{\pi} \sqrt[4]{(ab)}$

Figure 4-5. Fracture Toughness From Indented Ring Specimens

To provide a comparison of ring data with data obtained by internally pressurizing entire tubes, the line obtained from linear regression analysis of data obtained at Ceramatec on similar tubes is included in Figure 4-4. The Weibull modulus has precisely the same value for the ring data and the tube data, that is, the plots have the same slope. A lower value for σ_o is expected for the tube failures because the population of flaws is much larger in the tubes than in the rings. Specifically, in the Weibull theory, for specimens with different volumes but with the same flaw-size distribution, failure stresses (at a given failure probability) should be related by
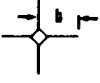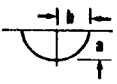
$$\sigma_1/\sigma_2 = (V_1/V_2)^{1/m} ,$$

where m is the Weibull modulus. If the ratio of the tube volume to the ring volume is used to predict the failure stresses for the tubes from the ring data, the dotted curve in Figure 4-4 is obtained. It is obvious that the tubes performed much better than predicted from the volume relationship.

Consequently, although this experiment has shown that the Weibull modulus obtained from ring data can be used to calculate failure probabilities for tubes, it also shows that it is necessary to obtain failure data on a few full-size tubes in order to obtain a reliable value for σ_o used in the calculations.

The value of 1.85 MPa m$^{1/2}$ for K_{1c} is somewhat lower than the value of 2.0 to 2.3 reported by Ceramatec for its Zeta-process beta"-alumina. It is in good agreement with values obtained from measurement of dimensions of process flaws in the ring strength specimens.

Beta"-Alumina Degradation

Anil Virkar, University of Utah

One approach to improving the mechanical response of beta"-alumina is to add zirconia powder to the batch prior to sintering. One clear result of that addition is the disappearance of the very large grains responsible for many of the failures in beta"-alumina.

109

The suppression of exaggerated grain growth can be achieved by adding either fully stabilized zirconia or partially stabilized zirconia to the beta″-alumina. However, the addition of partially stabilized zirconia may also improve the mechanical performance by what is termed *transformation toughening*. Substantial increases in fracture toughness and strength have been obtained in alpha-alumina and other materials by transformation toughening with zirconia additions.

One of the features of transformation toughening is that the stress field at the crack tip promotes the transformation of the zirconia to a lower density phase. As a consequence, the material at the crack tip is driven into compression (Figure 4-6). The question being addressed in the current study is how the local compressive stress developed by transformation toughening (or other tensile or compressive stresses present in the tube wall) might affect the electrolytic degradation processes. In beta″-alumina, degradation in the form of cracks extending into the electrolyte can occur at high ion-current densities. This degradation is a result of pressure generated in existing surface cracks as sodium flows into the crack through its walls. The magnitude of that pressure is determined by the resistance to the flow of the sodium out of the crack.
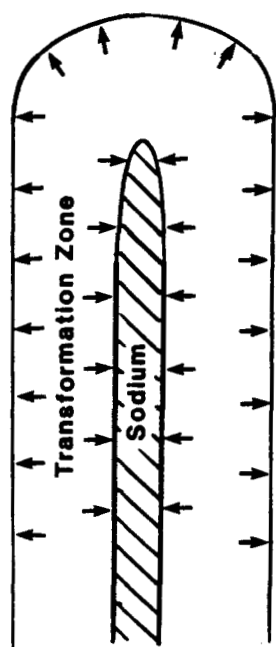

Figure 4-6. Material at Crack Tip Compresses as a Result of Transformation Toughening

Mechanical pressure on the crack from residual stresses or transformation of zirconia could affect the growth of the crack in several ways. The most obvious way would be to change the stress intensity factor at the crack tip. A compressive stress would reduce the stress intensity, slowing the crack; tensile stress would enhance the stress intensity and accelerate the crack. However, compressive stress might also close the mouth of the crack, restricting the sodium flow and raising the pressure so that crack growth is enhanced. Tensile stress might produce the opposite result.

Experimental Work

Ultimately, testing will be conducted at 300°C. However, for a preliminary assessment of the effect, experiments have been conducted at room temperature with the apparatus sketched in Figure 4-7. Fifty test bars of lithia-stabilized beta″-alumina have been prepared, and a number of these have been tested. The test procedure consisted of an initial electrolysis of 3 s at 7 mA for all specimens. Then half the sample set was subjected to a bending load while it was electrolyzed for an additional 16 s. The bending load produced a compressive stress of 50 MPa at the silver-painted surface (where the sodium was deposited). The other half of the sample set was also electrolyzed for an additional 13 s, but with no applied stress. Samples were subsequently loaded to failure in bending with the silver-painted surface in tension. For the bars that were mechanically stressed during electrolysis, this had been the surface in compression.
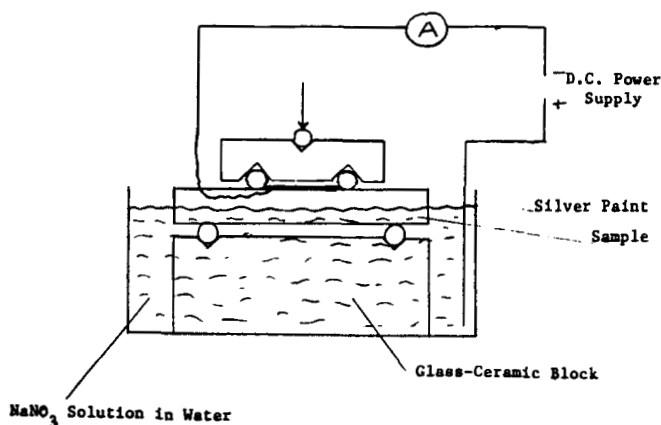
Figure 4-7. Schematic of Apparatus Used to Electrolyze Beta″-Alumina Samples Under Load

Preliminary results showed that the bars that had been electrolyzed with no load failed at 70 MPa. Those that had been loaded to 50 MPa during electrolysis failed at 110 MPa. For comparison, pristine specimens (no electrolysis) failed at 170 MPa. The superposed compression appears to have retarded degradation.

Future work will include examination of the effects of tensile stress in addition to tests at high temperature.

Chromium-Plating Studies of Sulfur Electrode Containers

Chrome-plating of sulfur containers is a common technique used by many manufacturers of sodium/sulfur batteries to protect the container from the very aggressive sodium polysulfides produced during the discharge of the battery. FACC chose a proprietary solution for its chrome-plating operation (M&T Unichrome CF-500). Plating conditions were identified as a critical factor affecting the durability of the resulting chrome deposit. Failure analysis of actual FACC cells revealed very erratic corrosion behavior of their sulfur containers. Examination of the early chrome deposits indicated that significant cracking in the plating often occurred. With this evidence, a small study was initiated at SNL (Livermore) in late 1983. The objective was to profile both the plating solution and operating conditions and then to identify changes that would reduce the cracking problem. The study was completed in 1985.

To reduce cracking, the tensile stress in the deposit had to be reduced, optimally to the point that compressive stresses exist. This work showed that with changes in the plating conditions (e.g., different temperature, higher current density), additions to the plating solution (vanadium pentoxide), and modifications to the plating technique (pulse-plating), a relatively crack-free deposit could be produced that actually was under compression.

Before conclusion of the FACC contract, a version of this new plating technique was successfully used by FACC in four of its sodium/sulfur cells. Two of the cells were removed voluntarily from cycle testing for postmortem analysis; the other two cells had completed 1206 cycles as of the end of December 1985, with continuing stable performance. These latter two cells have been on test a total of 16 months, with no corrosion problems evident. These results represent a dramatic improvement in container performance. This plating technique was subsequently transferred to the plating shop at the SNL's Albuquerque facility and used to plate the sulfur containers that will be used in the laboratory measurements associated with electrolyte stress and sulfur electrode contamination. In a related study, the SNL (Livermore) group is currently working on a method to directly measure stress in the such platings. This method, if successful, may be useful as a screening tool for plating quality.

Water and Oxygen in the Positive Electrode of a Sodium/Sulfur Cell

In the past, investigations of processes that occur in the positive electrode and that are deleterious to cell performance related to electronic and ionic conduction, to the physical distribution of reactants, and to metal corrosion at the cell case. Except for the acknowledgment that leaks through the hermetic seal can cause cell failure, deleterious processes in the positive electrode due to the presence of water and oxygen (either residual from the manufacturing process or from leaks in the hermetic seal) have received little attention.

Recent work at Brown, Boveri, and Cie (reported at the 1984 Fall Meeting of the American Electrochemical Society, New Orleans) showed that hydrogen sulfide, resulting from the reaction of sulfur with residual water, may exist in the gas phase of the positive electrode. Furthermore, their work suggested that the hydrogen sulfide partial pressure cycled as the cell was electrically cycled in a manner directly opposite to that predicted by volume changes in the cell if the total amount present were constant. In addition, it was suggested that hydrogen sulfide might promote a corrosion reaction of the sodium beta″-alumina. This suggestion has major implications for sodium/sulfur battery technology, and it is thus desirable to explore the possibility.

During 1985, a task was initiated at SNL to explore the deleterious effects caused by the presence of water and oxygen in the positive electrode of a sodium/sulfur cell. Knowledge of these effects was desirable so that the maximum quantities allowable could be defined. Thus, the optimal processes and specifications for the manufacture of sodium/sulfur cells could be determined. In the project we will first duplicate the Brown, Boveri, and Cie results in a laboratory cell, and then devise experiments to determine the deleterious effects of excess water and oxygen.

Work on this project in 1985 was limited to designing the laboratory cell, procuring the needed cell parts, and exploring possible reactions in a system containing carbon, sulfur, sodium polysulfide, water, and oxygen. Figure 4-8 shows the cell designed for this work. The design incorporated a tube with an orifice to restrict sodium flow in case of electrolyte failure. The electrolyte, provided by Cerametec, was

glass-mounted to an alpha-alumina collar. A finish $>20 \, \mu m$ on both sides of the alpha-alumina collar was required. The metal flanges on both the sulfur containment case and the sodium containment case contained a machined ring 1.5 mm wide, raised 0.25 mm. Hermetic seals were obtained by compressing a fully annealed aluminum (alloy 1100) gasket between the ring and the mirror-like finish on the alpha-alumina collar. Helium leak tests of the seals using this arrangement have shown leak rates $<10^{-9}$ cc-He/s. Thermal expansion of the bolts (which keeps the pressure on the gasket) is matched to that of the assembly by the addition of an extra thickness of aluminum carefully calculated to keep the assembly in compression. The hermetic seal in the sodium containment case is achieved by a commercially available part from Varian, held together with bolts.

The inside of the sulfur containment case is plated with chromium following a procedure developed by Bonivert and reported in the previous section. Some sulfur containment cases contain a side port to allow gas sampling and introduction of impurities. All metal parts of the containment cases (except the chrome plating) are 304 stainless steel.

By the end of 1985, the cell design had been completed, all piece parts had been procured, the plating technique had been developed in the plating shop, a process for casting the sulfur electrode had been developed, and the first cell was ready for assembly.

In addition to cell design, free-energy data were used to identify thermodynamically possible reactions in a system containing carbon, sulfur, sodium polysulfide, water, and oxygen. Over 70 reactions are thermo-
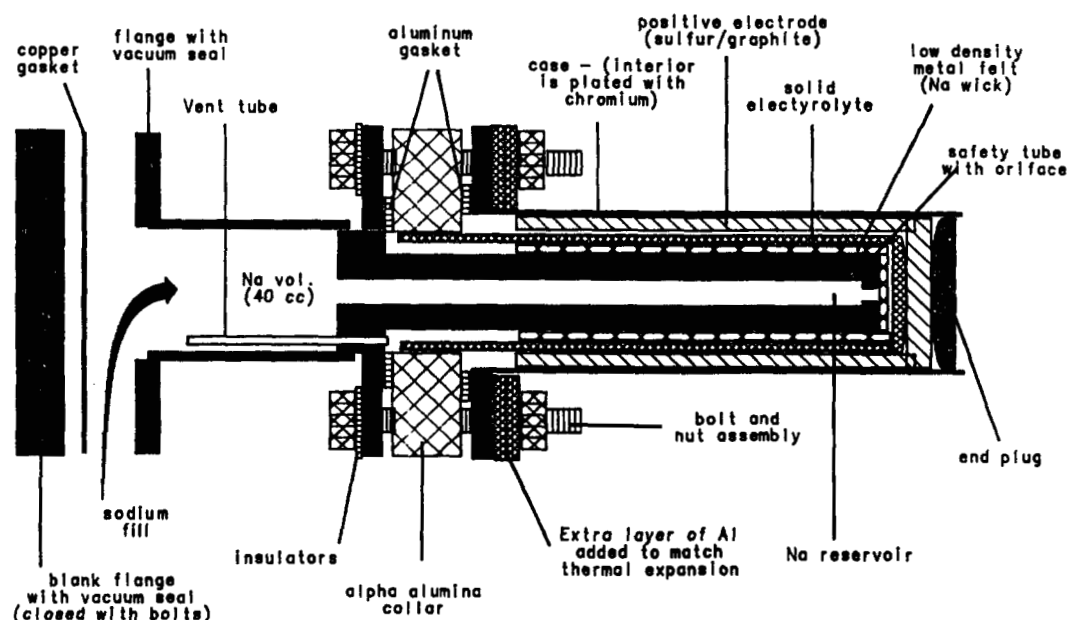

Figure 4-8. Laboratory Cell Design to Explore Deleterious Effects of Excess Water and Oxygen

dynamically possible in this system and, using only equilibrium data, it is possible to predict hydrogen sulfide partial pressures that cycle as the cell cycles electrically. This prediction does not include the reactions that involve the hydrogen polysulfide series known to exist, and almost surely would be soluble in sodium polysulfide. Equilibrium data on these materials are not known. Additionally, activities to address possible hydrogen sulfide reactions with the sodium beta″-alumina were not started.

Stress on the Solid Electrolyte of a Sodium/Sulfur Cell During a Freeze/Thaw Cycle

The sodium/sulfur system utilizes a solid electrolyte and operates in the temperature range of 300°C to 350°C. Sodium, sulfur, and sodium polysulfides are all liquid at operating temperature, but become solid at ambient temperature. Consequently, if for any reason a sodium/sulfur battery is cooled to ambient temperature, the liquids freeze and this causes volume changes and stress on the solid electrolyte. If this stress exceeds the strength of the solid electrolyte, fractures can occur that lead to cell failure. Failure of a significant number of cells in a battery leads to battery failure.

Cell survival during the freeze/thaw cycle is a critical requirement for successful utilization of the sodium/sulfur system, especially for EV applications. A very credible scenario requiring this capability is one analogous to an empty fuel tank miles away from a service station. In this situation, there would be no power available to keep the battery hot, and eventually the battery would cool. Battery failure in this scenario leads to an unacceptable cost, since the battery is expected to be a significant fraction of the capital cost of an electric vehicle. It is questionable whether consumers will accept a product that requires a significant expense each time the user is negligent. For this reason, it is important that cells be designed to withstand the freeze/thaw cycle.

Developers of the sodium/sulfur battery have made significant progress toward improving cell resistance in freeze/thaw cycles, especially for cells in a charged state. Over the years, a consensus has emerged among developers that the stresses leading to electrolyte failure during freeze/thaw cycles originate in the positive electrode. At the Beta Battery Workshop in Snowbird, Utah (May 1985), developers from Germany (Brown, Boveri, and Cie) and Japan (Yuasa Battery Company and Hitachi, Ltd.) reported significant progress on the problem with cells in a discharged state. The Japanese developers are considering this technology only for stationary applications and are apparently satisfied with the current progress on this problem. Despite the progress made for EV applications, more is needed. Furthermore, data on progress made in the Japanese and German programs are not readily available to programs funded by the US Department of Energy.

During 1985, a task was initiated at SNL that will allow electrolyte stresses during freeze/thaw cycling to be predicted for a number of different cell designs. This task has three primary components:

1. Development of suitable materials models and incorporation into a thermomechanical computer code for predicting electrolyte stresses at any SOC.

2. Measurement of the physical and mechanical properties of the positive electrode materials as a function of SOC and temperature. This information, especially for sodium polysulfides, is currently not well-known but is a very necessary input to the materials model contained in the thermomechanical computer code.

3. Direct measurement of the stresses generated in the positive electrode at any SOC. Initially, these actual measurements are needed to help identify the important processes leading to electrolyte stress and, thus, the simplifying assumption that can be used in the stress calculations. Near the completion of this task, these measurements will be used to validate the results obtained by the final computer code.

Once an adequate model for the stresses in a test cell is achieved, calculations for several other designs will be made. A proprietary solution to the problem of freeze/thaw survivability will not be developed by SNL. The stress results for the various designs and the analysis tool itself will be made available to any interested developer.

SNL has several computer codes available on a CRAY computer that can be adapted to calculate stresses for almost any thermomechanical problem. Currently, what is unknown in the modeling effort relates to material behavior and the source of electrolyte stress. Consequently, most of our efforts to date have been directed toward measuring the stresses and the needed material properties. The modeling activities that have been completed include selecting a suitable code (JAC) and formatting the general experimental approach. Actual calculations cannot begin until more data for the material properties become available.

To determine the physical and mechanical properties for the sodium polysulfides or for the polysulfide/carbon-felt composite, it was necessary to synthesize enough sodium polysulfide at the desired composition to make these measurements. An open central-sulfur cell was designed to operate in a glove box for the required synthesis. Figure 4-9 illustrates the apparatus. In this apparatus, the solid electrolyte becomes a container for the molten sodium polysulfide. When a synthesis is complete, the electrolyte/container is removed from the sodium bath and the molten sodium polysulfide is poured into a molybdenum beaker. Two initial runs have been made with this apparatus, and an analysis of the resulting sodium polysulfide indicates that the composition of the melt was not homogeneous throughout the melt, and unusually high amounts of trace metals (calcium and zinc) were present. Better starting materials and a more careful procedure should eliminate these problems.

Our initial approach to measuring the stresses involved casting cathodes of sodium polysulfide with compositions equivalent to a given SOC. Conversations with personnel from Chloride Silent Power, Ltd. suggest several possible deficiencies in this approach, and we had difficulties casting the higher melting sodium polysulfides. For these reasons, we redirected our effort. Our current approach utilizes a modification of the cell described in the previous section. The modifications to that cell are illustrated in Figure 4-10. The major changes included use of an electrolyte

with a wall thick enough to withstand the stresses and a reduction in the diameter of the protection tube to accommodate the electrolyte's decreased inner diameter.
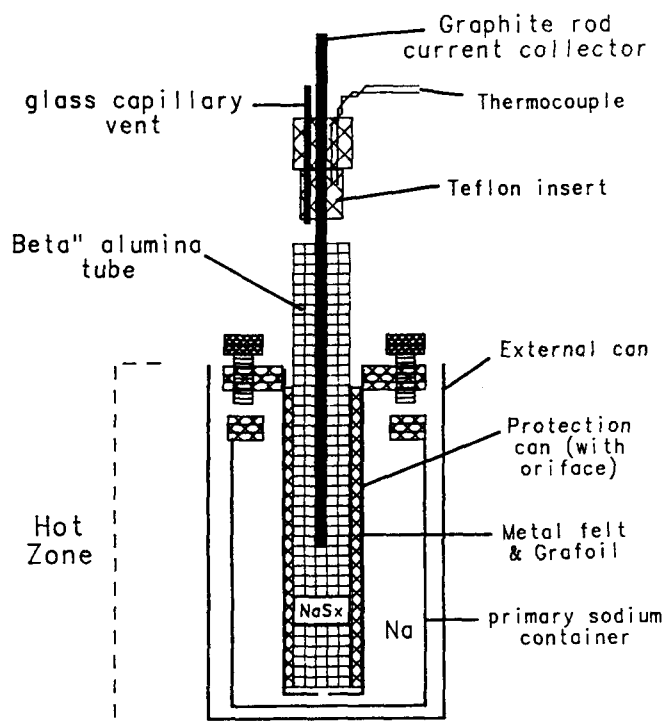

Figure 4-9. Apparatus Used for Open Central-Sulfur Cell to Operate in a Glove Box
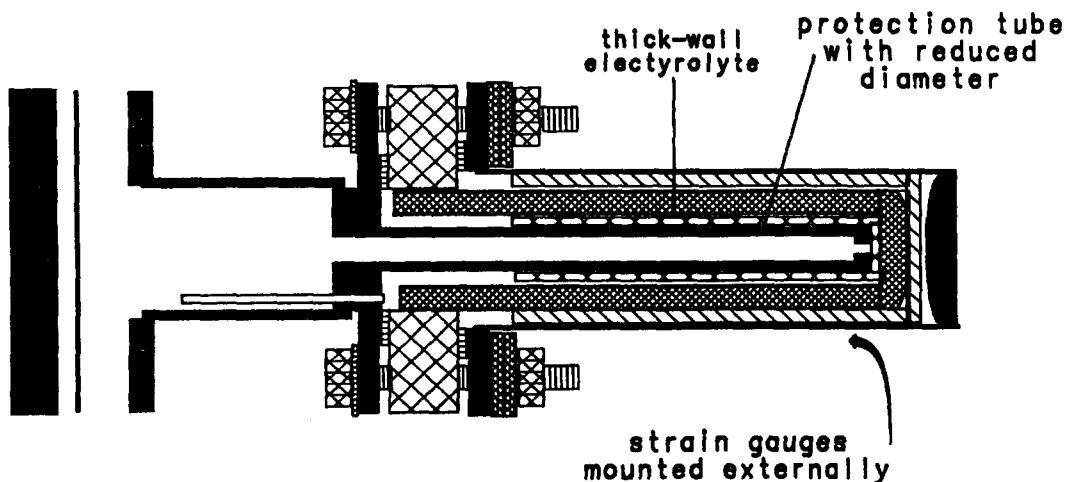

Figure 4-10. Modified Cell

The current experimental technique for measuring electrolyte stress uses strain gauges mounted on the external surface of the cell case to measure the strain generated during freeze/thaw. The theory supporting this technique is that the important electrolyte stress is caused by stresses in the positive electrode. Thus, the stress on the case should be similar to the stress applied to the electrolyte. The strain gauges are calibrated with isostatic pressure in order to relate the measurements to stress. The thick-walled electrolyte still conducts ions (although not very efficiently). This allows the cell to be electrically cycled to any desired state of charge, and the freeze/thaw cycle can be repeated. Data generated in this manner are expected to be quite variable since the location at which a phase change occurs cannot be determined a priori. We expect to perform the freeze/thaw cycle a number of times for a given state of charge. In this manner, we will define an envelope of stress within which realistic calculations must fall. Additionally, to assist in the identification of the regions of high stress, a new technique involving holographic interferometry is being investigated.

By the end of 1985 we had procured all parts for the cell, developed procedures for mounting weldable strain gauges to test cans, developed calibration procedures for the strain gauges, developed techniques for casting cathodes, and developed data acquisition programs for the experiment. We were essentially ready to assemble the first modified cell.

After successfully measuring the pressures generated in the modified cell, we plan to mount strain gauges on cells provided by CSPL and repeat the experiment. We also plan to later include the CSPL geometry as one of several used for modeling.

Development of New Beta″-Alumina Electrolytes at ORNL

The major objective of this research was to increase the conductivity of sodium beta″-alumina below 200°C by using zinc cations rather than lithium cations to stabilize the beta″ phase. The results obtained for various zinc-stabilized ceramic specimens were summarized in the 1984 report. None of these specimens exhibited a significantly reduced low-temperature activation energy [determined from the linear region of $\ln(\sigma T)$ vs $1/T$ below ~200°C] compared to commercial lithium-stabilized material: the lowest activation energy for a large-grained, hot-pressed, zinc-stabilized electrolyte was 0.27 eV compared to 0.32 eV for the lithium-stabilized samples from Ceramatec.

It was found from earlier studies at ORNL that the activation energies of zinc-stabilized sodium beta″-alumina single crystals grown at high temperatures (~1200°C) varied with the zinc concentration and were as low as 0.14 eV. To test the effect of high temperature on the polycrystalline samples, several of the hot-pressed specimens synthesized previously were heated in a covered platinum crucible for various lengths of time at temperatures >1600°C. The most significant change in the electrical properties was observed after heating a specimen hot-pressed at 1610°C (BAZ-43) for 42 h at ~1610°C. After heat treatment, the outer edge of the disc-shaped specimen (and approximate 1- to 2-mm-thick rim) was light blue, similar to the color of single crystals grown at a comparable temperature. Figure 4-11 compares the results of conductivity measurements (see 1984 report for experimental details) made on a small section of the blue rim with those obtained before heat treatment. Because of the shape of heat-treated conductivity specimens, there is at least a 10% relative uncertainty in the σT values. This uncertainty, however, does not affect the determination of the activation energy, and it is clear that a significant reduction in activation energy was achieved: E=0.23 eV after heat treatment compared to E=0.29 eV before heat treatment. X-ray fluorescence measurements in a scanning electron microscope showed a significant reduction in the zinc concentration in the specimen following heat treatment. The microstructure of the heat-treated specimen appears to be comparable to that of the parent sample, so that the reduction in activation energy is probably due to the change in the zinc concentration rather than to any change in the relative grain sizes. While these results should be viewed with caution, since only a single specimen was examined, they suggest that it may be possible to significantly alter the conductivity of zinc-stabilized sodium beta″-alumina ceramics by making a small adjustment in its composition.
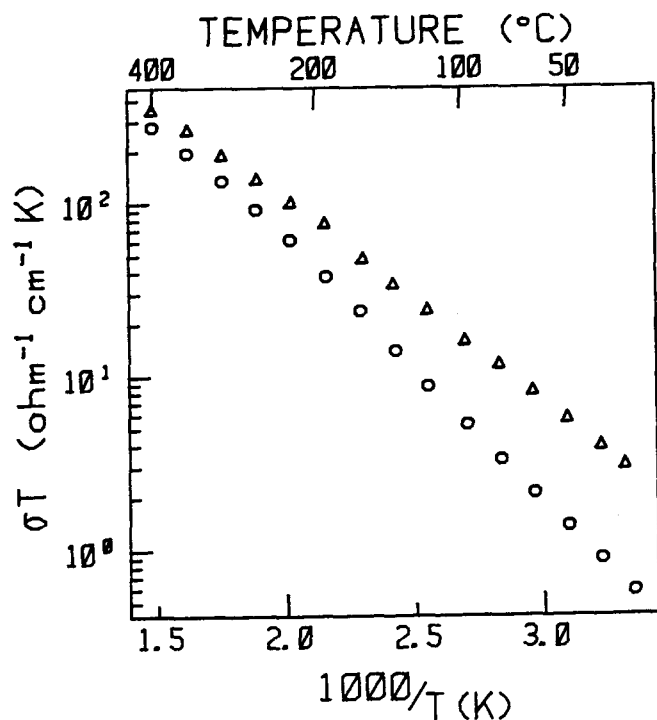
TEMPERATURE (°C)

Figure 4-11. Conductivity of a Hot-Pressed, Zinc-Stabilized Sodium Beta″-Alumina Specimen (BAZ-43) Before (O) and After (△) Heating at 1610°C in a Covered Platinum Crucible

A secondary objective of this research effort was to attempt to increase by metal particle addition the fracture toughness of sodium beta″-alumina without altering its electrical properties. Ceramic specimens of lithium-stabilized sodium beta″-alumina containing ~1% by volume of dispersed platinum particles were prepared by mixing the precursor electrolyte powder (Ceramatec) with hexachloroplatinic acid (H_2PtCl_6) in ethyl alcohol, drying the mixture, and then heating it to 500°C for 30 min. The mixture was hot-pressed at 1675°C for 15 min under vacuum at 8×10^3 psi, and the resulting specimen was then heated in air at 1480°C for 2 h. The final density of the cermet was 3.3 g/cm³.

Figure 4-12 shows the results of conductivity measurements on the cermet. At 300°C, $\rho = 81$ Ω-cm. There is no evidence of an increase in the electronic

conductivity of the electrolyte due to the metal particles and indeed none was expected, as the low concentration and dispersion precludes the formation of a continuous metal path. The fracture toughness measured at 25°C using an indentation technique was $K_{1c} = 4.9 \pm 0.2$ MPa m$^{1/2}$. After further heat treatment of the specimen at 1600°C in air for 1 h, followed by 2 h of heating at 1480°C, the conductivity was improved considerably (Figure 4-12) with little change in fracture toughness: $\rho = 27$ Ω-cm at 300°C and $K_{1c} = 4.6 \pm 0.2$ MPa m$^{1/2}$ at 25°C. Microscopic examination of the specimen revealed essentially no change in the microstructure after the second heat treatment. The material consists mainly of fine elongated grains measuring ~10 μm along the long axis and 1 to 2 μm along the short axis (Figure 4-13).
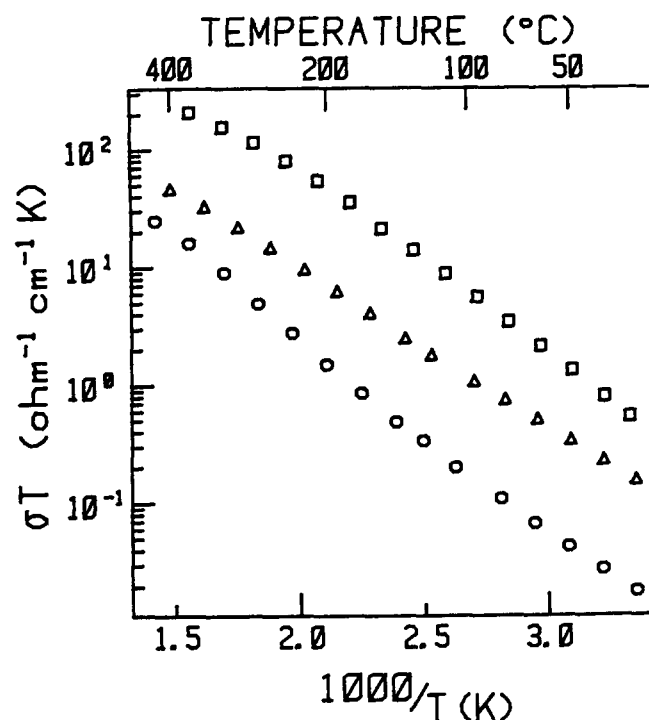
TEMPERATURE (°C)

Figure 4-12. Conductivity of the Cermet Electrolyte As-Prepared (O) and After Additional Heat Treatment in Air (△). Data for a Commercial sample of sodium beta″-alumina are shown for comparison (□).
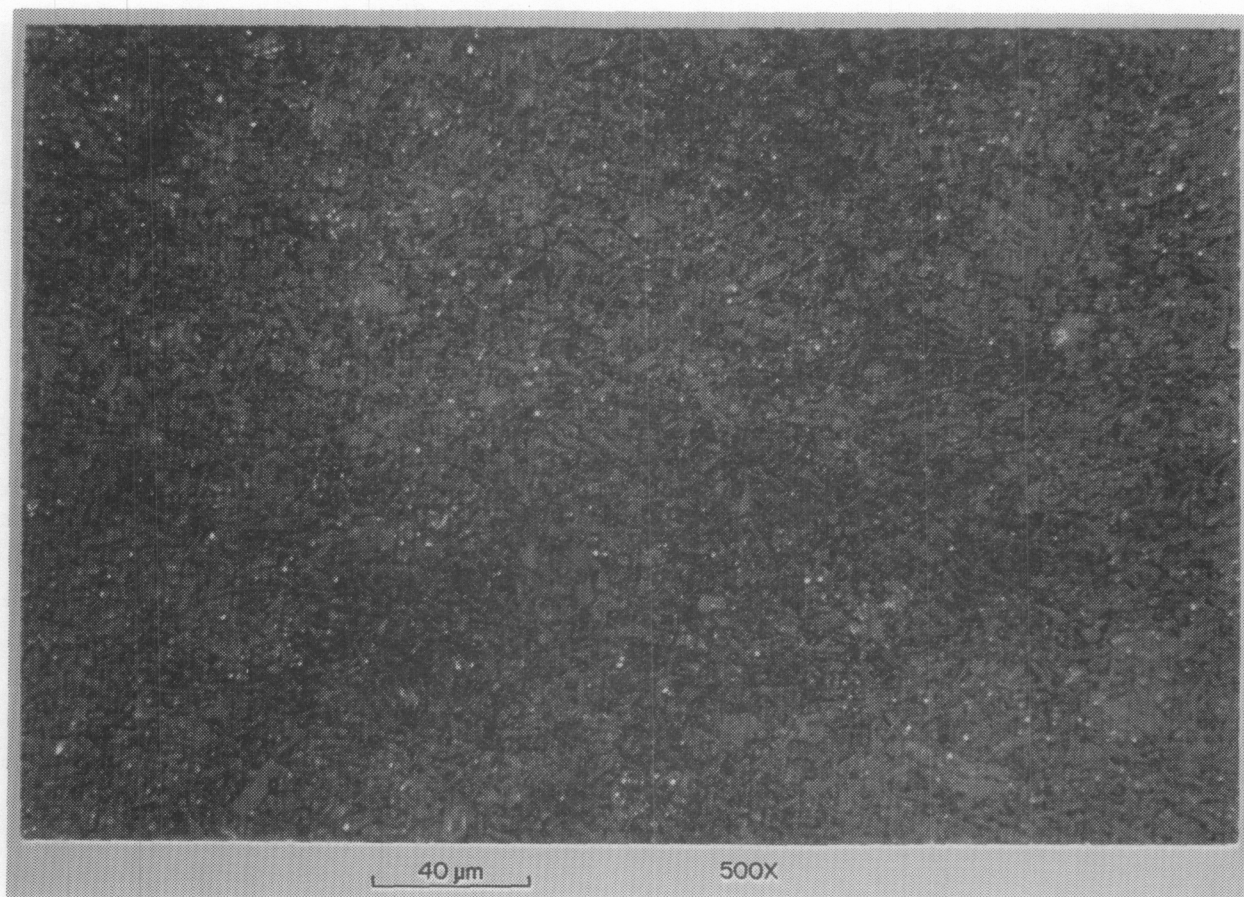
116

Figure 4-13. Optical Micrograph of the Cermet Electrolyte After Heat Treatment of the As-Prepared Specimen. The small bright specks are the platinum particles.

Aside from the fine grain structure of the cermet, the probable major cause of the low conductivity is that the cermet consisted mainly of sodium beta-alumina with only a small fraction of beta″-alumina. This was revealed from x-ray diffraction measurements. A check on the precursor electrolyte powder showed that the conversion of beta″-alumina to beta-alumina occurred during some stage of synthesis of the cermet. Further studies are needed to identify and correct this problem. Since the cermet was essentially a beta-alumina electrolyte, it is interesting to compare its resistivity at 300°C, $\rho = 27$ Ω-cm, with that of pure polycrystalline sodium beta-alumina, $\rho = 18$ Ω-cm, at the same temperature.

Chapter 5. Project Analysis

The objectives of the Project Analysis activities are to determine battery requirements in various end-use applications by analyzing the technical and economic aspects of such systems, to provide models that allow computer simulation of battery performance in a variety of situations, and to perform planning studies that will assist the Lead Center in providing effective program direction and management. These objectives were attained through both in-house efforts and outside contracts.

In-House Work

During 1985 the CSOM storage battery load-leveling facility was analyzed using a risk-adjusted approach to the capital budgeting decision. Capital budgeting is a process whereby firms identify and evaluate potential investment projects. Risk adjustments to the capital budgeting process are required to determine a project's appropriate rate of return on investment. The CSOM analysis presents a capital budgeting methodology that is more theoretically correct and technically elegant than other methods previously applied to advanced energy system projects.

The preferred capital budgeting technique is net present value (NPV) analysis using the firm's weighted average cost of capital (WACC), but using this discount rate assumes a level of project risk that is not often understood. The WACC is the appropriate discount rate when the riskiness of the project to be undertaken is the same as the riskiness of the firm's returns (i.e., the riskiness of the firm's past investment projects). When the project has a greater (or lesser) risk than the firm as a whole, an alternative method of determining the appropriate discount rate is necessary. The cash flows of higher risk projects should be discounted using higher discount rates, and the cash flows of lower risk projects should be discounted using lower discount rates.

A model exists to identify the risk-adjusted required rate of return for risky projects. The model, called the Capital Asset Pricing Model (CAPM), shows the relationship between the required rate of return and risk. A site-specific CSOM storage battery project for a textile manufacturer was evaluated using the CAPM and a project NPV sensitivity analysis.

The CSOM facility consists of a nominal 500-kWh/500-kW battery. Two different investment scenarios were considered for this CSOM facility analysis. The first assumed that the 500-kWh/500-kW battery (an air-lift design, lead-acid battery manufactured by GNB Batteries) and the 500-kW converter that EPRI purchased for testing at the BEST Facility could be repurchased (after testing) by the textile manufacturer. This situation was referred to as the BEST Battery and Converter (Case #1) scenario. Total project cost for Case #1 was estimated to be $392,600 (1983 dollars), including $62,500 for the battery ($125/kWh) and $37,500 for the converter; $132,100 for balance-of-plant costs; and $160,500 for engineering and project management costs. The second scenario, designated New Battery and Converter (Case #4), assumed that a totally new battery and converter was purchased. Total project cost for Case #4 was $624,900, including $168,400 for the battery ($337/kWh) and $163,900 for the converter; $132,100 for balance-of-plant costs; and $160,500 for engineering and project management costs. Project NPV was calculated using a CAPM-determined discount rate. The CAPM rate, 10.38%, was based on a historical risk-free rate of 4.0%, a market risk premium of 5.1%, and a textile industry beta of 1.34. The project NPV for the cost-subsidized initial investment scenario (Case #1) was $102,719, while the NPV for the full cost initial investment scenario (Case #4) was a negative $568.

The sensitivity of project NPV to variations in two key cash flow variables—the on-peak demand charge rate and the demand charge escalation rate—illustrates the risk associated with the CSOM project. Figure 5-1 is a graphic representation of the on-peak demand charge rate sensitivity analysis results (only the high on-peak demand charge rates are shown). As one can see, for both scenarios, the NPV is very sensitive to changes in the on-peak demand charge rate. Figure 5-2 is a graphic representation of the demand charge escalation rate sensitivity analysis results. The value of the CSOM storage battery facility project is also very sensitive to the demand charge escalation rate. The importance of an EPRI cost-subsidized battery and converter is obvious.
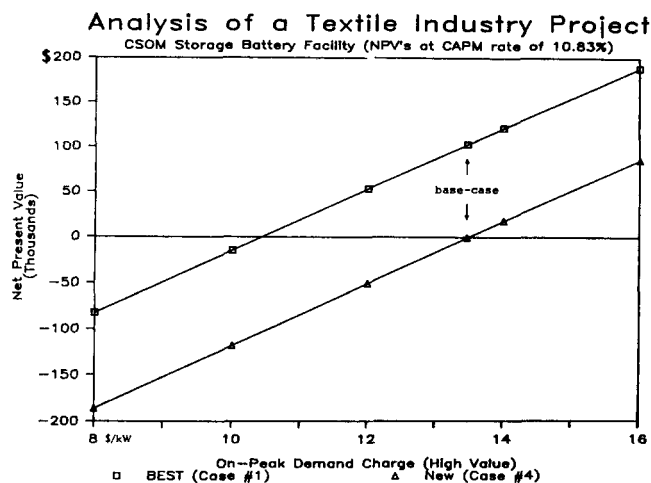
Analysis of a Textile Industry Project

CSOM Storage Battery Facility (NPV's at CAPM rate of 10.83%)

Figure 5-1. Sensitivity Analysis of On-Peak Demand Charge Rate

Analysis of a Textile Industry Project

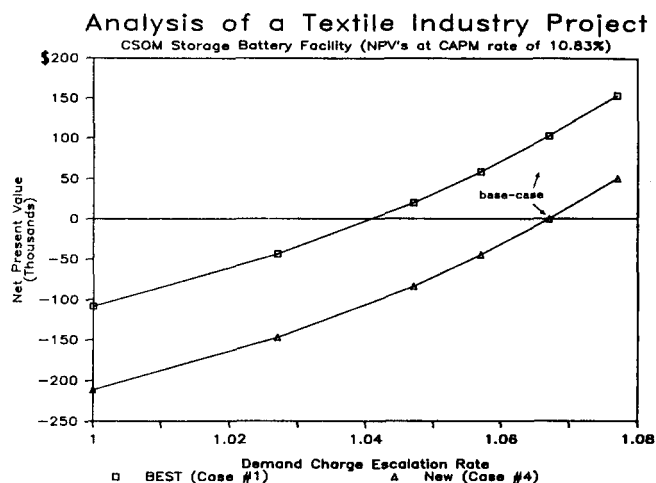CSOM Storage Battery Facility (NPV's at CAPM rate of 10.83%)

Figure 5-2. Sensitivity Analysis of Demand Charge Escalation Rate

It was concluded that the textile manufacturer's CSOM investment project is riskier than originally thought.

Another major in-house effort during 1985 concerned a cost study on the hydrogen/nickel oxide battery. The study compared the hydrogen/nickel oxide system with the flooded lead-acid and sealed lead-acid battery technologies in a residential stand-alone photovoltaic application. The life-cycle cost analysis results show that the higher initial cost for the hydrogen/nickel oxide battery is ameliorated by its very low maintenance and long life, resulting in the lowest present-value cost of the three battery systems studied.

Contracted Work

Technology Transfer Plan—Jaycor

Jaycor, a consulting firm in Alexandria, Virginia, was awarded a contract in late 1983 to develop a technology transfer plan for the DOE/ESD Branch. The contracted work was completed and a final report was received during 1985.

APPENDIX

Publications and Presentations, 1985

Burant, L., and W. Gentry. "An Interim Cost Study of a Terrestrial Hydrogen/Nickel Oxide Battery." Presented at the 18th Photovoltaic Specialists Conference, Las Vegas, Nevada, October 1985.

Bush, D. M. "Using the Pressure-Time Slope to Terminate Charging of Nickel/Hydrogen Batteries." Presented at Fall Meeting of the Electrochemical Society, Las Vegas, Nevada, October 1985.

Bush, D. M., J. D. Sealey, and D. W. Miller. *Testing of Sealed Lead-Acid Batteries.* SAND85-2334, Revised. Albuquerque, NM: Sandia National Laboratories, May 1985.

Bush, D. M., and J. Sindorf. "Tests of Hydrogen/Nickel Oxide and Lead-Acid Battery Systems." Presented at Seventh Battery and Electrochemical Contractors' Conference, Washington, DC, November 1985.

Butler, P. C. *Final Battery Evaluation Report: Energy Research Corporation Zinc/Bromine Battery.* SAND84-0799. Albuquerque, NM: Sandia National Laboratories, March 1985.

Butler, P. C. "Overview of Rechargeable Battery Testing in the United States." Presented at International Workshop on Battery Testing, Heidelberg, West Germany, October 1985.

Butler, P. C. "EHP Battery Test Working Task Force Activities." Presented at Seventh DOE Battery and Electrochemical Contractors' Conference, Washington, DC, November 1985.

Butler, P. C., and J. M. Freese. "Flow Battery and Sodium/Sulfur Cell Testing at SNL." Presented at Seventh DOE Battery and Electrochemical Contractors' Conference, Washington, DC, November 1985.

Butler, P. C., and C. E. Robinson. "Flowing Electrolyte Batteries Test Methods and Results." Presented at International Workshop on Battery Testing, Heidelberg, West Germany, October 1985.

Chreitzberg, A. M. *Testing, Data Analysis, and Engineering Services on Lead-Acid Load-Leveling Batteries, Phase II.* SAND85-7235. Albuquerque, NM: Sandia National Laboratories, September 1985.

Chreitzberg, A. M. "Accelerated Testing of Lead-Acid Batteries." Presented at Seventh Battery and Electrochemical Contractors' Conference, Washington, DC, November 1985.

Dunlop, J., M. Earl, M. Brown, H. Vaidyanathan, W. Gentry, R. Beauchamp, and J. Sindorf. *Design and Development of a Sealed 100-Ah Hydrogen/Nickel Oxide Battery.* SAND85-7219. Albuquerque, NM: Sandia National Laboratories, September 1985.

Dunlop, J., and R. Beauchamp. "Development of the Hydrogen/Nickel Oxide Battery System." Presented at the Seventh Battery and Electrochemical Contractors' Conference, Washington, DC, November 1985.

Hornstra, F. "Autonormalization of Battery Test Data to Significantly Reduce Impact of Battery Aging on Test Results." *Extended Abstracts: First International Workshop on Battery Testing, Heidelberg, West Germany, 30 September-2 October 1985,* pp 58-62.

Hornstra, F. "A Simple Methodology for Obtaining Battery Discharge Times (and Vehicle Ranges) for Arbitrarily Structured Load Profiles." *Extended Abstracts: First International Workshop on Battery Testing, Heidelberg, West Germany, 30 September-2 October 1985,* pp 179-184.

Hornstra, F. "Test Programs at the National Battery Test Laboratory." *Extended Abstracts: First International Workshop on Battery Testing, Heidelberg, West Germany, 30 September-2 October 1985,* pp 38-42.

Hornstra, F. "Summary Report of First International Workshop on Battery Testing, 30 September through 2 October 1985, Heidelberg, FRG." *Extended Abstracts: Seventh Battery and Electrochemical Contractors' Conference, Crystal City, Virginia, 18-21 November 1985,* pp 175-78.

Hornstra, F., W. H. DeLuca, and T. P. Mulcahey. "Testing Activities at the National Battery Test Laboratory." *Extended Abstracts: Seventh Battery and Electrochemical Contractors' Conference, Crystal City, Virginia, 18-21 November 1985,* pp 175-78.

Lee, J., J. D. Arntzen, E. C. Gay, F. Hornstra, and C. C. Christianson. "Characterization of Thermal Behavior of Sealed Starved-Electrolyte Lead-Acid Batteries." *Extended Abstracts: 168th Electrochemical Society Meeting, Las Vegas, Nevada, 13-18 October 1985,* 85(2):55-6.

Magnani, N. J., R. P. Clark, D. M. Bush, P. C. Butler, J. L. Chamberlin, J. M. Freese, K. R. Grothaus, K. D. Murphy, and P. E. Schumaker. *Exploratory Battery Technology Development and Testing Report for 1984.* SAND85-1446. Albuquerque, NM: Sandia National Laboratories, October 1985.

Miller, J. F., C. C. Christianson, F. Hornstra, E. C. Gay, J. D. Arntzen, and N. P. Yao. "Impact of Simulated Electric Vehicle Operation on the Cycle Life of EV-2300 Lead-Acid Batteries." *Extended Abstracts: 168th Electrochemical Society Meeting, Las Vegas, Nevada, 13-18 October 1985,* 85(2):53-4.

Sindorf, J., L. Burant, and J. Dunlop. "Design and Cost Study of a 15-kWh Hydrogen/Nickel Oxide Battery for Photovoltaic Applications." Presented at the 20th Intersociety Energy Conversion Conference, Miami Beach, Florida, August 1985.

DISTRIBUTION:

US Department of Energy (34)
Energy Storage and Distribution
Attn: R. Eaton
M. Gurevich
K. Klein
A. Landgrebe
J. Quinn (30)
CE-32
FORSTL
Washington, DC 20585

US Department of Energy (4)
Electric and Hybrid Propulsion Div.
Attn: K. Barber
P. J. Brown
R. Kirk
P. Patil
CE-132
FORSTL
Washington, DC 20585

US Department of Energy (5)
Albuquerque Operations Office
Attn: D. L. Krenz (2)
C. B. Quinn (2)
K. Smith
Energy Technologies Div.
Albuquerque, NM 87115

US Department of Energy
Sandia Area Office
Attn: A. R. Sneddon, Jr.
PO Box 5800
Albuquerque, NM 87115

Lawrence Berkeley Laboratory (3)
University of California
Attn: E. Cairns
K. Kinoshita
F. McLarnon
No. 1 Cyclotron Road
Berkeley, CA 94720

Electric Power Research Institute (7)
Attn: R. Schainker
PO Box 10412
Palo Alto, CA 94303

Argonne National Laboratory (5)
Attn: C. Christianson
T. Mulcahey (3)
P. Nelson
9700 South Cass Ave.
Argonne, IL 60439

EG&G Idaho, Inc.
Idaho National Engineering Lab
Attn: G. L. Hunt
PO Box 1625
Idaho Falls, ID 83415

Wright Patterson AFB
Attn: W. Bishop
Air Force Wright Aeronautical Labs
AFWAL/POOC-1
Wright Patterson AFB, OH 45433

Trebor, Inc.
Attn: Dr. Robert Meredith
173 River Road
Charles Town, WV 25414

Battelle (2)
Pacific Northwest Laboratories
Attn: B. Ashton
R. Sen
2030 M Street NW
Washington, DC 20036

Battelle (6)
Pacific Northwest Laboratories
Attn: L. Fassbender (5)
L. Kannberg
Battelle Blvd.
Richland, WA 99352

Martin Marietta Energy Systems, Inc.
Attn: J. Stovall
PO Box X
Oak Ridge, TN 37831

Energetics (3)
Attn: J. Hurwitch
H. Lowitt
R. Scheer
9210 Route 108
Columbia, MD 21044

DISTRIBUTION (continued):

20	O. E. Jones
140	W. W. Hollis
	Attn: H. A. Romme, 143
400	A. N. Blackwell
1521	R. D. Krieg
1521	C. M. Stone
1524	A. K. Miller
1524	S. R. Subia
1810	R. G. Kepler
1811	C. Arnold, Jr.
1811	R. L. Clough
1812	R. A. Assink
1812	J. M. Zeigler
1820	R. E. Whan
1840	R. J. Eagan
1845	E. K. Beauchamp
1845	R. P. Gerstle, Jr.
2000	L. K. Anderson
2500	D. B. Hayes, Actg.
2520	N. J. Magnani
2522	R. D. Wehrle
2523	J. Q. Searcy
2525	R. P. Clark (150)
2526	R. C. Lincoln
3710	A. J. Arenholz
	Attn: R. W. Williams, 3712
6200	V. L. Dugan
6220	D. G. Schueler
6221	E. C. Boes
6223	G. J. Jones
8313	W. D. Bonivert
8313	L. R. Thorne
8024	P. W. Dean
3141	S. A. Landenberger (5)
3151	W. L. Garner (3)
3154-1	C. H. Dalin (28)
	For DOE/TIC (Unlimited Release)